Effects of different perturbative methods of the system-bath coupling on the reduced system dynamics

von der Fakultät für Naturwissenschaften der
Technischen Universität Chemnitz genehmigte Dissertation
zur Erlangung des akademischen Grades

doctor rerum naturalium

(Dr. rer. nat.)

Vorgelegt von Dipl. Phys. Markus Schröder
geboren am 15.05.1977 in Verden (Aller)
Eingereicht am 18.10.2006

Bibliographische Beschreibung

Referat

Diese Dissertation befasst sich mit der numerischen Behandlung dissipativer quantenmechanischer Prozesse im Rahmen der reduzierten Dichtematrix-Theorie. Zunächst werden Elektronen-Transferprozesse mit Hilfe einer hierarchischen Methode zur Lösung der Bewegungsgleichung der System-Dichtematrix untersucht. Hier liegt der Fokus auf der Untersuchung des Konvergenzverhaltens der Hierarchie mit der Anzahl der berücksichtigten Ebenen bei unterschiedlichen Abbruchverfahren. Es wird gezeigt, dass die Konvergenz stark von der Abbruchmethode und der Observablen abhängt.

Weiterhin wird das lineare Absorptionsspektrum des B850 Pigment-Rings von *Rhodispirillum molischianum* mit verschiedenen Methoden zur Berücksichtigung der Effekte eines angekoppelten Bades berechnet. Diese Methoden basieren auf störungstheoretischen Ansätzen in der System-Bad-Kopplung. Es gelang unter Verwendung der modifizierten Redfield Theorie (MRT) einen Ausdruck für das Absorptionsspektrum herzuleiten. Bei der MRT werden Teile der System-Bad-Wechselwirkung exakt behandelt. Diese Methode wird in zwei Varianten diskutiert und anderen Methoden gegenübergestellt. Modellrechnungen werden für verschiedene Spektraldichten angefertigt, darunter eine, die aus einer Molekulardynamik(MD)- Simulation stammt. Ebenso wird der Einfluss statischer Unordnung der Pigment-Energien auf die Form des Absorptionsspektrums diskutiert. Dazu werden Spektren sowohl einer einzelnen Realisierung als auch des Ensembles dargestellt. Im Falle der Spektraldichte aus der MD-Simulation werden die Ensemble-Spektren zusätzlich mit experimentellen Daten verglichen. Weiterhin wird eine Rechnung mit der Hierarchie zum Spektrum des B850 Rings und weitere zur Populationsdynamik eines kleineren Systems diskutiert und mit Ergebnissen aus der MRT verglichen.

Außerdem wird eine Methode zur stochastischen Propagation von mehrdimensionalen Wellenfunktionen entwickelt. Mit Hilfe von Sprung- Prozessen gelingt es die Freiheitsgrade des Systems zu entkoppeln, sodass mehrere eindimensionale Wellenfunktionen stochastisch propagiert werden können. Die exakte Wellenfunktion kann so als Ensemblemittel von Produkten eindimensionaler stochastischer Wellenfunktionen beschrieben werden.

Schlagwörter

Exzitonentransfer, Elektronentransfer, dissipative Quantendynamik, Störungstheorie, reduzierte Dichtematrix, lineares Absorptionsspektrum, Pigment-Protein-Komplex, B850, stochastische Wellenfunktion

Contents

1 Introduction

In this work various methods for treating the dynamics of a quantum mechanical subsystem coupled to external systems are discussed and compared. This includes dissipative dynamics as well as coherent motion in a multi-dimensional system. In this chapter an introduction to the systems under consideration and a motivation for their treatment are given.

1.1 Pigment complexes

Pigment complexes are widespread within nature, in biological as well as in anorganic systems, and play also an important role in technological applications where, however, in the vast majority of cases synthetic pigments are used. Pigments absorb light in a selected frequency range while other wavelengths are reflected or transmitted such that the impression of color arises. In biological systems pigments not only serve for coloring but often have particular functions such as photoreception or energy and charge transport. Chlorophyll molecules are a famous example for such pigments.

To transport excitation energy, spatially separated pigments have to be coupled. This coupling usually consists of several contributions where the most important are Coulomb and exchange interaction.[1,2] If the spatial distance is large enough, the exchange contribution can be neglected and the Coulomb interaction, which can be expanded in a multipole series, is the dominating mechanism. If the pigment molecules are uncharged the dominating contribution of the multipole series is the dipole-dipole interaction. A pigment which is in an electronically excited state can interact via the dipole-dipole interaction with a neighboring pigment which is in its electronic ground state and cause a transition of this pigment to the excited state while decaying into the ground state itself. This mechanism is the so-called Förster interaction[1,2] and describes a radiationless transfer process for excitation energy. For most pigment systems it is sufficient to take into account only nearest neighbor interaction since the dipole-dipole term decays with r^{-3} where r is the distance between two pigments.

From a quantum mechanical point of view such coupled pigment systems form a combined structure where the single pigments cannot be treated separately. While the eigenstates of the uncoupled pigment system are located at the pigments, the eigenstates of the coupled complex are no longer identical with the eigenstates of the separated pigments and hence are spread over a number of sites. These eigenstates are also called *excitons*. It should be mentioned that *exciton* in this case describes a delocalized excited state in a finite organic aggregate and is somewhat different from the usual definition as an electron-hole pair in an infinite crystal as known from solid state physics.

Usually the pigment complexes are embedded in an environment such as solvents or solids. In biological systems often a protein matrix keeps the pigment complexes in a certain shape which guarantees its function. This environment is in many cases not

optically active in the same frequency range as the pigment complex but its vibronic degrees of freedom (DOFs) are usually coupled to the pigments and cause transitions between the excitonic states and exchange of energy between the pigments and their environment.

The existence of excitons and their coupling to the environment has also consequences for the absorption spectra of the pigment complexes. The spectra are no longer identical with those of the single pigments. If the pigmet complex is much smaller than the wavelength of the absorbed light it can be assumed that not the individual pigments but the pigment complex as a whole absorbs energy from the electromagnetic field at the transition frequency between the ground state and the excitonic states. In addition the life-time of the excitonic states is limited due to the coupling between the excitons and the environment such that broadening of the absorption lines can be observed.

The exact quantum mechanical and even a classical treatment of these kinds of systems is rather difficult, especially for biological systems, since a large number of different atoms is involved. An exact numerical description of large systems usually exceeds the computational capacity of modern computers. Hence (partly very rough) approximations have to be applied for a numerical description.

In the present work two excitonic systems will be examined within simplified models. In chapter 4 the absorption spectrum of the B850 pigment ring of the light-harvesting system II (LH2) of the purple bacterium *Rhodospirillum* (*Rhs.*) *molischianum* is calculated. The LH2 rings are together with the larger LH1 rings part of the photosynthetic system of purple bacteria. Both complexes are embedded in the cell membrane and are usually arranged in groups where several LH2 rings surround one LH1 system.[3] The structure of the arrangement and also the structure of the pigment complexes itself differs depending on the species. For *Rhs. molischianum* the structure of the LH2 systems has been determined in 1996[4] such that further studies became possible. The LH2 systems only serve as light absorbing antennas that transfer the excitation energy to the LH1 systems. In the center of the LH1 systems a reaction center is located[5,6] where the excitation is transfered to such that the energy can be used to trigger a charge separation process. The charge separation drives further mechanisms so that adenosine triphosphate (ATP) can be produced.[7] The light harvesting systems contain two different rings of bacteriochlorophylls (BChls) which are named after the wavelength where the maxima of their absorption spectra are located. In the case of *Rhs. molischianum* the LH2 system consists of the so-called B800 and B850 rings that absorb at approximately 800 and 850 nanometers, respectively. The B800 and B850 rings consist of 8 and 16 BChl *a* molecules (the pigments), respectively, which are arranged in a circular pattern. The *a* here labels a special type of BChl of which several variants are known. The various BChl types mainly differ in the side groups and also have different absorption spectra.

Several theoretical approaches have been developed to determine absorption lineshapes as for instance the stochastic line-shape theory[8] or the Brownian oscillator model.[9,10,11] For larger systems such as the LH2 system there have been non-perturbative[12,13] studies as well as perturbative approaches to treat the interaction of the pigment system and an environment.[14,15,16] In this work the linear absorption of only a part, the B850 ring, of the LH2 pigment complex of *Rhs. molischianum* is studied using different methods based on second order perturbation theory. The perturbative treatment is used for both, for the coupling between the electronic states of the pigments to their environment as well as to the electromagnetic light field. Also an

additional method based on the so-called (Markovian) modified Redfield theory (MRT) proposed by Zhang and coworkers[17] is developed and used to calculate the linear absorption profile of the B850 ring. This is also done with a time-dependent variant (TDMRT) of the Markovian MRT. Within MRT parts of the interaction between the pigment system and its environment are treated exactly such that one can expect more reliable results.

The calculations with the different methods are performed also using input data from a molecular dynamics (MD) simulation published in Ref. [18]. The obtained spectra are compared and discussed with special focus on the influence of the bath and the reliability of results of the various methods. There have been ongoing discussions about which of the approaches yields the most precise results. This question cannot be answered in general within this study, however, for the results obtained with the data of the MD simulation arguments pointing to one of second-order perturbative treatments will be identified.

Except from the results obtained with the hierarchical method described in section 4.2.4 and those obtained with the TDMRT approach with unshifted bath, the results discussed in chapter 4 have already been published in Refs. [19, 20, 21].

In chapter 5 the population dynamics of the excitonic states of a similar but smaller ring shaped pigment system under the influence of a surrounding environment are calculated. This is done within reduced density matrix theory and to various orders of perturbation theory and using the MRT and TDMRT approaches. The focus of this chapter lies on the comparison between the MRT and TDMRT methods and usual perturbative approaches. The MRT and TDMRT methods are assumed to be more precise as other perturbative techniques since here parts of the perturbation are treated exactly. The results of both methods are compared in order to verify their limits and convergence behavior.

1.2 Electron transfer processes

Besides transfer processes of excitation energy also charge transfer processes are one of the most important processes in chemistry and chemical physics. There are several types of charge transfer processes known, such as electron, proton or hole transfer processes. All these kinds of processes are of high importance in anorganic chemistry and in biological systems as well. Examples are redox reactions or acid and base reactions in anorganic chemistry or, in biological systems, for example, the final charge separation in the photosynthetic reaction center or the production of ATP. There are many other examples of such transfer reactions. Recently several studies of charge transfer reactions in molecular wires[22] especially DNA as a model for molecular wires were published.[23, 24, 25, 26] Both, electron and hole transfer processes have been studied within this system.[27, 28] The following discussion will be restricted to the transfer process of a single electron.

There are several types of electron transfer processes such as intra- and inter molecular transfers.[2] Both can be understood as (spatial) redistributions of charge within one or between several molecules, respectively, where in the latter case also so-called bridge molecules, that can be temporarily populated, can be involved. Within the theoretical treatment of electron transfer processes it is usually possible to restrict the number of electronic states to a single donor and a single acceptor state and, if bridge

molecules are involved, single electronic states for each bridge molecule.[2] These electronic states can be understood as eigenstates of different effective potentials comprising all different kinds of interaction which the electron experiences when located at a respective molecule. To allow for electron transport, however, these eigenstates have to be coupled such that the electron can travel from the initially populated donor state to the acceptor state. Since the acceptor state is energetically lower, excitation energy has to dissipate out of the system so that the acceptor state can be populated. Otherwise the population will be transfered back to the donor state. Responsible for dissipation can be a thermal bath of internal vibrational modes of the molecule or of surrounding molecules that are coupled to the electronic donor, acceptor and bridge states.

In addition, the vibrational DOFs of the molecules play an important role for the electron transfer process since the thermal energy of the molecular modes can enable the electron to pass a potential energy barrier between donor and acceptor state faster or even hinder the transfer by reducing the transfer integral between the states. Since the electron moves much faster than the nuclei of the molecule it is usually assumed that the electronic wave function can be parametrized in terms of the nuclei positions and that the electronic wave function creates a potential energy surface encountered by the nuclei. The nuclear motion, i.e., the vibrational DOFs, can then be treated independently from the electronic wave functions. This procedure is called the Born-Oppenheimer approximation. In addition, it is reasonable to assume that for small deviations from the equilibrium position the nuclei move in almost harmonic potential surfaces.

In chapter 3 a simple model system of a donor and an acceptor state coupled to a surrounding bath will be modeled by harmonic potential surfaces. The interaction with the bath will be treated to several orders. It will be of special interest to show the convergence behavior of a hierarchical method for density matrix propagation proposed by Tanimura and others.[29,30,31,32,33,34,35,36,37] There have been questions of whether a time-local or a time-nonlocal treatment of such systems performs superiorly.[38] This will also be discussed in more detail in chapters 3 to 5.

1.3 Wave packet dynamics

The systems discussed above are usually treated within density matrix theory where only a few DOFs are treated explicitly. In many cases, however, especially in the area of femtochemistry,[39,40,41,42,43] one is interested in detailed time evolution of wave functions instead of density matrices. Examples of such systems are nuclear dynamics in large molecules or clusters[44] where in most cases many DOF are involved. Several methods have been developed to treat such systems numerically, however, with today's computational capacities the direct quantum mechanical treatment is limited to four to six DOFs, even with advanced methods[45,46,47,48] since the requirements for memory and CPU time grow very fast with the number of dimensions.

A lot of effort has been spent on developing algorithms that separate an M-dimensional problem into a number of one-dimensional problems that are numerically much more easy to deal with. A simple method of this kind is the time-dependent Hartree method[49,50] which can be derived from a variational ansatz. Within this method the complete multi-dimensional state vector is approximated by an outer product of single mode wave functions that evolve on effective potential energy surfaces that, in turn,

depend on the states of all other modes. Unfortunately much of the correlations such as entanglements between the wave functions of the various modes are neglected in this scheme. This can be overcome by using a number of such product states to approximate the correct wave function. This method is called the multi-configurational time-dependent Hartree (MCTDH) method[51,52,53] which turned out to be a powerful tool for multi-dimensional wave-packet propagation where also damping had been taken into account.[54,55]

In chapter 6 the ansatz of decomposing the multi-dimensional wave function into an outer product of single mode wave functions is used as well, however, inspired by the so-called Monte Carlo wave-function (MCWF) methods or quantum trajectories, the coupling between the various DOFs will not be treated in a deterministic way as within the other methods, but with stochastic processes. As will be discussed later, stochastic processes enable the formal breakup of coupled equations of motion (EOMs) of parts of a (quantum) system. Of course, the correlations are still present but have been transfered to the stochastic events. The MCWF methods were inspired by the observation of spontaneous quantum jumps that appear in a stochastic manner and should, in the limit of infinitely many realizations, unravel quantum master equations that describe the same process in terms of *deterministic* quantum probabilities. Here and in the following the term deterministic is used in the sense that no explicit stochastic process is involved and is kept separated from the probabilistic nature of quantum mechanics. Besides the applications in optics, the MCWF scheme has also been applied to a number of other fields as electron transfer problems[56,57,58] and has also been extended in several ways,[59,60,61] including a scheme to unravel general time-local quantum master equations[62,63] and to calculate multi-time correlation functions of open quantum systems.[64,65] Based on this algorithm the EOM of the multi-dimensional wave function will be decoupled into a number of one-dimensional but stochastic EOMs that in the limit of infinitely many realizations unravel the Schrödinger equation of the combined system. The derivation of this algorithm and the results displayed in chapter 6 have allready been published in Ref. [66].

2 Reduced density matrix theory

2.1 Introductory remarks

The state of a quantum mechanical particle is, different from a classical particle, not given in terms of single momentum and position vectors, i.e. a single point in phase space. In contrast, the state of a quantum mechanical particle is blurred and has to be described by a state vector $|\Psi\rangle$ or, in coordinate representation, a wave function

$$|\Psi(t)\rangle \equiv \Psi(\mathbf{x}, t) \tag{2.1}$$

which can be understood as a superposition of many possible and orthogonal states to find the system in upon measurement. Here the notation $|\Psi(t)\rangle$ describes a general state vector at time t without a particular representation chosen and $\Psi(\mathbf{x}, t)$ means the wave function in coordinate representation with coordinate vector $\mathbf{x}$. The time evolution of such a state vector is determined by the time-dependent Schrödinger equation

$$\frac{\partial}{\partial t}|\psi(t)\rangle = -\frac{i}{\hbar}H(t)|\psi(t)\rangle, \tag{2.2}$$

where $\hbar = h/2\pi$ with h being the Planck constant. In the following $\hbar$ is set to unity.

$$H(t) = \frac{\mathbf{p}^2}{2m} + V(t) \tag{2.3}$$

is a general time-dependent Hamilton operator or *Hamiltonian* of the complete system with the momentum operator $\mathbf{p}$, reduced mass m and a possibly time-dependent potential V. In general H can be time-dependent, for example if a (classical) laser field couples to the state vector. During this work $H(t) = H$ will be assumed to be time-independent. This is mainly done to simplify notation as the methods discussed below in most cases also work for time-dependent Hamiltonians. This is also the case in chapter 4 where a laser field couples to the system. However, in this case only the system's second order response on the laser radiation is to be calculated which only involves the Hamiltonian without the laser field.

The actual representation of a state vector and the operators, however, is not limited to the coordinate representation as done in Eq. (2.1) but can be chosen arbitrarily according to any complete set $\{|\phi_i\rangle\}$ of orthogonal state vectors. The state vector can be decomposed as

$$|\Psi(t)\rangle = \sum_i c_i(t)|\phi_i\rangle, \tag{2.4}$$

where the coefficients c_i contain the information on how much the orthogonal basis states $|\phi_i\rangle$ contribute to the state vector $|\Psi\rangle$. The knowledge of the c_i together with the specification of the basis therefore completely represents the state vector. Hence, for numerical treatment the set of coefficients can be stored in the computer memory to represent the state vector in a certain basis set.

Unfortunately, the number of basis states is in general not finite so that in practice not all coefficients can be stored. It is, however, possible to skip all those basis states whose coefficients will remain zero during the calculations so that a finite number of relevant coefficients can be stored. But even though the number of coefficients may be finite, it can, depending on the system under consideration, still be very large. This is especially true for multi-dimensional problems with many DOFs. Even though each single mode might be described accurately by a small number of basis vectors, entanglements of the single mode state vectors cannot be represented by separate sets of coefficients. Instead a combined set of coefficients has to be used. If, for example, an M-dimensional system can be sufficiently represented by N basis states per dimension, in general the total number of coefficients to be stored is N^M. Hence, the direct numerical treatment of quantum mechanical systems is strongly limited by computer memory and CPU time and one is limited to low-dimensional problems with a few DOFs as already mentioned in section 1.3.

The treatment of larger systems therefore requires an alternative way of numerical calculation and much effort has been spent to find methods which demand less computational capacities. One possibility is the so-called reduced density matrix theory which will also be used within this work and discussed later in more detail. The general idea is that in most cases where a large system has to be treated only a small part of it is really of interest. This could be for example a molecule in a solvent or impurities in a crystal structure. It seems reasonable to separate the complete system into a relevant part describing the structure of interest and a bath part containing all remaining DOFs of the complete system. Often, instead of 'relevant system', also the short-hand notation 'system' is used for the relevant part. Fig. 2.1 visualizes the separation into system and bath. Note that the combined system plus bath is assumed
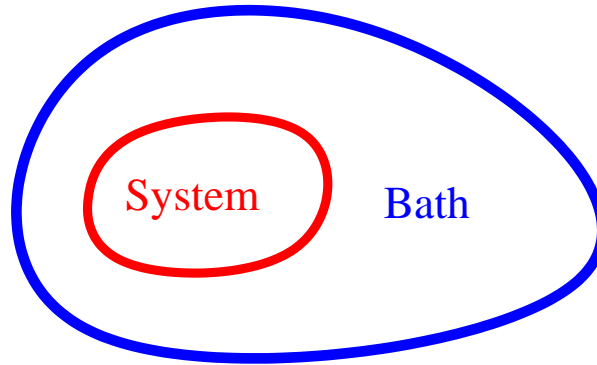
Figure 2.1: Schematic separation of the complete system into a relevant part and a bath part.

to be closed, i.e., there is no interaction with an outside world. This especially means that the time evolution of a state describing this system is unitary which is not the case for the relevant system. Interactions with the surrounding bath may lead to a non-unitary evolution of the relevant system. This separation, though, allows for the detailed treatment of the relevant part while taking into account the remaining part only in an indirect way without storing all detailed information of its state. Especially the time evolution of the relevant part under the influence of the bath is of interest. The influence of the bath can lead to a variety of effects for the relevant system. Energy may dissipate into the bath or from the bath to the system, the system state can lose coherence or the environment may cause energetic shifts etc. Observing the

time evolution of such systems therefore can lead to a detailed understanding of the processes that occur within the relevant part under 'natural' circumstances.

A huge variety of different formalisms have been developed to treat such separated system-bath problems, most of these methods are of approximative character such as perturbative approaches based on the projection operator formalism. Well known in this field are the Nakajima-Zwanzig identity[67,68,69] and the Hashitsume-Shibata-Takahashi identity[70,71] which both lead to effective EOMs of the relevant part alone by using a projection of the bath dynamics onto the system.[72] Most of the perturbative treatments are to second and fourth order[73,74] in the system-bath-coupling. But also numerical exact treatments are known as for example based on the Nakajima-Zwanzig identity,[72] the path integral technique,[75,76] self-consistent hybrid schemes[54,55] or Monte-Carlo approaches.[33,77,78,79,80,81] Also a hierarchical schemes that are in principle exact have been developed by Tanimura and others.[29,30,31,32,33,34,35,36,37] A similar scheme will also be used in the present work.

If not indicated differently, the numerical calculations within this work have been performed with standard numerical libraries. Differential equations such as the EOMs of the system state have been solved with the Runge-Kutta algorithm. Numerical integrations of usual functions have been performed with appropriate procedures provided by the NAG Fortran library and matrix operations such as the solution of eigenvalue problems have been treated with the LAPACK/BLAS package.

2.2 Statistical operator

In systems containing more than one particle, for instance a cloud of molecules, it is usually not possible to describe the state of the system with a single state vector but with a mixture of different (not necessarily orthogonal) state vectors. For this purpose one introduces the so-called density operator

$$W(t) = \sum_n w_n \left| \psi_n(t) \right\rangle \left\langle \psi_n(t) \right|, \tag{2.5}$$

which is a sum of outer products of states $\left| \psi_n(t) \right\rangle$ in which the particles might appear with probability w_n, i.e.,

$$\sum_n w_n = 1. \tag{2.6}$$

The statistical operator is Hermitian and normalized such that

$$W(t) = W^\dagger(t) \tag{2.7}$$

and

$$\mathrm{tr}\left\{ W(t) \right\} = 1. \tag{2.8}$$

Its EOM can be obtained from the Schrödinger equation (2.2) by using the product rule for differentiation as

$$\frac{\partial}{\partial t} W(t) = -i\mathcal{L} W(t). \tag{2.9}$$

Here

$$\mathcal{L} = [H, \bullet] \tag{2.10}$$

is the so-called Liouville superoperator. The EOM (2.9) can be formally solved as

$$W(t) = \mathcal{U}(t, t_0) W(t_0), \tag{2.11}$$

where the statistical operator is assumed to be known at the initial time t_0 and

$$\mathcal{U}(t, t_0) = \exp\left(-i\mathcal{L}(t - t_0)\right) \tag{2.12}$$

is the time evolution superoperator.

The Liouville equation (2.9) can be seen as a more general form of the Schrödinger equation (2.2). It describes the coherent motion of the complete statistical operator. It is interesting to note that if no influence from the outside world disturbs the motion of $W(t)$, no dissipation can occur since the system is closed and energy is conserved.

2.3 Reduced statistical operator

As mentioned above one is, in many cases, only interested in the dynamics of a small part of the complete system, for example the dynamics of a molecule in a solvent or the properties of a small structure like a quantum dot surrounded by a substrate. Due to the interaction of both, the small part and its surrounding, one would have to calculate the dynamics of the combined system and then extract the properties of subsystem of interest. The inclusion of the environment usually leads to very large systems with many DOFs so that the complete density operator cannot be stored in the computer. As mentioned above, in this case one often separates the total system into the relevant part and treats all remaining DOFs as a bath which is usually assumed to be in thermal equilibrium. To describe the relevant system a reduced density operator

$$\rho(t) = \text{tr}_B \{W(t)\} \tag{2.13}$$

is introduced. The trace with subscript "B" indicates that only the bath DOFs are affected by the trace operation and hence the result is an operator exclusively defined in the system DOFs.

According to the distinction of system and bath also the complete Hamiltonian is split as

$$H = H_S + H_{SB} + H_B + H_{ren} \tag{2.14}$$

where H_S and H_B are Hamiltonians defined exclusively in the DOFs of system and bath, respectively, and are responsible for the free motion of those two subsystems if they were uncoupled. H_{SB} covers the interaction of system and bath. In addition one often adds a renormalization term H_{ren} to counter artificial shifts in the system energies caused by the introduction of H_{SB}. Since the renormalization Hamiltonian is defined in the system DOFs one often defines the effective system Hamiltonian

$$H_S^{\text{eff}} = H_S + H_{ren}. \tag{2.15}$$

The EOM of the reduced density operator can (in most cases) be expressed as

$$
\begin{aligned}
\frac{\partial}{\partial t}\rho(t) &= \frac{\partial}{\partial t}\text{tr}_B \{W(t)\} \\
&= -i\,\text{tr}_B \{\mathcal{L}W(t)\} \\
&= -i\,\mathcal{L}_S^{\text{eff}}\rho(t) - i\,\text{tr}_B \{\mathcal{L}_{SB}W(t)\}.
\end{aligned}
\tag{2.16}
$$

Here the abbreviations

$$
\begin{aligned}
\mathcal{L}_S^{\text{eff}} &= \left[H_S^{\text{eff}}, \bullet\right], \\
\mathcal{L}_{SB} &= \left[H_{SB}, \bullet\right]
\end{aligned}
\tag{2.17}
$$

have been used. The operator $\mathcal{L}_\mathrm{B} = [H_\mathrm{B}, \bullet]$ does not appear in Eq. (2.16) since the complete trace over a commutator is always zero.

The main difficulty in Eq. (2.16) is that the term $\mathrm{tr}_\mathrm{B}\{\mathcal{L}_\mathrm{SB}W(t)\}$ is in most cases unknown. For real systems, especially those with a large number of bath-DOFs, it is hardly possible to calculate the complete statistical operator or find an exact expression for the bath Hamiltonian or the system-bath interaction. At this point it is interesting to note that in contrast to Eq. (2.9) the relevant system is not closed anymore and exchange of energy between the two subsystems can occur.

2.4 Projection operator technique

To derive an equation of motion exclusively for a part of some general system the projection operator $\mathcal{P}$ is introduced which projects the combined system onto the part of interest. Usually as also in this work $\mathcal{P}$ is chosen time-independent and the subsystem is identical with the relevant system discussed above, but also other definitions of $\mathcal{P}$ are possible, as, for instance, used to derive the MRT, where $\mathcal{P}$ projects onto the populations of the eigenstates of H_S only (cf. section 2.8 and Appendix B). Often the standard projector

$$\mathcal{P}\bullet = R_\mathrm{ref}\,\mathrm{tr}_\mathrm{B}\{\bullet\}, \tag{2.18}$$

is used, where R_ref is a reference operator defined only in the bath DOFs which has to fulfill the constraint

$$\mathrm{tr}_\mathrm{B}\{R_\mathrm{ref}\} = 1 \tag{2.19}$$

such that the projector property $\mathcal{P}^2 = \mathcal{P}$ is satisfied. Due to Eq. (2.19) R_ref can be interpreted as a statistical operator in the bath DOFs and it is obvious that for later approximate use R_ref should be chosen close to the real state of the bath which is in most cases the thermal equilibrium state, i.e.,

$$R_\mathrm{ref} = \frac{\exp\left(-\beta H_\mathrm{B}\right)}{\mathrm{tr}_\mathrm{B}\{\exp\left(-\beta H_\mathrm{B}\right)\}} = R_\mathrm{eq}. \tag{2.20}$$

This identification is a good approximation especially in the weak coupling limit between the system and bath DOFs and helpful for later perturbative treatments.

Without any restrictions to the particular form of $\mathcal{P}$ one often introduces the orthogonal complement $\mathcal{Q}$ of $\mathcal{P}$ as

$$\mathcal{Q} = 1 - \mathcal{P}. \tag{2.21}$$

Using the projector properties of $\mathcal{P}$ one can verify that $\mathcal{P}\mathcal{Q} = \mathcal{Q}\mathcal{P} = 0$ and that $\mathcal{Q}^2 = \mathcal{Q}$, i.e., $\mathcal{Q}$ is a projector as well.

With help of the projectors $\mathcal{P}$ and $\mathcal{Q}$, especially using the identity operation $\mathcal{P} + \mathcal{Q} = 1$ the EOM of the total statistical operator $W(t)$ can be split into two parts:

$$\frac{\partial}{\partial t}W(t) = \frac{\partial}{\partial t}\mathcal{P}W(t) + \frac{\partial}{\partial t}\mathcal{Q}W(t) \tag{2.22}$$

which allows to consider the two terms on the right hand side separately. With help of the projection operators it is possible to derive two formal EOMs of the projected part, the Nakajima-Zwanzig identity[67,68,69]

$$\frac{\partial}{\partial t}\mathcal{P}W(t) = -i\mathcal{P}\mathcal{L}\mathcal{P}W(t) - \int\limits_{t_0}^{t} d\tau\,\mathcal{P}\mathcal{L}\mathcal{U}_\mathcal{Q}(t,\tau)\mathcal{Q}\mathcal{L}\mathcal{P}W(\tau) - i\mathcal{P}\mathcal{L}\mathcal{U}_\mathcal{Q}(t,t_0)\mathcal{Q}W(t_0). \tag{2.23}$$

and the Hashitsume-Takahashi-Shibata identity[70,71]

$$\frac{\partial}{\partial t}\mathcal{P}W(t) = -i\mathcal{P}\mathcal{L}\left[1 + i\int_{t_0}^{t}d\tau\,\mathcal{U}_{\mathcal{Q}}(t,\tau)\mathcal{Q}\mathcal{L}\mathcal{P}\mathcal{U}(\tau,t)\right]^{-1}\left(\mathcal{P}W(t) + \mathcal{U}_{\mathcal{Q}}(t,t_0)\mathcal{Q}W(t_0)\right) \quad (2.24)$$

with the projected time evolution operator

$$\mathcal{U}_{\mathcal{Q}}(t,\tau) = \exp\left(-i\mathcal{Q}\mathcal{L}(t-\tau)\right). \quad (2.25)$$

The terms containing $\mathcal{Q}W(t_0)$ are the so-called initial correlations since they contain the entanglements of system and bath at time t_0.

The main difference between the Hashitsume-Takahashi-Shibata identity (2.24) and the Nakajima-Zwanzig identity (2.23) is that the EOM of the relevant part does not depend on past times in Eq. (2.24), i.e., the EOM is local in time while Eq. (2.23) contains an integral over past times of the system state. This distinction results in a different operator governing the coherent motion and dissipation from the relevant system to the bath as well as a different treatment of the initial correlations. In general, however, neither the Hashitsume-Takahashi-Shibata identity (2.24) nor the Nakajima-Zwanzig identity (2.23) can be used for numerical calculations such that perturbative techniques have to be applied and model assumptions have to be embraced. This is especially true for macroscopic baths where a detailed description of all DOFs is hardly possible as well as for the coupling between system and bath.

2.5 General assumptions

2.5.1 Harmonic bath approximation

Usually in density matrix theory the bath modes (in most cases vibrational DOFs) are approximated by an infinite number of uncoupled (though the real bath modes might be coupled) harmonic oscillators with momentum p_ξ, mass m_ξ, frequency ω_ξ and coordinate x_ξ such that the bath Hamiltonian reads

$$H_{\mathrm{B}} = \frac{1}{2}\sum_{\xi}\left(\frac{p_\xi^2}{m_\xi} + m_\xi\omega_\xi^2 x_\xi^2\right). \quad (2.26)$$

This approximation holds especially for solid environments, low temperatures and small coupling between system and bath. In this case the fluctuations around the equilibrium position are small such that the restoring force is approximately linear in the deviation from the equilibrium position. In addition the influence of the system onto the bath is small for weak couplings such that the fluctuations do not enter the non-linear regime where the harmonic approximation does not hold. A realistic vibrational bath usually is dominated by a limited number of modes whose spectrum is broadened due to couplings within the bath. Within the harmonic bath approximation this broadening is emulated by an infinite number of bath oscillators with different frequencies and different weight such that the spectral properties of the bath are imitated. In contrast to the real bath modes, these modes are not coupled to each other such that there is no redistribution of energy within the bath.

2.5.2 Linear system-bath coupling

As mentioned above, the interaction Hamiltonian H_{SB} is defined in both, the system and the bath DOFs. At this point no particular form of the interaction has been assumed. It is, however, always possible to express a general operator as a sum of products of one system and one bath operator, respectively. Hence, the system-bath interaction can be written as

$$H_{\mathrm{SB}} = \sum_k K_k \Phi_k \tag{2.27}$$

where K_k is a system operator and ϕ_k a bath operator.

In addition to the model of a harmonic bath one often assumes linear coupling of the system to the bath modes. This can be interpreted as a Taylor expansion of the real bath operators in Eq. (2.27) up to first order in the bath coordinate such that the interaction term reads

$$H_{\mathrm{SB}} = \sum_k K_k \sum_\xi c_{k\xi} x_\xi. \tag{2.28}$$

Here $c_{k\xi}$ determines the coupling strength to the ξth bath mode through the kth system operator.

2.5.3 The renormalization

Due to the introduction of the system-bath interaction (2.28) the potential energy surfaces of the bath modes are shifted along the respective coordinate axes while the minima in the absence of H_{SB} is located at $x_{\xi,\mathrm{min}} = 0$. The minimum positions in the presence of H_{SB} can be obtained by calculating the functional derivative of the Hamiltonian $\bar{H} = H - H_{\mathrm{ren}}$ without renormalization and setting

$$\frac{\delta}{\delta x_\xi} \bar{H} = 0 \tag{2.29}$$

which yields

$$x'_{\xi,\mathrm{min}} = -\sum_k \frac{K_k c_{k\xi}}{m_\xi \omega_\xi^2}. \tag{2.30}$$

Upon inserting the minimum positions $x'_{\xi,\mathrm{min}}$ and $x_{\xi,\mathrm{min}}$ into the Hamiltonian $\bar{H}$ and comparing both results one notices that

$$\bar{H}\left(\mathbf{x}'_{\mathrm{min}}\right) - \bar{H}\left(\mathbf{x}_{\mathrm{min}}\right) = -\sum_{k,l} \sum_\xi \frac{K_k K_l c_{k\xi} c_{l\xi}}{2m_\xi \omega_\xi^2}. \tag{2.31}$$

Here the bold face notation indicates that $\mathbf{x}_{\mathrm{min}}$ and $\mathbf{x}'_{\mathrm{min}}$ are vectors with components $x_{\xi,\mathrm{min}}$ and $x'_{\xi,\mathrm{min}}$, respectively. Hence, to compensate for the shift (2.30), one has to add the term

$$\begin{aligned} H_{\mathrm{ren}} &= \sum_{kl} K_k K_l \sum_\xi \frac{c_{k\xi} c_{l\xi}}{2m_\xi \omega_\xi^2} \\ &= \sum_{kl} K_k K_l \lambda_{kl} \end{aligned} \tag{2.32}$$

to $\bar{H}$. Here λ_{kl} is the so-called reorganization energy which can be obtained from the bath correlation functions[76] as discussed in section 2.6.3. With the reorganization energy one can describe reorganization processes such as shifts in the bath coordinates that can occur when a transition to an excited state of the system takes place.

Although H_{ren} is a system operator it has to be considered as part of the interaction since it originates from the introduction of H_{SB} by definition.

The final Hamiltonian reads

$$H = H_{\text{S}} + \sum_k K_k \sum_\xi c_{k\xi} x_\xi + \frac{1}{2} \sum_\xi \left(\frac{p_\xi^2}{m_\xi} + m_\xi \omega_\xi^2 x_\xi^2 \right) + \sum_{k,l} K_k K_l \sum_\xi \frac{c_{k,\xi} c_{l,\xi}}{2 m_\xi \omega_\xi^2}, \qquad (2.33)$$

where the system Hamiltonian H_{S}, the system parts of the interaction K_k and the coupling constants $c_{k\xi}$ still have to be adapted to a particular model under consideration.

2.6 Perturbation theory

Even with the model assumptions made in section 2.5 it is in most cases not possible to solve the EOM (2.16) for the reduced density operator exactly. One possibility to find approximative expressions for $\dot{\rho}$ is the application of perturbative techniques. One possibility is to expand the Nakajima-Zwanzig or the Hashitsume-Takahashi-Shibata identity with respect to the interaction H_{SB}. But also other techniques can be used, as done in section 2.7 where higher order perturbative EOMs for the relevant system are given. In the following the standard projector (2.18) with the bath state (2.20) is used and it is assumed that in the initial moment t_0 the state of the combined system plus bath factorizes as

$$W(t_0) = \rho(t_0) R_{\text{eq}}, \qquad (2.34)$$

such that the initial correlations vanish, i.e., $\mathcal{Q}W(t_0) = 0$.

2.6.1 Second-order time-local EOMs

The time-local (TL) EOMs for the reduced density matrix are derived from the Hashitsume-Takahashi-Shibata identity (2.24) which, without initial correlations, simplifies to

$$\frac{\partial}{\partial t} \mathcal{P}W(t) = -i\mathcal{P}\mathcal{L} \left[1 + i \int_{t_0}^t d\tau \, \mathcal{U}_{\mathcal{Q}}(t,\tau) \mathcal{Q}\mathcal{L}\mathcal{P}\mathcal{U}(\tau,t)(t) \right]^{-1} \mathcal{P}W(t). \qquad (2.35)$$

The inverse term in brackets can be Taylor expanded as

$$\left[1 + i \int_{t_0}^t d\tau \, \mathcal{U}_{\mathcal{Q}}(t,\tau) \mathcal{Q}\mathcal{L}\mathcal{P}\mathcal{U}(\tau,t) \right]^{-1} \approx 1 - i \int_{t_0}^t d\tau \, \mathcal{U}_{\mathcal{Q}}(t,\tau) \mathcal{Q}\mathcal{L}\mathcal{P}\mathcal{U}(\tau,t). \qquad (2.36)$$

Inserting this into Eq. (2.35) one notices that the Liouville operator containing the system-bath interaction already appears explicitly in second order so that one may neglect it in the time evolution operators. Using the properties

$$\begin{aligned}
\mathcal{Q}\mathcal{L}\mathcal{P} &= \mathcal{L}_{\text{SB}}\mathcal{P} \\
\mathcal{P}\mathcal{L}\mathcal{Q} &= \mathcal{P}\mathcal{L}_{\text{SB}} \\
\mathcal{P}\mathcal{L}\mathcal{P} &= \mathcal{L}_{\text{S}}^{\text{eff}}\mathcal{P}
\end{aligned} \qquad (2.37)$$

one gets

$$\frac{\partial}{\partial t}\mathcal{P}W(t) = -i\mathcal{L}_{\mathrm{S}}^{\mathrm{eff}}\mathcal{P}W(t) - \int_{t_0}^{t} d\tau\, \mathcal{P}\mathcal{L}_{\mathrm{SB}}\mathcal{U}_0(t,\tau)\mathcal{L}_{\mathrm{SB}}\mathcal{U}_0(\tau,t)\mathcal{P}W(t). \qquad (2.38)$$

For the projector identities listed above it was made use of the fact that in thermal equilibrium the expectation value of the coordinate operator in which the system-bath interaction is assumed to be linear, is zero. Otherwise one would get additional terms in K_k multiplied with a constant, namely the expectation value of the bath operator. The change from $\mathcal{U}_{\mathcal{Q}}$ to $\mathcal{U}_0$ with

$$\mathcal{U}_0(t,\tau) = \exp\left(-i\left(\mathcal{L}_{\mathrm{S}} + \mathcal{L}_{\mathrm{B}}\right)(t - \tau)\right) = \exp\left(-i\mathcal{L}_0\left(t - \tau\right)\right) \qquad (2.39)$$

can be derived by using a Taylor expansion of $\mathcal{U}_{\mathcal{Q}}$ and applying the projector properties listed above. After tracing out the bath DOFs and inserting the explicit expressions (2.18) and (2.20) for $\mathcal{P}$ the EOM of the reduced density matrix reads

$$\frac{\partial}{\partial t}\rho(t) = -i\mathcal{L}_{\mathrm{S}}^{\mathrm{eff}}\rho(t) - \int_{t_0}^{t} d\tau\, \mathrm{tr}_{\mathrm{B}}\left\{\mathcal{L}_{\mathrm{SB}}\mathcal{U}_0(t,\tau)\mathcal{L}_{\mathrm{SB}}\mathcal{U}_0(\tau,t)\,R_{\mathrm{eq}}\right\}\rho(t). \qquad (2.40)$$

As mentioned previously, H_{ren} is of second order in the system-bath interaction. Therefore it does not appear in the integral part.

Eq. (2.40), however, still contains explicit bath operators. After expanding the commutators $\mathcal{L}_{\mathrm{SB}}$ and inserting the factorization (2.27), Eq. (2.40) can be re-written as

$$\frac{\partial}{\partial t}\rho(t) = -i\mathcal{L}_{\mathrm{S}}^{\mathrm{eff}}\rho(t) - \sum_k \left[K_k, \Lambda_k(t)\rho(t) - \rho(t)\Lambda_k^\dagger(t)\right], \qquad (2.41)$$

with the time dependent operators

$$\Lambda_k(t) = \sum_l \int_{t_0}^{t} d\tau\, C_{kl}(t - \tau)K_l(\tau - t) \qquad (2.42)$$

and the so-called free bath correlation functions

$$C_{kl}(t) = \mathrm{tr}_{\mathrm{B}}\left\{\Phi_k(t)\Phi_l R_{\mathrm{eq}}\right\}. \qquad (2.43)$$

Here $\Phi_k(t)$ and $K_k(t)$ evolve according to the interaction representation with respect to H_{SB}.

The actual form of the bath correlation functions strongly depends on the system under consideration. It determines the strength of the coupling between system and bath and furthermore determines the time scales on which relaxation in the bath occurs, i.e., to what extent past perturbations of the bath influence the present dynamics of the system. Indirectly, $C_{kl}(t)$ can be determined by experiments or, e.g., by MD simulations and can therefore serve as input for further calculations. A more detailed discussion is given in section 2.6.3.

Markov Approximation

Typically the correlation functions decay exponentially with growing time. For fast decaying functions the integral over the correlation functions, e.g. in Eq. (2.42),

can be extended to infinity without too much loss of information about the system dynamics, i.e.,

$$\Lambda_k(t) \rightarrow \Lambda_k = \sum_l \int_0^\infty d\tau \, C_{kl}(\tau) K_l(-\tau).$$ (2.44)

Here also a change of the integration variable has been applied. The physical interpretation of this procedure is that one assumes that past perturbations of the bath do not affect the present system dynamics such that the dissipative part of Eq. (2.41) is time-independent.

Redfield Theory

The dissipative terms in Eq. (2.41) still contain imaginary parts which cause a frequency shift also called Lamb shift[82, 83] in the system dynamics. It is often argued, that this shift usually compensates the frequency shift caused by the renormalization to some degree, such that neglecting both only leads to minor effects.

Having chosen a basis set, the (real) dissipative parts of Eq. (2.41) can be summarized in a fourth order tensor $R_{\mu\nu\mu'\nu'}$, the so-called Redfield Tensor. In energy representation the EOM for the matrix elements of the reduced density matrix reads

$$\frac{\partial}{\partial t}\rho_{\mu\nu}(t) = -i\omega_{\mu\nu}\rho_{\mu\nu}(t) + \sum_{\mu'\nu'} R_{\mu\nu\mu'\nu'}\rho_{\mu'\nu'}(t)$$ (2.45)

with

$$R_{\mu\nu\mu'\nu'} = -\mathrm{Re}\left[\delta_{\mu\mu'}\sum_{\upsilon}\Gamma_{\nu\upsilon\upsilon\nu'} + \delta_{\nu\nu'}\sum_{\upsilon}\Gamma_{\mu\upsilon\upsilon\mu'} - \Gamma_{\mu'\mu\nu\nu'} - \Gamma_{\nu'\nu\mu\mu'}\right]$$ (2.46)

and

$$\Gamma_{\mu\nu\mu'\nu'} = \sum_k \langle\mu|\,K_k\,|\nu\rangle\,\langle\mu'|\,\Lambda_k\,|\nu'\rangle.$$ (2.47)

Especially in energy representation one can assign functions to the elements of the Redfield tensor. The elements $R_{\mu\mu\nu\nu}$, e.g., are responsible for population transfer and the elements $R_{\mu\nu\mu\nu}$ are responsible for coherence dephasing. All other terms cause transfer between coherences and between populations and coherences.[2]

Secular Approximation

In the interaction picture with respect to H_S the Redfield tensor becomes time dependent as

$$R_{\mu\nu\mu'\nu'}(t) = R_{\mu\nu\mu'\nu'}e^{-i\left(\omega_{\mu\nu}-\omega_{\mu'\nu'}\right)(t-t_0)}.$$ (2.48)

Upon integration of the EOM of the reduced density matrix terms containing oscillating elements of the Redfield tensor will almost vanish and only those terms couple that oscillate at the same frequency.[84] Hence one may only take into account all those contributions where

$$\omega_{\mu\nu} - \omega_{\mu'\nu'} = 0.$$ (2.49)

These are especially contributions containing

$$\omega_{\mu\mu} - \omega_{\nu\nu} = 0,$$ (2.50)

i.e., the terms responsible for population transfer and those contributions containing

$$\omega_{\mu\nu} - \omega_{\nu\mu} = 0, \tag{2.51}$$

which are responsible for coherence dephasing. Care has to be taken whether other combinations also fulfill condition (2.49). Using only those contributions mentioned above the population transfer can be decoupled from the dephasing which significantly reduces the numerical effort needed for solving the EOM of the system density matrix. This procedure is called the secular approximation.[2] The EOM for the matrix elements (in energy representation and Schrödinger picture) is split into two parts:

$$\frac{\partial}{\partial t}\rho_{\mu\mu}(t) = \sum_{\nu} R_{\mu\mu\nu\nu}\rho_{\nu\nu}(t) \tag{2.52}$$

for the populations and

$$\frac{\partial}{\partial t}\rho_{\mu\nu}(t) = -i\omega_{\mu\nu}\rho_{\mu\nu}(t) + (1 - \delta_{\mu\nu})\,R_{\mu\nu\mu\nu}\rho_{\mu\nu}(t) \tag{2.53}$$

for the coherences.[2] It should be mentioned that the secular approximation does in general not hold for systems with degenerate eigenstates where additional contributions will have to be taken into account.

2.6.2 Second order time non-local EOM

In addition to the TL EOMs given above it is possible to derive time non-local (TNL) EOMs based on the Nakajima-Zwanzig identity (2.23). As in the previous subsection the initial correlations are set to zero and the projector identities (2.37) are used to derive a second-order perturbative EOM of the reduced density matrix as

$$\frac{\partial}{\partial t}\rho(t) = -i\mathcal{L}_{\mathrm{S}}^{\mathrm{eff}}\rho(t) - \sum_{kl}\int_{t_0}^{t}d\tau\left[K_k, e^{-i\mathcal{L}_{\mathrm{S}}(t-\tau)}\left(K_l\,\rho(\tau)C_{kl}(t-\tau) - \rho(\tau)\,K_l\,C_{kl}^{*}(\tau - t)\right)\right]. \tag{2.54}$$

It is interesting to note that upon applying the approximation $\rho(t) \approx \mathcal{U}_{\mathrm{S}}(t - \tau)\rho(\tau)$ the TNL EOM (2.54) can be transformed into the TL EOM (2.41).

2.6.3 Correlation functions and spectral densities

As mentioned above the general form of the correlation functions introduced in Eq. (2.43) is strongly related to the model under consideration and can be, in principle, indirectly measured by obtaining the second-order response function of the bath.[2] In this section the matrix of correlation functions (2.43) is evaluated under the assumption of a harmonic bath with linear coupling to the system. Starting with Eq. (2.43) and using $\Phi_k = \sum_{\xi} c_{k\xi}x_{\xi}$ the correlation function reads

$$C_{kl}(t) = \sum_{\xi\xi'}c_{k\xi}c_{l\xi'}\mathrm{tr}_{\mathrm{B}}\left\{x_{\xi}(t)x_{\xi'}R_{\mathrm{eq}}\right\}. \tag{2.55}$$

This expression can be evaluated in coordinate representation using Eqs. (C.7) and (C.28) leading to

$$C_{kl}(t) = \sum_{\xi}\frac{c_{k\xi}c_{l\xi}}{2m_{\xi}\omega_{\xi}}\left[\coth\left(\frac{\beta\omega_{\xi}}{2}\right)\cos\left(\omega_{\xi}t\right) - i\sin\left(\omega_{\xi}t\right)\right]. \tag{2.56}$$

Here the trace over the bath cancels the sum over ξ' since only quadratic terms in the bath coordinate are nonzero such that terms with $\xi \neq \xi'$ vanish.

The correlation function $C_{kl}(t)$ connects the two operators K_k and K_l via the bath, i.e., the perturbation of the bath caused by the coupling with K_k affects the system again via the operator K_l. If $k \neq l$ this kind of interaction is usually small compared to the case $k = l$. Hence, one often neglects the offdiagonal parts of the matrix of correlation functions using the approximation[2]

$$C_{kl}(t) = \delta_{kl}\, C_k(t). \tag{2.57}$$

In addition, one often assumes all correlation functions to be identical, i.e., it is assumed that those parts of the bath connected to the system via the operators K_k are identical and separated from each other and that they are coupled in the same way to the system. In this case the matrix of correlation functions can be given as

$$C_{kl}(t) = \delta_{kl}\, C(t), \tag{2.58}$$

such that a single correlation function comprises the influence of the complete bath. Eqs. (2.57) and (2.58) are also called the local bath approximation[2] where in Eq. (2.58) also identical baths are assumed. The term *local* here accounts for the fact that for systems where the local bath approximation holds, different ϕ_k have to be defined in different parts of the bath. As an example consider spatially separated molecules surrounded by solvent particles. Each molecule is coupled to the solvent by an operator K_k where k labels a particular molecule. The solvent surrounding can be assumed to be of the same kind for each molecule and an indirect interaction via the bath can be neglected due to the spatial separation of the sites. So every molecule sees an equal surrounding.

In the following only the single correlation function $C(t)$ will be considered such that the Latin indices of the coupling constants $c_{k\xi}$ in the correlation matrix (2.55) can be skipped such that

$$C(t) = \sum_{\xi} \frac{c_\xi^2}{2m_\xi\omega_\xi} \left[\coth\left(\frac{\beta\omega_\xi}{2}\right) \cos\left(\omega_\xi t\right) - i \sin\left(\omega_\xi t\right) \right]. \tag{2.59}$$

In the Fourier domain the correlation function can be written as

$$C(\omega) = \int_{-\infty}^{\infty} dt\, e^{i\omega t} C(t) = [n(\omega) + 1]\, [J(\omega) - J(-\omega)] \tag{2.60}$$

where $n(\omega) = [\exp(\beta\omega) - 1]^{-1}$ is the Bose-Einstein distribution function and $J(\omega)$ is the so-called spectral density function with

$$J(\omega) = \frac{\pi}{2} \sum_{\xi} \frac{c_\xi^2}{m_\xi\omega_\xi} \delta(\omega - \omega_\xi). \tag{2.61}$$

$J(\omega)$ can be interpreted as a weighted density of states that contains detailed information about the bath modes and their coupling to the reduced system. The correlation function is therefore completely determined by the spectral density and the temperature of the bath such that $J(\omega)$ can serve as the input quantity that characterizes the bath modes and their coupling to the system.

In the continuum limit of infinitely many bath modes, the spectral density can be written as a continuous function. In many cases, however, $J(\omega)$ is given as a data set from measurements or numerical simulations such that a concrete analytical expression for it is not available. Also, even if an analytical expression is known e.g. by model assumptions, analytical treatment can be difficult for a general form of $J(\omega)$. To enable analytical treatment, Meier and Tannor[85] introduced a numerical decomposition of the spectral density into a sum of Lorentzians according to

$$J(\omega) = \sum_{j=1}^{n} p_j \frac{\omega}{\left[(\omega + \Omega_j)^2 + \Gamma_j^2\right]\left[(\omega - \Omega_j)^2 + \Gamma_j^2\right]} \tag{2.62}$$

where p_j, Ω_j and Γ_j are real parameters that can be obtained numerically with standard optimization procedures and can, without restrictions, be adapted to any continuous form of $J(\omega)$. In Eq. (2.62) the spectral density has been extended to negative frequencies via $J(-\omega) = -J(\omega)$ which allows for a more convenient notation and automatically guarantees $J(\omega) \propto \omega$ around $\omega = 0$ which cancels the singularity of $n(\omega)$ at this point. As a consequence the correlation function in time domain is given by

$$C(t) = \int_{-\infty}^{\infty} \frac{d\omega}{\pi} J(\omega) \frac{e^{i\omega t}}{e^{\beta\omega} - 1}. \tag{2.63}$$

The advantage of finding analytical expressions for $J(\omega)$ in terms of Lorentzians is that the integral Eq. (2.63) can be calculated using the theorem of residues. The correlation function then assumes an analytical expression as

$$C(t) = \sum_{j=1}^{n} \frac{p_j}{4\Omega_j\Gamma_j} \left\{ e^{i\Omega_j^+ t} n(\Omega_j^+) + e^{-i\Omega_j^- t}\left[n(\Omega_j^-) + 1\right] \right\} + \frac{2i}{\beta}\sum_{j=1}^{n'} J(i\nu_j) e^{-\nu_j t}. \tag{2.64}$$

Here $\Omega_j^+ = \Omega_j + i\Gamma_j$ and $\Omega_j^- = \Omega_j - i\Gamma_j$ have been used to simplify notation. In addition to the residues of the spectral density the residues of the Bose-Einstein term in Eq. (2.63) yield a sum over the Matsubara frequencies $\nu_j = 2\pi j/\beta$ which, in principle, is an infinite one but can be truncated for practical purposes at a temperature-dependent finite value of n'.

Since in the master equations also the complex conjugate appears one often splits the correlation function into real and imaginary parts, $C(t) = a(t) + ib(t)$ with

$$\begin{aligned} a(t) &= \sum_{j=1}^{n} \frac{p_j}{8\Omega_j\Gamma_j}\left[\coth\left(\frac{\beta\Omega_j^-}{2}\right)e^{-i\Omega_j^- t} + \coth\left(\frac{\beta\Omega_j^+}{2}\right)e^{i\Omega_j^+ t}\right] + \frac{2i}{\beta}\sum_{j=1}^{n'} J(i\nu_j)e^{-\nu_j t}, \\ b(t) &= -\sum_{j=1}^{n} \frac{ip_j}{8\Omega_j\Gamma_j}\left(e^{-i\Omega_j^- t} - e^{i\Omega_j^+ t}\right), \end{aligned} \tag{2.65}$$

which allows a separate treatment of the real and imaginary parts. The time dependence of the correlation function is now given in terms of exponential functions which allows for further analytical treatment in the quantum master equations given in the previous subsections. Following Refs. [76] and [85] one can introduce the abbreviations

$$a(t) = \sum_{j=1}^{n_{\mathrm{r}}} \alpha_j^{\mathrm{r}} e^{\gamma_j^{\mathrm{r}} t} \quad b(t) = \sum_{j=1}^{n_{\mathrm{i}}} \alpha_j^{\mathrm{i}} e^{\gamma_j^{\mathrm{i}} t} \tag{2.66}$$

with $n_\mathrm{r} = 2n + n'$ and $n_\mathrm{i} = 2n$.

With the definition of $J(\omega)$ it is in addition possible to determine the reorganization energy λ_{kl} as defined in Eq. (2.32). Assuming that the local bath approximation holds one can skip the indices as above in such manner that

$$\lambda = \int\limits_0^\infty \frac{d\omega}{\pi} \, \frac{J(\omega)}{w} \tag{2.67}$$

as it is used in the present work.

2.7 Hierarchical approach

As mentioned above higher-order perturbative master equations can be obtained from the Nakajima-Zwanzig or the Hashitsume-Takahashi-Shibata identity by expanding the time-evolution operators with respect to the interaction term. In this section a different approach previously proposed by Tanimura and others[29, 30, 31, 32, 33, 34, 36, 35, 37] is used to derive a hierarchical set of EOMs for the reduced density matrix. The original derivation has been performed using path integrals[29, 30, 31, 36, 37] but also recursive techniques[35] are known. In this section a slightly modified version of the derivation proposed by Shao, Yan and Yang[33, 34] using stochastic fields, so-called Wiener processes,[86] is presented.

2.7.1 Wiener processes and Itó calculus

Wiener processes $\nu_k(t)$, also called Brownian motion, are stochastic processes that are continuous in time in the sense that the stochastic increments $d\nu_k(t) = \nu_k(t+dt) - \nu_k(t)$ are small, i.e., of the order $\sqrt{dt}$ but with random sign so that no jumps of larger order occur. A numerical realization of such a process could be, for example, $d\nu_k = \pm\sqrt{dt}$ with random sign.[87] Wiener processes are Gaussian distributed with variance t and independent from their past and from other processes. For the expectation values these properties yield

$$\begin{aligned}
E\{\nu_k(t)\} &= 0 \\
E\{\nu_k(t)\,\nu_l(t')\} &= \delta_{kl}\,\delta(t-t') \\
E\{d\nu_k(t)\} &= 0 \\
E\{d\nu_k(t)\,d\nu_l(t)\} &= \delta_{kl}\,dt,
\end{aligned} \tag{2.68}$$

where $E\{\bullet\}$ denotes the ensemble mean operation, i.e., the calculation of the expectation value with respect to the stochastic process. Note the difference to quantum mechanical expectation values which will be denoted as $\langle\bullet\rangle$.

The differential of a general (one dimensional) stochastic process $X(\{\nu\}, t)$ that depends explicitly on time t and various Wiener processes ν_k reads

$$dX(\nu, t) = u(X, t)\,dt + \sum_k v_k(X, t)\,d\nu_k. \tag{2.69}$$

In this expression $u(X, t)$ can be interpreted as a drift coefficient which describes the deterministic part of the motion of X and $v_k(X, t)$ are diffusion coefficients that determine the impact of the stochastic increments on the motion of X.

However, since the stochastic increments are of order $\sqrt{dt}$ the stochastic differential of a function $Y = Y(\{X\}, t)$ of a set of different processes X_l has to be Taylor expanded to second order so that all contributions to order dt are taken into account such that

$$dY(\{X\}, t) = \frac{\partial}{\partial t} Y(\{X\}, t) dt + \sum_l \frac{\partial}{\partial X_l} Y(\{X\}, t) dX_l + \frac{1}{2} \sum_{lj} \frac{\partial^2}{\partial X_l \partial X_j} Y(\{X\}, t) dX_l dX_j. \quad (2.70)$$

This expression is the so-called Itó formula. Upon inserting Eq. (2.69) and setting

$$d\nu_k \, d\nu_l \;\; = \;\; \delta_{kl} \, dt, \quad (2.71)$$

one obtains the stochastic differential of $Y(X, t)$. Here all higher orders of dt, i.e., the terms containing dt^2 and $dt \, d\nu_k$, are set to zero.

2.7.2 Decoupling of system and bath

In Eq. (2.71) the squared stochastic increment yields a term in dt and hence causes additional contributions to the drift. This can be used to decouple the dynamics of the system and bath into separate but stochastic EOMs if the coupling terms are equipped with stochastic increments so that upon calculation of the differential of the product state a term in dt re-connecting the coupling terms appears.

Shao, Yan and Yang[33,34] have achieved this goal via the so-called Hubbard-Stratonovich-transformation.[77] Alternatively one can use an ansatz of separated but stochastic EOMs for system and bath, respectively, as

$$\begin{aligned}
d\,\hat{\rho}(t) \;\; &= \;\; -i \left[H_{\mathrm{S}}^{\mathrm{eff}}, \hat{\rho}(t) \right] dt - \frac{i}{2} \sum_k [K_k, \hat{\rho}(t)] \, (d\nu_{1,k} + i d\nu_{2,k}) + \frac{1}{2} \sum_k [K_k, \hat{\rho}(t)]_+ \, (d\nu_{3,k} - i d\nu_{4,k}) \\
d\,\hat{R}(t) \;\; &= \;\; -i \left[H_{\mathrm{B}}, \hat{R}(t) \right] dt - \frac{i}{2} \sum_k \left[\Phi_k, \hat{R}(t) \right] (d\nu_{3,k} + i d\nu_{4,k}) + \frac{1}{2} \sum_k \left[\Phi_k, \hat{R}(t) \right]_+ (d\nu_{1,k} - i d\nu_{2,k}).
\end{aligned} \quad (2.72)$$

Here $\hat{\rho}$ and $\hat{R}(t)$ are stochastic system and bath operators, respectively. At this point it should be emphasized that $\hat{\rho}$ is not identical with the deterministic system density matrix ρ. In Eq. (2.72) four different stochastic fields $\nu_{j,k}$ per coupling operator have been used to separate one coupling term in the EOMs though two would have been sufficient. The two additional fields cancel for additional deterministic contributions that would appear due to Eq. (2.71) upon formal integration of the EOMs (2.72). With help of the Itó formula (2.70) one obtains for the differential of the product state

$$\begin{aligned}
d \left(\hat{\rho}(t) \hat{R}(t) \right) \;\; &= \;\; \hat{R}(t) \, d\hat{\rho}(t) + \hat{\rho}(t) \, d\hat{R}(t) + d\hat{\rho}(t) d\hat{R}(t) \\
&= \;\; -i \left[H, \hat{\rho}(t) \hat{R}(t) \right] dt \\
&\quad - \frac{i}{2} \sum_k \left[K_k, \hat{\rho}(t) \hat{R}(t) \right] (d\nu_{1,k} + i d\nu_{2,k}) + \frac{1}{2} \sum_k \left[K_k, \hat{\rho}(t) \hat{R}(t) \right]_+ (d\nu_{3,k} - i d\nu_{4,k}) \\
&\quad - \frac{i}{2} \sum_k \left[\Phi_k, \hat{\rho}(t) \hat{R}(t) \right] (d\nu_{3,k} + i d\nu_{4,k}) + \frac{1}{2} \sum_k \left[\Phi_k, \hat{\rho}(t) \hat{R}(t) \right]_+ (d\nu_{1,k} - i d\nu_{2,k}).
\end{aligned} \quad (2.73)$$

After applying the mean operation only the deterministic term remains. If the initial complete density operator $W(0)$ of the combined system can be written as $W(0) = \rho(0)R(0) = \hat{\rho}(0)\hat{R}(0)$ the mean of the differential of the product state resembles the Liouville equation for the complete density operator

$$E \left\{ d \left(\hat{\rho}(t) R(t) \right) \right\} = -i \left[H, E \left\{ \left(\rho(t) R(t) \right) \right\} \right] dt \quad (2.74)$$

and due to the same initial conditions for the stochastic and deterministic EOMs it follows

$$E\left\{\left(\hat{\rho}(t)R(t)\right)\right\} = W(t).\tag{2.75}$$

It is therefore possible to integrate the stochastic EOMs of $\hat{\rho}$ and $\hat{R}(t)$ separately and only calculate the mean of the product state.

This separation has the advantage that the trace and the mean operation commute, i.e., the exact system density matrix is given as

$$\rho(t) = \text{tr}_{\text{B}}\left\{W(t)\right\} = E\left\{\hat{\rho}(t)\,\text{tr}_{\text{B}}\left\{R(t)\right\}\right\}.\tag{2.76}$$

The term $\text{tr}_{\text{B}}\left\{R(t)\right\}$ comprises the complete influence of the bath onto the system evolution and is merely a scalar but stochastic function of time. The stochastic differential of this function can be obtained by applying the trace operation to the second line of Eq. (2.72) which yields

$$d\,\text{tr}_{\text{B}}\left\{R(t)\right\} = \sum_k \text{tr}_{\text{B}}\left\{R(t)\Phi_k\right\}(d\nu_{1,k} - id\nu_{2,k}).\tag{2.77}$$

This expression can be formally integrated to

$$\text{tr}_{\text{B}}\left\{R(t)\right\} = \exp\left(\sum_k \int_0^t g_k(\tau)\left(d\nu_{1,k}(\tau) - id\nu_{2,k}(\tau)\right)\right)\tag{2.78}$$

where $g_k(t) = \text{tr}_{\text{B}}\left\{\Phi_k R(t)\right\}/\text{tr}_{\text{B}}\left\{R(t)\right\}$ again is a scalar but stochastic function of time.

For a harmonic bath which is initially in thermal equilibrium, i.e., $R(0) = R_{\text{eq}}$, and linearly coupled to the system according to Eq. (2.28) one can solve Eq. (2.77) analytically. This is shown in detail in appendix C. Direct comparison with the solution (C.42) of the bath influence leads to

$$g_k(t) = \sum_l \int_0^t \left[a_{k,l}(t-\tau)\left(d\nu_{1,l}(\tau) - i\,d\nu_{2,l}(\tau)\right) + b_{k,l}(t-\tau)\left(d\nu_{3,l}(\tau) + i\,d\nu_{4,l}(\tau)\right)\right]\tag{2.79}$$

with $a_{ij}(t)$ and $b_{ij}(t)$ being the real and imaginary parts of the bath correlation functions as given in Eq. (2.65).

The expressions (2.78) or (C.42) are strongly related to the Feynman-Vernon form of the influence functional[33,88] known from path integral technique. Here only the contributions from the paths in the system DOFs are replaced by the fluctuating fields.

2.7.3 Hierarchical set of EOMs

The differential of the exact system density matrix can be calculated using Eqs. (2.76) and (2.78). For later convenience a new stochastic system density matrix

$$\tilde{\rho}(t) = \hat{\rho}(t)\exp\left(\sum_k \int_0^t g_k(\tau)\left(d\nu_{1,k}(\tau) - id\nu_{2,k}(\tau)\right)\right)\tag{2.80}$$

is defined such that the exact system density matrix is just given as the mean

$$\rho(t) = E\left\{\tilde{\rho}(t)\right\}.\tag{2.81}$$

This definition of a new density matrix is equivalent to performing a Girsanov transformation as done in the original proposal by Shao.[33] Since the mean operation and the differential commute one can first apply the Itó formula to Eq. (2.81) and then take the ensemble average which yields

$$d\rho(t) = -i\left[H_{\mathrm{S}}^{\mathrm{eff}}, \rho(t)\right] + \sum_k \left[K_k, E\left\{g_k(t)\,\tilde{\rho}(t)\right\}\right]dt, \tag{2.82}$$

where the expectation value $E\left\{g_k(t)\,\tilde{\rho}(t)\right\}$ on the right hand side of this expression is still unknown. However, with help of the Itó formula it is possible to derive an EOM for it. The resulting expression will be similar to Eq. (2.82) but contains both, the differential and higher-order terms in g_k. This is also true for the differentials of the higher-order terms and so forth. The differentials of g_k, however, contain the time derivative of the bath-correlation function. If the time derivative can be expressed in terms of the correlation functions itself, a hierarchy of differential equations in different orders of g_k can be derived. This goal can be reached by using the decomposition (2.65) of the bath correlation function.

In the following it is assumed that the local bath approximation (2.58) holds so that Eq. (2.79) simplifies to

$$g_k(t) = \int_0^t \left[a\left(t-\tau\right)\left(d\nu_{1,k}(\tau) - i\,d\nu_{2,k}(\tau)\right) + b(t-\tau)\left(d\nu_{3,k}(\tau) + i\,d\nu_{4,k}(\tau)\right)\right]. \tag{2.83}$$

For a general matrix of correlation functions the following expressions would have a similar but much more complex structure. Using the decomposition (2.66) of the bath correlation function into a sum of exponentials one can split $g_k(t)$ into a sum of stochastically integrated exponentials as

$$g_k(t) = \sum_{j=1}^{n_{\mathrm{r}}} g_{jk}^{\mathrm{r}}(t) + \sum_{j=1}^{n_{\mathrm{i}}} g_{jk}^{\mathrm{i}}(t) \tag{2.84}$$

with

$$
\begin{aligned}
g_{jk}^{\mathrm{r}}(t) &= \int_0^t \alpha_j^{\mathrm{r}} e^{\gamma_j^{\mathrm{r}}(t-\tau)}\left(d\nu_{1,k}(\tau) - i d\nu_{2,k}(\tau)\right), \\
g_{jk}^{\mathrm{i}}(t) &= \int_0^t \alpha_j^{\mathrm{i}} e^{\gamma_j^{\mathrm{i}}(t-\tau)}\left(d\nu_{3,k}(\tau) + i d\nu_{4,k}(\tau)\right).
\end{aligned} \tag{2.85}
$$

Using the Itó formula (2.70) one gets for the differentials

$$
\begin{aligned}
d\,g_{jk}^{\mathrm{r}}(t) &= \alpha_j^{\mathrm{r}}\left(d\nu_{1,k}(\tau) - i d\nu_{2,k}(\tau)\right) + \gamma_j^{\mathrm{r}}\,g_{jk}^{\mathrm{r}}(t), \\
d\,g_{jk}^{\mathrm{i}}(t) &= \alpha_j^{\mathrm{i}}\left(d\nu_{3,k}(\tau) + i d\nu_{4,k}(\tau)\right) + \gamma_j^{\mathrm{i}}\,g_{jk}^{\mathrm{i}}(t).
\end{aligned} \tag{2.86}
$$

With help of these definitions the differentials of the unknown part in Eq. (2.82) can be expressed in terms of powers of the components (2.84) of g_k. Hence, it is convenient to define the auxiliary density matrices

$$\rho_{\{I\}}(t) = E\left\{\left(g_{11}^{\mathrm{r}}(t)\right)^{I_1}\ldots\left(g_{n_{\mathrm{r}}1}^{\mathrm{r}}(t)\right)^{I_{n_{\mathrm{r}}}}\left(g_{11}^{\mathrm{i}}(t)\right)^{I_{n_{\mathrm{r}}+1}}\ldots\left(g_{n_{\mathrm{i}}N}^{\mathrm{i}}(t)\right)^{I_{N(n_{\mathrm{r}}+n_{\mathrm{i}})}}\,\hat{\rho}(t)\right\}, \tag{2.87}$$

with the multi-index $\{I\} = \{I_1, I_2, ..., I_{N(N_r+N_i)}\}$ indicating the integer exponents of all possible components $g_{jk}^{\mathrm{M}}(t)$ of the integrated correlation function. The differential of these auxiliary density matrices can be obtained by applying the Itó formula and calculating the mean as

$$
\begin{aligned}
\frac{d\rho_{\{I\}}(t)}{dt} &= \left(\sum_k^N \left(\sum_j^{n_r} \gamma_j^r \, I_{(k-1)(n_r+n_i)+j} + \sum_j^{n_i} \gamma_j^i \, I_{(k-1)(n_r+n_i)+n_r+j} \right) - i\mathcal{L}_S^{\mathrm{eff}} \right) \rho_{\{I\}}(t) \\
&+ \sum_k^N \mathcal{L}_k^- \sum_j^{n_r+n_i} \rho_{\{I;I_{(k-1)(n_r+n_i)+j}+1\}} \\
&+ \sum_k^N \mathcal{L}_k^- \sum_j^{n_r} \alpha_j^r \, I_{(k-1)(n_r+n_i)+j} \, \rho_{\{I;I_{(k-1)(n_r+n_i)+j}-1\}} \\
&+ \sum_k^N \mathcal{L}_k^+ \sum_j^{n_i} \alpha_j^i \, I_{(k-1)(n_r+n_i)+n_r+j} \, \rho_{\{I;I_{(k-1)(n_r+n_i)+n_r+j}-1\}}.
\end{aligned}
\tag{2.88}
$$

The EOM of each member of the hierarchy can be expressed in terms of members in the neighboring upper and lower levels. The notation $\{I; I_j \pm 1\}$ indicates a change in the index $I_j \to I_j \pm 1$. In terms of the auxiliary density matrices (2.87) the system density matrix which is the quantity of interest is given as $\rho(t) = \rho_{\{0\}}(t)$, i.e., with all indices being zero. It serves as the root of a tree-like hierarchy of auxiliary density matrices. The unknown part $E\{g_k(t)\tilde{\rho}(t)\}$ in Eq. (2.82) refers to the sum of auxiliary density matrices of type $\rho_{\{0,...,1,...0\}}$, i.e., one index being 1 and all others being 0. A graphical scheme of the hierarchy can be found in Fig. 2.2.

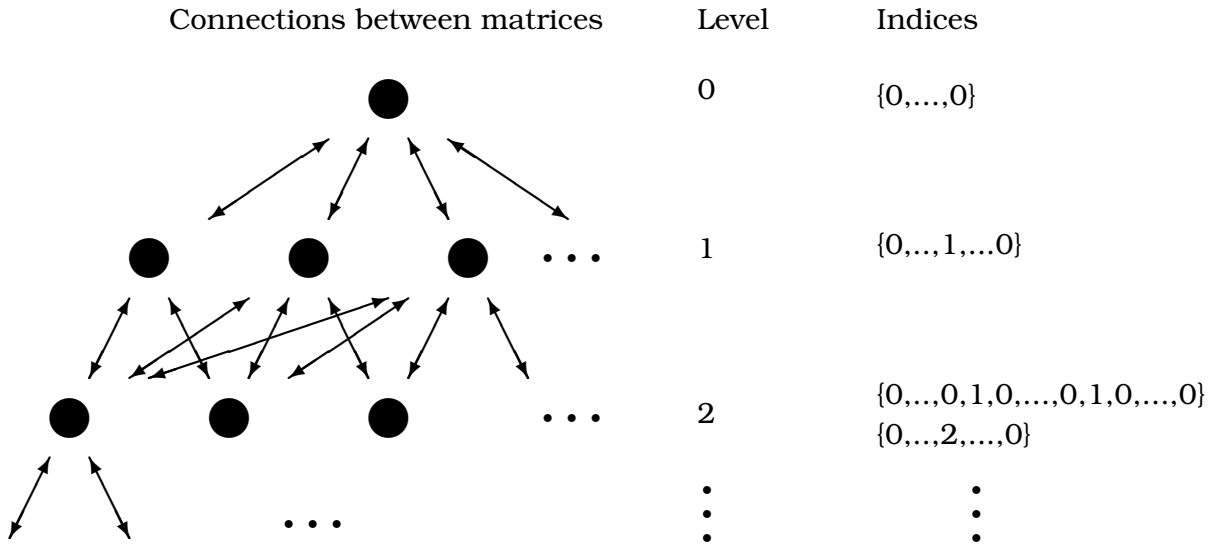Figure 2.2: Scheme of the hierarchy. The auxiliary density matrices are indicated by black circles and their interdependencies are marked by arrows. Only neighboring levels are connected by the EOM (2.88).

2.7.4 Truncation schemes

The hierarchical scheme (2.88) is in principle correct, however not closed so that for an exact treatment infinitely many auxiliary density matrices would have to be taken

into account. For practical purposes the scheme has to be truncated at some point. This truncation can be safely chosen such that[37]

$$L_{\max}\gamma_{\min} \gg \omega_{\mathrm{S}} \tag{2.89}$$

where $L_{\max}$ is the highest level in the hierarchy which is treated explicitly, $\gamma_{\min}$ is the smallest exponent of the bath correlation function (2.65) and ω_{S} is a characteristic frequency of the system, e.g. the largest transition frequency of the system Hamiltonian.

Shao *et al.* proposed dropping all levels of the hierarchy which are member of a higher level than $L_{\max}$. Since neighboring levels are connected by two interactions (upward and downward) via the coupling operators one can conclude that the system density matrix ρ is of twice the order as levels $L_{\max}$ are included in the hierarchy. The level L of an auxiliary density matrix can be obtained by summing over all indices of an auxiliary density matrix., i.e.,

$$L = \sum_l I_l. \tag{2.90}$$

It is interesting to note, that this truncation scheme is identical with a TNL propagation scheme Meier and Tannor proposed earlier[85] if only terms to second order in the system-bath coupling are taken into account. In this case, the (second-order) hierarchy can also be derived from the second order TNL EOM (2.54) by using the decomposition (2.66) of the correlation function (provided that the local bath approximation (2.58) holds). Hence, we will call the method of dropping all higher order terms the TNL truncation of the hierarchy.

A different truncation scheme has been proposed by Xu *et al.*[36] which is a modification of the original truncation proposed by Tanimura (see e.g. Ref. [37]). In the latter the Markov approximation is applied for the last level in the hierarchy which is then formally integrated. However, this scheme does not involve the system frequencies in the truncating term but only contains an integral over the bath correlation function. Xu *et al.* deduced from the structure of the hierarchy (2.88) which is basically the same in all levels except from integer coefficients that the levels of higher order than $L_{\max}$ in the hierarchy should be approximated by replacing the linking term to the last level by a time dependent operator involving also the system frequencies. Following Xu *et al.* the last order in the hierarchy (2.88) should be approximated by

$$\sum_{n}^{N_{\mathrm{r}}+N_{\mathrm{i}}} \rho_{\{I;I_{(k-1)(N_{\mathrm{r}}+N_{\mathrm{i}})+n}+1\}} \approx \Lambda_k(t)\rho_{\{I\}} + \rho_{\{I\}}\Lambda_k^\dagger(t) \tag{2.91}$$

where Λ_k is given in Eq. (2.42). This implies that any of the second order schemes can be used to approximate the next higher level. The only difference to the original scheme proposed by Tanimura *et al.* is that Λ_k is evaluated including the time evolution due to the system Hamiltonian.

2.7.5 Numerical scaling

As one may guess from the large number of indexes in Eq. (2.88) the numerical scaling strongly depends on the number of exponentials used to decompose the correlation function as well as the number of terms in the system-bath interaction. Each level in the hierarchy contains $(N(n_{\mathrm{r}}+n_{\mathrm{i}})+L-1)!/L!/(N(n_{\mathrm{r}}+n_{\mathrm{i}})-1)!$ auxiliary density matrices.

This not only leads to a fast increase of computer memory needed but also leads to a computational bottleneck upon calculating the time derivative of the single members of the hierarchy since each member is linked to various other members which have to be loaded from the RAM into the cache of the processor. All this leads to the fact that only small systems and a few orders in system-bath interaction can be treated properly on standard computers and that the condition (2.89) cannot be fulfilled in every case.

2.8 Modified Redfield theory

As discussed previously all perturbative methods are based on the splitting of the combined Hamiltonian (2.33) into one part which is responsible for the free evolution of a subsystem and a remaining part which is responsible for a perturbation of the free evolution. This separation, however, is in principle completely free and can be arbitrarily chosen. In the cases discussed above the system and the bath Hamiltonian were chosen to be responsible for the free evolution and the interaction terms were defined as the perturbation.

2.8.1 Separation of the Hamiltonian

Within the MRT[17,89] one is only interested in the population dynamics in eigenstate representation of the system Hamiltonian and hence a different separation of the complete Hamiltonian can be made. For a harmonic bath with linear coupling to the system the diagonal part of the interaction (in energy representation of the system) can be treated exactly.[17] Hence, besides the system and bath Hamiltonian one can also include the diagonal parts of the interaction in the unperturbed system and treat the remaining parts, i.e., the off-diagonal parts of the interaction, perturbatively.

The complete Hamiltonian is split as

$$
\begin{aligned}
H_0 &= H_{\mathrm{S}} + H_{\mathrm{B}} + \sum_\mu |\mu\rangle \langle\mu| H_{\mathrm{SB}} |\mu\rangle \langle\mu| , \\
H' &= \sum_{\binom{\mu\nu}{\mu\neq\nu}} |\mu\rangle \langle\mu| H_{\mathrm{SB}} |\nu\rangle \langle\nu|
\end{aligned}
\tag{2.92}
$$

with $|\mu\rangle$ and $|\nu\rangle$ being eigenstates of H_{S}, and H_0 and H' being responsible for the free evolution and the perturbation, respectively. The matrix elements in the system DOFs of H_0 can be obtained in eigenstate representation of H_{S} as

$$
\langle\mu| H_0 |\mu\rangle = E_\mu - \lambda_{\mu\mu\mu\mu} + H_{\mathrm{B}}(\mu)
\tag{2.93}
$$

where E_μ is the eigenenergy of the state $|\mu\rangle$ and

$$
\lambda_{\mu\nu\mu'\nu'} = \sum_{kl} \langle\mu| K_k |\nu\rangle \langle\mu'| K_l |\nu'\rangle \sum_\xi \frac{c_{k\xi} c_{l\xi}}{2 m_\xi \omega_\xi^2} .
\tag{2.94}
$$

is the weighted reorganization energy that is strongly related to the renormalization Hamiltonian (2.32). In the following it will be assumed that the local bath approximation (2.58) holds such that

$$
\begin{aligned}
\lambda_{\mu\nu\mu'\nu'} &= \sum_k \langle\mu| K_k |\nu\rangle \langle\mu'| K_k |\nu'\rangle \sum_\xi \frac{c_\xi^2}{2 m_\xi \omega_\xi^2} \\
&= \sum_k \langle\mu| K_k |\nu\rangle \langle\mu'| K_k |\nu'\rangle \lambda
\end{aligned}
\tag{2.95}
$$

where λ can be obtained from the spectral density according to Eq. (2.67). The term

$$H_{\mathrm{B}}(\mu) = \frac{1}{2}\sum_\xi \left(\frac{p_\xi^2}{m_\xi} + m_\xi \omega_\xi^2 \left(x_\xi + \sum_k \frac{\langle \mu | K_k | \mu \rangle c_\xi}{m_\xi \omega_\xi^2} \right)^2 \right). \qquad (2.96)$$

denotes a set of bath oscillators shifted according to the excitonic state $|\mu\rangle$.

Since within MRT one is only interested in the population dynamics in eigenstate representation of the system a different type of projection operator is used which only projects onto the populations of the system eigenstates. The projector within MRT is defined as

$$\begin{aligned}
\tilde{\mathcal{P}} &= \sum_\mu \mathcal{P}_\mu, \\
\mathcal{P}_\mu \bullet &= R_{\mathrm{eq}}^\mu \mathrm{tr}\left\{ |\mu\rangle \langle \mu | \bullet \right\}.
\end{aligned} \qquad (2.97)$$

Here the projectors $\mathcal{P}_\mu$ determine the μth diagonal element in eigenstate representation of H_{S} and $R_{\mathrm{eq}}^\mu = \exp\left(-\beta H_{\mathrm{B}}(\mu) \right)/\mathrm{tr}\left\{ \exp\left(-\beta H_{\mathrm{B}}(\mu) \right) \right\}$ is the equilibrium density matrix of the bath with respect to the shifted bath Hamiltonian $H_{\mathrm{B}}(\mu)$. In this case the shifted bath Hamiltonian has been chosen since in an excited state the potential energy surfaces are usually shifted compared to the ground state. The equilibrium density matrix R_{eq}^μ can be interpreted as an approximate expression for the thermal equilibrium state of the bath if the system is in state $|\mu\rangle$.

With help of the projectors (2.97) the population $\rho_{\mu\mu}$ of the eigenstate $|\mu\rangle$ can be obtained as

$$\rho_{\mu\mu}(t) = \mathrm{tr}\left\{ \mathcal{P}_\mu W(t) \right\}, \qquad (2.98)$$

where the trace operation is used to integrate over the bath DOFs.

2.8.2 Population dynamics

As within the usual second-order perturbative techniques described in section 2.6 one can now use the Nakajima-Zwanzig identity (2.23) or the Hashitsume-Takahashi-Shibata identity (2.24) to derive TNL or TL EOMs for the populations, respectively. In the following only the TL form will be discussed since the TNL has not been used in this work. Upon inserting the definitions (2.92) and (2.97) into the Hashitsume-Takahashi-Shibata identity and expanding it up to second order in H' one obtains a TL EOM for the populations as

$$\frac{\partial}{\partial t}\rho_{\mu\mu}(t) = \sum_{\nu \neq \mu} \left(\overline{R}_{\mu\mu\nu\nu}(t)\rho_{\nu\nu}(t) - \overline{R}_{\nu\nu\mu\mu}(t)\rho_{\mu\mu}(t) \right) \qquad (2.99)$$

with the population transfer rates $R_{\mu\mu\nu\nu}$ also called the modified Redfield tensor.[17,89]

Expanding the Hashitsume-Takahashi-Shibata identity to second order in H' yields

$$\begin{aligned}
\overline{R}_{\nu\nu\mu\mu} &= 2\mathrm{Re}\int_0^t d\tau\, \mathrm{tr}\left\{ |\nu\rangle \langle \nu | \exp\left(-iH_0\tau \right) H' |\mu\rangle \langle \mu | R_{\mathrm{eq}}^\mu \exp\left(iH_0\tau \right) H' \right\} \\
&\approx 2\mathrm{Re}\int_0^t d\tau \exp\left(-i\left(\omega_{\nu\mu} + 2\left(\lambda_{\mu\mu\mu\mu} - \lambda_{\nu\nu\nu\nu} \right) \right)\tau - G_{\nu\nu\nu\nu}(\tau) - G_{\mu\mu\mu\mu}(\tau) + 2G_{\nu\nu\mu\mu}(\tau) \right) \\
&\quad \times \left[\ddot{G}_{\nu\mu\nu\mu}(\tau) - \left(\dot{G}_{\nu\mu\nu\nu}(\tau) - \dot{G}_{\nu\mu\mu\mu}(\tau) + 2i\lambda_{\mu\mu\mu\nu} \right)^2 \right]
\end{aligned}$$

$$(2.100)$$

where the second line has been obtained by applying the local-bath approximation (2.58) and the second-order cumulant expansion technique as shown in detail in appendix B. The functions

$$G_{\mu\nu\mu'\nu'}(t) = \sum_k \langle\mu|\,K_k\,|\nu\rangle\,\langle\mu'|\,K_k\,|\nu'\rangle \int\limits_0^t d\tau \int\limits_0^\tau d\tau' C(\tau') \tag{2.101}$$

are weighted doubly integrated bath correlation functions. Note that the diagonal part of the system-bath coupling is treated exactly.[17] In the Markovian limit the integral in Eq. (2.100) is raised to infinity such that the population transfer rates become time-independent and Eq. (2.99) becomes

$$\frac{\partial}{\partial t}\rho_{\mu\mu}(t) = \sum_{\nu\neq\mu}\left(\overline{R}_{\mu\mu\nu\nu}\rho_{\nu\nu}(t) - \overline{R}_{\nu\nu\mu\mu}\rho_{\mu\mu}(t)\right). \tag{2.102}$$

In the following the non-Markovian form of the MRT will be denoted as time-dependent MRT (TDMRT).

Note, that the Markovian modified Redfield tensor is identical with the usual Redfield tensor (2.46) if the diagonal parts of the system-bath coupling vanish. In this case the bath operators (2.96) are not shifted and $H_0 = H_S + H_B$ as in the usual second-order schemes.

2.9 Linear absorption theory

When light interacts with a macroscopic sample of a dielectric medium the system responds with a polarization **P** which, to first order in the electric field, is given by

$$\mathbf{P} = \chi\mathbf{E} \tag{2.103}$$

where **E** denotes the electric field vector of the light and χ the so-called linear susceptibility which is also called the linear response function of the medium. It describes the reaction of the medium to an external perturbation. In general, χ is a tensor, i.e. the direction of the polarization vector does not necessarily have to coincide with the direction of the applied electrical field. For simplicity, however, it will be assumed in the following that χ is scalar.

The quantity that describes the linear optical absorption of a medium, however, is the so-called linear absorption coefficient $\alpha(\omega)$ which is in general frequency dependent. It describes the exponential decrease of the intensity A of light that travels through a medium in z direction as

$$A(z) = A(0)e^{-\alpha z}. \tag{2.104}$$

This expression is also known as the Lambert-Beer law.[1,2] The absorption coefficient α can be expressed in terms of the linear susceptibility as

$$\alpha(\omega) = \frac{4\pi\omega}{nc}\mathrm{Im}\chi(\omega). \tag{2.105}$$

Here n is the refraction index and c denotes the speed of light. In a semi-classical approach, i.e. if the light field can be treated classically while the system under consideration is treated quantum mechanically the linear response function of the

system in time domain can be calculated using second-order perturbation theory. In time domain it is given in terms of the dipole-dipole correlation function as[2,90]

$$\chi(t) = n_{\mathrm{mol}} i \mathrm{tr}\left\{W_{\mathrm{eq}}\left[\hat{\mu}(t), \hat{\mu}\right]\right\} \tag{2.106}$$

where n_{mol} is the molar concentration of dipoles and $\hat{\mu}(t)$ denotes the dipole operator $\hat{\mu}$ which is evolving according to the Heisenberg representation with respect to the Hamiltonian of the unperturbed system, i.e., without the coupling to the electric field. From the dipole-dipole correlation function the absorption coefficient in frequency domain can be obtained by applying the Fourier transformation. Note that

$$\chi(t) = -2n_{\mathrm{mol}} \mathrm{Im}\, \mathrm{tr}\left\{U(t)\hat{\mu}W_{\mathrm{eq}}U^{\dagger}(t)\hat{\mu}\right\} \tag{2.107}$$

is real valued which can be verified by evaluating the commutator within the trace of Eq. (2.106) and using the invariance of the trace upon cyclic permutation of its arguments.

Usually the equilibrium density matrix W_{eq} can be assumed to be in the electronic ground state at room temperature since the energy difference between the electronic ground and the excited states is large compared to the thermal energy. Another important quantity is the so-called line shape of absorption. It is related to the absorption coefficient as[18]

$$I(\omega) = \frac{3c}{4\pi^2 \omega |d|^2}\alpha(\omega) \tag{2.108}$$

where $|d|^2$ is the mean square dipole moment of the system. To compare calculated data to experimental data, one often normalizes all spectra to a maximum peak height equal to unity or uses an integral normalization. I.e.,

$$I(\omega) \propto \mathrm{Re} \int\limits_{0}^{\infty} dt\, e^{i\omega t}\chi(t). \tag{2.109}$$

where prefactors are neglected.

From Eq. (2.107) it can be seen that, instead of the density matrix, the dipole operator times the equilibrium density operator has to be propagated according to the Hamiltonian of the complete system (without the interaction with the light). If the dipole operator is defined exclusively in the system DOFs it becomes possible to apply the above mentioned propagation schemes for density matrices to the dipole operator (times the system parts of W_{eq}) instead of the reduced density matrix and apply the trace in the system DOFs later.

3 Electron transfer in a donor-acceptor complex

In the present chapter the evolution of a reduced density matrix coupled to a thermal bath is calculated to several orders in the system-bath interaction using the hierarchical method discussed in section 2.7. The calculations will be restricted to model systems of one and two coupled harmonic oscillators, respectively, that are linearly coupled to a collection of bath oscillators.

To demonstrate the effect of different spectral densities, i.e., different kinds of coupling strength to the various bath modes, in section 3.1 the population dynamics of the third eigenstate of a single harmonic oscillator and the dynamics of the variance $\langle q^2 \rangle$ are shown, where q is the coordinate operator in the system DOF.

In section 3.2 the model system is extended to a set of two coupled harmonic oscillators. This kind of system is often used to model donor-acceptor systems.[26] Here the effects of different orders in the system-bath interaction will be demonstrated by means of the population dynamics of the donor state.

In both cases the total Hamiltonian has the structure

$$H \;=\; H_\mathrm{S} + K\Phi + H_\mathrm{B} + H_\mathrm{ren}. \tag{3.1}$$

Due to the fact that one coupling term $K\Phi$ exists in the total Hamiltonian the indices labeling the different interaction operators can be skipped such that the bath part of the coupling reads

$$\Phi = \sum_\xi c_\xi x_\xi \tag{3.2}$$

and the renormalization (2.32) reduces to

$$H_\mathrm{ren} = K^2 \sum_\xi \frac{c_\xi^2}{2 m_\xi \omega_\xi^2} = K^2 \lambda. \tag{3.3}$$

Also the structure of the hierarchy (2.88) simplifies to

$$
\frac{\partial}{\partial t}\rho_{\{I\}}(t) \;=\; -i\left[H_\mathrm{S}^\mathrm{eff}, \rho_{\{I\}}(t) \right] + \left(\sum_{j=1}^{n_\mathrm{r}} I_j \gamma_j^\mathrm{r} + \sum_{j=1}^{n_\mathrm{i}} I_{n_\mathrm{r}+j} \gamma_j^\mathrm{i} \right) \rho_{\{I\}}(t) - i \sum_{j=1}^{n_\mathrm{r}+n_\mathrm{i}} \left[K, \rho_{\{I;\, I_j+1\}}(t) \right]
$$

$$
-i\sum_{j=1}^{n_\mathrm{r}} \alpha_j^\mathrm{r}\, I_j \left[K, \rho_{\{I;\, I_j-1\}}(t) \right] + \sum_{j=1}^{n_\mathrm{i}} \alpha_j^\mathrm{i}\, I_{n_\mathrm{r}+j} \left[K, \rho_{\{I;\, I_{n_\mathrm{r}+j}-1\}}(t) \right]_+ . \tag{3.4}
$$

Here the effective system Hamiltonian $H_\mathrm{S}^\mathrm{eff}$ has been defined according to Eq. (2.15) and the bath Hamiltonian H_B is chosen according to Eq. (2.26). These definitions will be used in the following sections, where, according to the particular model under consideration the remaining operators will be specified.

3.1 Damped harmonic oscillator

For the single damped harmonic oscillator the same parameters as in Ref. [76] have been used, i.e., mass m_0 and frequency ω_0 of the oscillator have been set to unity and the calculations have been performed at an inverse bath temperature of $\beta = 1$ a.u. In Ref. [76] the TL and TNL second order schemes have been used and especially for the population dynamics very different results have been obtained and the question was raised which of the methods gave the more reliable results. This question can be answered by taking into account higher orders of H_{SB}.

The spectral density has been chosen to be of Drude form, i.e.,

$$J(\omega) = \frac{\eta\omega}{1 + (\omega/\omega_d)^2}, \tag{3.5}$$

with η being a prefactor determining the coupling strength and ω_d being the so-called Drude frequency determining the frequency range in which the bath modes can couple to the system or, in time domain, the bath correlation time. The use of a Drude spectral density has the advantage that the spectral density does not have to be decomposed into a number of Lorentzians in order to decompose the correlation function into a sum of exponentials. Instead, the theorem of residues can be directly used to evaluate the correlation function (2.66).[76]

Using the definitions given above and setting the system part of the interaction to $K = q$ with q being the coordinate operator in the system DOF, the total Hamiltonian (3.1) reads

$$H = \frac{1}{2}\left(\frac{p^2}{m_0} + m_0\omega_0^2 q^2\right) + q\sum_\xi c_\xi x_\xi + \sum_\xi \frac{1}{2}\left(\frac{p_\xi^2}{m_\xi} + m_\xi\omega_\xi^2 x_\xi^2\right) + q^2\sum_\xi \frac{c_\xi}{2m_\xi\omega_\xi^2} \tag{3.6}$$

where p denotes the momentum operator of the system. In order to provide comparable damping strength in all calculations the integral

$$\int_0^\infty d\omega \frac{J(\omega)}{\omega} = \mathrm{const} \tag{3.7}$$

was identical in all examples.[91] Furthermore, the initial state of the complete system has been set to $W(0) = |3\rangle\langle 3| R_{\mathrm{eq}}$ where $|3\rangle$ denotes the third excited eigenstate of the system oscillator which in total was described using the lowest 10 eigenstates.

3.1.1 Small bath relaxation time

The dynamics of the third eigenstate for a large cutoff frequency ω_d, i.e., short bath correlation time, and various orders of the system-bath coupling are displayed in Fig. 3.1. Here, as in the other figures in this chapter, the time scale is given in units of the oscillation period $t_0 = 2\pi/\omega_0$ of the unperturbed system oscillator. It can be nicely seen that the system relaxes towards thermal equilibrium which is almost reached at $t/t_0 = 8$. In the left panel of Fig. 3.1 the results obtained from a propagation using the TL truncation (2.91) of the hierarchy are given. In this case all curves lie on top of each other and the hierarchy seems to be converged already in second order of the system-bath coupling when the usual TL formalism discussed in section 2.6.1 is used. In the right panel of Fig. 3.1 the results obtained with the TNL truncation

method are displayed. Also here the curves lie almost on top of each other. Only the curve obtained with the second order TNL, i.e., the usual TNL method as proposed by Meier and Tannor[85] (see also section 2.6.2), deviates slightly from the other curves for $t/t_0 < 1$ a.u. The scheme seems to be converged in the fourth order of system-bath coupling.
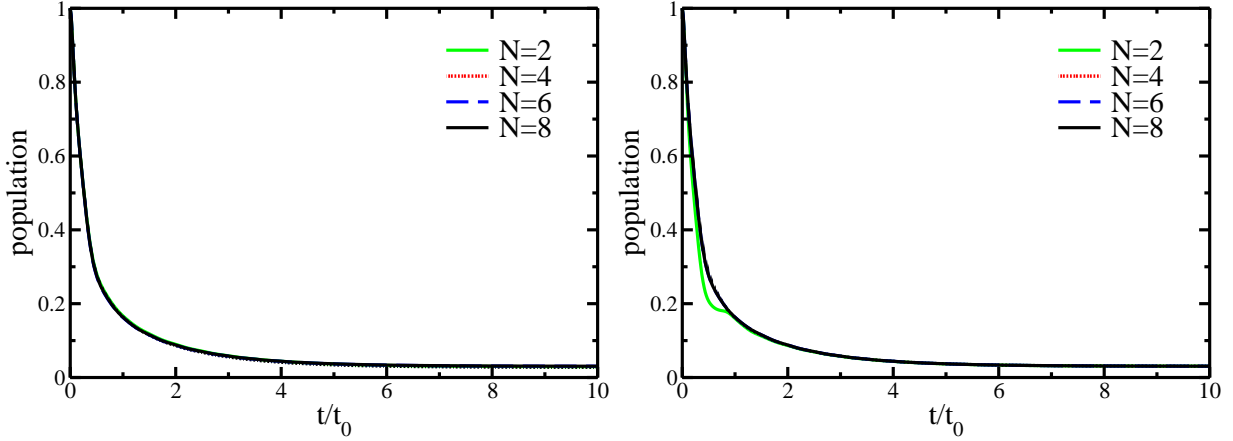

Figure 3.1: Population dynamics of the third excited state using the TL (left) and TNL (right) truncation scheme to different orders N of the system-bath coupling obtained with a Drude spectral density with $\eta = 0.136$ and $\omega_d = 2$ a.u.

The reason for this relatively fast convergence can be found in the EOMs for the higher levels of the hierarchy (3.4). The large cutoff frequency ω_d causes relatively short bath correlation times such that the exponents γ_j^r and γ_j^i of the dominating exponential functions within the decomposed correlation function (2.66) are large. This causes a strong damping of the higher levels within the hierarchy since here the exponents appear together with integer multiplicators such that the hierarchical set of EOMs converges fast.

Another aspect of interest is the dynamics of the expectation values calculated from the system density matrix. In Fig. 3.2 the expectation value $\langle q^2 \rangle = \text{tr} \{q^2 \rho\}$ is shown. In the present case this is equal to the variance of the system state since the expectation value $\langle q \rangle = \text{tr} \{q\rho\}$ vanishes for all times. The results obtained with the TL and the TNL methods of truncation are in good agreement for the various orders of the system-bath interaction and also with results from exact path integral calculations which have been taken from Refs. [75, 76]. It is worth mentioning that the results obtained with the TNL truncation seem to converge faster than those obtained with the TL truncation. Also here the equilibrium value is almost reached at $t/t_0 = 8$.

3.1.2 Large bath relaxation time

As mentioned before, the short bath correlation times cause a fast convergence of the EOMs. In the following the bath correlation times are increased, i.e., the Drude frequency is set to a smaller value compared to the previous example. The population
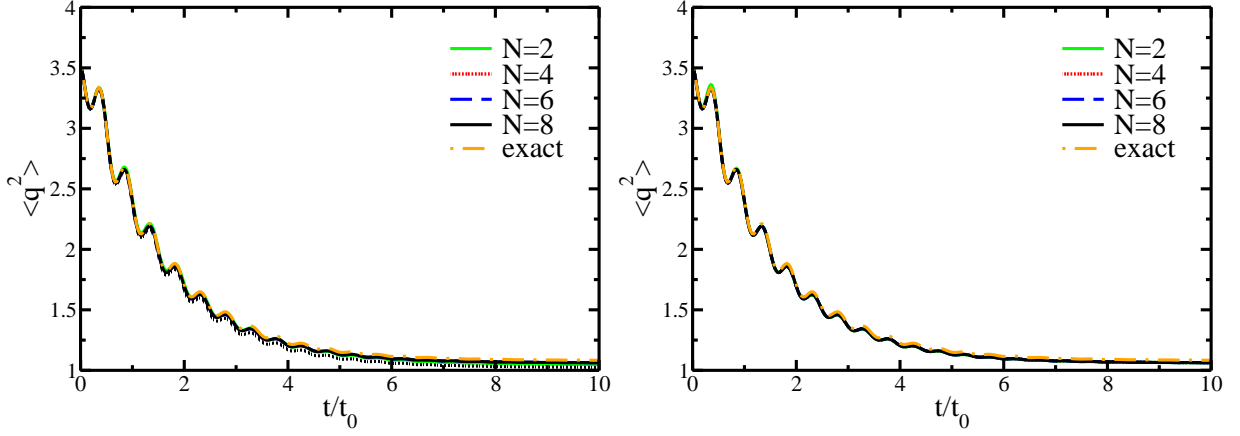
Figure 3.2: Expectation value of q^2 using the TL (left) and TNL (right) truncation scheme to different orders N of the system-bath coupling obtained with a Drude spectral density with $\eta = 0.136$ and $\omega_d = 2$ a.u.

dynamics of the third excited state are shown in Fig. 3.3. In the case where the TL truncation scheme has been used, all curves are in good agreement except from small deviations around $t/t_0 = 1$. The results obtained with the TNL truncation scheme, however, show large deviations in the various orders. The curve obtained with the second order TNL scheme shows large oscillations before it reaches the equilibrium value. This has also been observed in Ref. [76]. The curves obtained from higher order calculations show larger deviations as well until the scheme seems to be converged in 8th order of the system-bath interaction where it is in good agreement with the TL truncation scheme. The TL truncation therefore appears to yield far better results for population dynamics already in low orders of the perturbation theory.
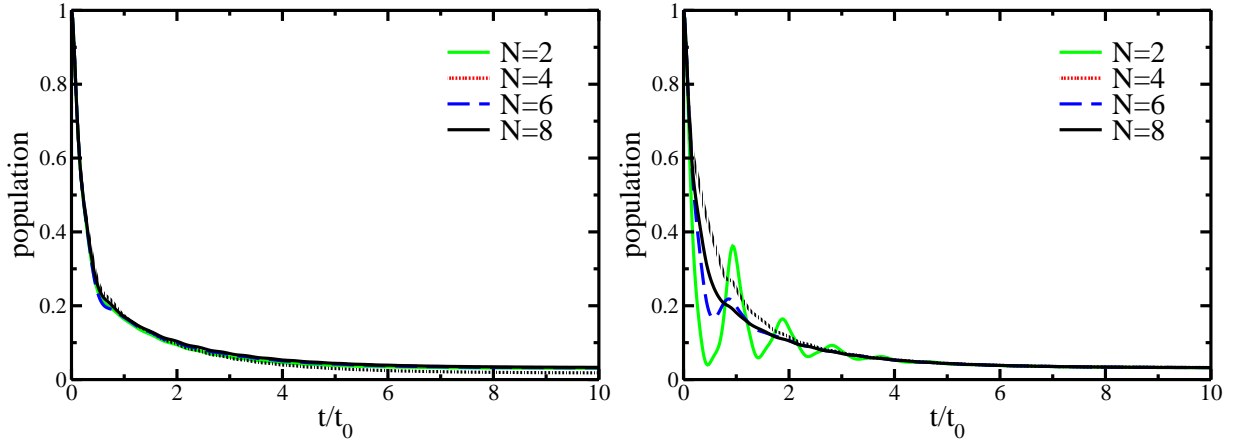

Figure 3.3: Same as Fig. 3.1 but with $\eta = 0.544$ and $\omega_d = 0.5$ a.u.

This is completely different for the expectation value of q^2 given in Fig. 3.4. For the small cutoff frequencies the curves obtained with the TL truncation scheme in fact show qualitatively a similar behavior, however, for the lower orders, especially for the fourth order, deviations from the exact results are observed. The scheme has not converged until the 6th order. In contrast, all curves obtained with the TNL truncation scheme are in good agreement with the exact path integral calculations. Only the

curve obtained with the second-order scheme deviates slightly from the others around $t/t_0 = 1/2$. In this case therefore the TNL truncation scheme apparently yields more reliable results.
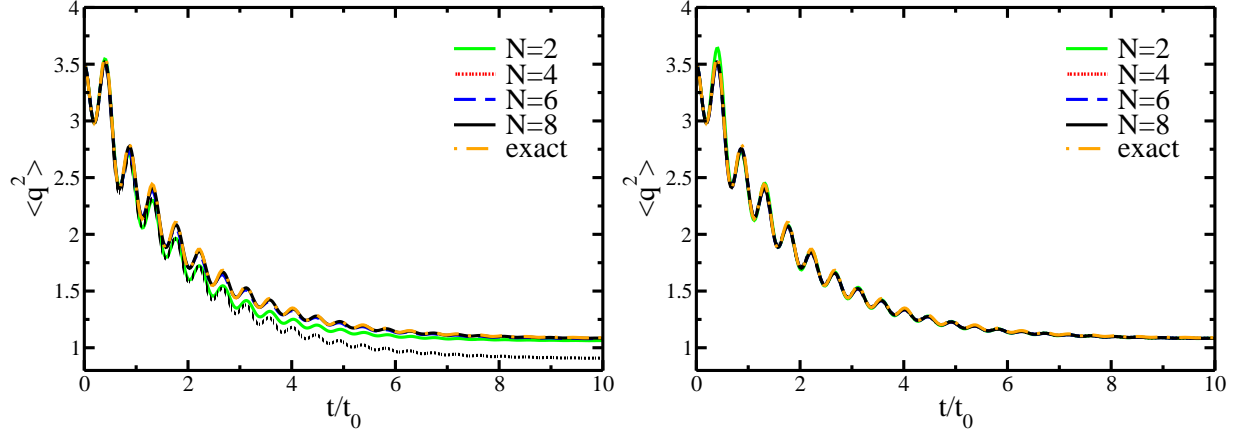

Figure 3.4: Same as Fig. 3.2 but with $\eta = 0.544$ and $\omega_d = 0.5$ a.u.

It is interesting to see that the deviations of $\langle q^2 \rangle$ in the various orders of the system-bath interaction for both, the TL and the TNL truncation scheme, are rather small compared to the large deviations of the population dynamics obtained with the TNL truncation method. A possible reason for this behavior can be found in the structure of the operators q and p (cf. Eq. (C.7)) as well as the initial state $\rho(0)$. In energy representation only the matrix element of ρ_{33} of the initial state is nonzero. With increasing time also other matrix elements ρ_{ij} with $i + j$ even can become nonzero. The calculation of $\langle q^2 \rangle$ involves the matrix elements ρ_{ii}, ρ_{ij} and ρ_{ji} with $j = \pm 2$. I.e., more matrix elements, especially all diagonal elements, are used. Since $\mathrm{tr}\,\{\rho\} = 1$ holds for all times it is most likely that the error, mainly caused by oscillations within the TNL scheme, is averaged out to some extent. A reduction of the oscillations in the population dynamics can also be observed when a general initial state is used.

3.2 Two coupled damped harmonic oscillators

In the following the model is extended to two coupled harmonic energy surfaces which are arranged along a common single reaction coordinate q as illustrated in Fig. 3.5. A formally similar system has been treated with a hierarchical method by Tanimura and Mukamel earlier.[32] In their model the oscillators were optically coupled and the pump-probe spectrum has been calculated. Furthermore the calculations were done in the high temperature limit, i.e., the Matsubara frequencies in (2.64) have been neglected such that high orders in the system-bath coupling could be calculated.

The Hamiltonian of such a system consists of single harmonic oscillators describing the vibronic levels of the donor and acceptor and an additional term that is responsible for their electronic coupling. The system Hamiltonian reads

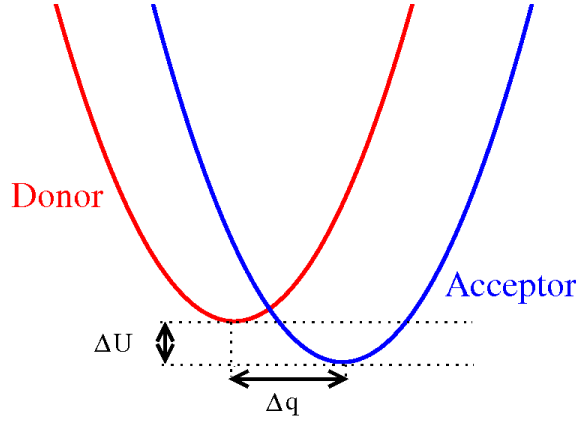$$H_S = \sum_n H_n(q) + \sum_{m \neq n} V_{mn}(q), \qquad (3.8)$$

Figure 3.5: Schematic view of donor-acceptor system

where

$$H_n = U_n + \left(a_n^\dagger a_n + \frac{1}{2} \right) \omega_n \tag{3.9}$$

is the vibrational Hamiltonian of the oscillator $n = 1, 2$ with frequency ω_n and the bosonic creation and annihilation operators $a_n^\dagger$ and a_n, respectively. The additional term $V_{mn}(q)$ denotes the electronic coupling between the different oscillators and U_n is a constant energy shift. The coupling term V_{mn} usually depends on the reaction coordinate. In the following it will be assumed that the Condon approximation holds[2] and $V_{mn}(q) = V_{mn}$ is independent from q. In this case the electronic coupling can then be written as[26]

$$V_{mn} = \sum_{MN} (1 - \delta_{mn}) \, v_{mn} F_{\mathrm{FC}}(m, n, M, N) \, |mM\rangle \, \langle nN| \, . \tag{3.10}$$

Here $v_{mn} = v$ determines the strength of the coupling between the potential energy surfaces m and n and $F_{\mathrm{FC}}(m, n, M, N)$ are the so-called Franck-Condon factors that render the overlap of the states $|mM\rangle$ and $|nN\rangle$. In the notation of the state vectors lower case indices label the energy surfaces and upper case indices label the vibronic levels of which 10 for each oscillator have been used for the calculations.

As in the previous example the Drude spectral density function (3.5) has been used for all calculations and the inverse temperature β is set to unity. The system-bath interaction is the same as in Eq. (3.6), however with

$$K = q = \sum_n \frac{1}{\sqrt{2\omega_n m_n}} \left(a_n^\dagger + a_n \right) \tag{3.11}$$

where m_n denotes the mass of the nth harmonic oscillator. All additional parameters can be found in Table 3.1. The system discussed in Ref. [26] is basically the same as discussed here, but for different parameters. For the parameters discussed in Ref. [26] only very small changes were obtained with higher-order perturbation theory since the system frequencies are very small such that the condition (2.89) is already fulfilled in second order of the system-bath coupling. Therefore here the parameters have been chosen such that effects of higher orders in the system-bath coupling clearly emerge.

In all calculations the initial state has been set to $|nN\rangle = |13\rangle$, i.e. only the third excited vibronic state of the donor is populated. The electronic population of the donor

Quantity		Value
Frequency	$\omega_1 = \omega_2 = \omega_0$	1 a.u.
Mass	$m_1 = m_2 = m_0$	1 a.u.
Electronic coupling	$v_{1,2} = v_{2,1} = v$	0.2 E_h
Distance	Δq	3.4 a_0
Energy difference between donor and acceptor	$\Delta U = U_2 - U_1$	-1.5 E_h

Table 3.1: Parameters of the donor-acceptor system with E_h and a_0 being the Hartree energy and Bohr radius, respectively.
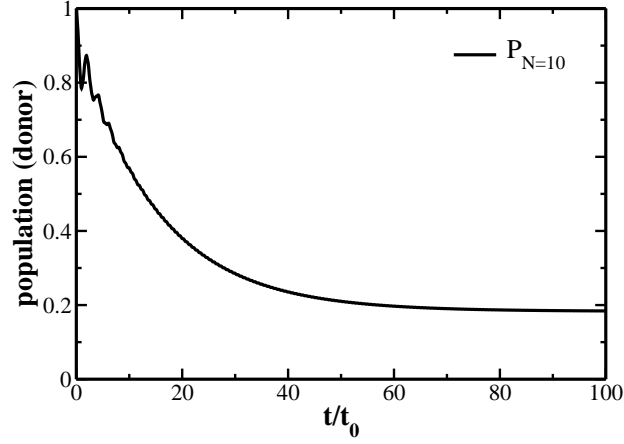

Figure 3.6: Example of the donor population P for a Drude spectral density with $\eta = 0.544$ and $\omega_d = 0.5$ a.u. calculated to order $N = 10$ in the system-bath coupling.

as a whole can be obtained by summing over all its vibronic populations. Fig. 3.6 shows one example of the time evolution of the donor population. It decays exponentially towards the thermal equilibrium while small oscillations are visible for early times. A similar behavior could be observed in all examples such that the convergence of the hierarchical approach can be better analyzed using difference plots for the populations obtained with the various methods. In the following only the difference to those results obtained using the hierarchical approach to 10th order of the system-bath interaction and TL truncation which serve as a reference, will be displayed.

3.2.1 Small bath relaxation time

The results obtained with a spectral density function with large Drude frequency, i.e., short bath correlation time are presented in Fig. 3.7. The deviations in the population of the donor state are of the order 10^{-2} for both, the TL and the TNL truncation method. Interestingly, the curve obtained with the second-order TL formalism shows the largest deviations for early times while the 4th-order curve approaches a different equilibrium state. In contrast, for the TNL truncation the 4th-order curve deviates only for short times slightly from the 10th-order but here the curve obtained with the second order TNL method relaxes to a different equilibrium value.

The different equilibrium states here and also in the following result from different effective Hamiltonians created by the perturbative treatment of the full Hamiltonian.
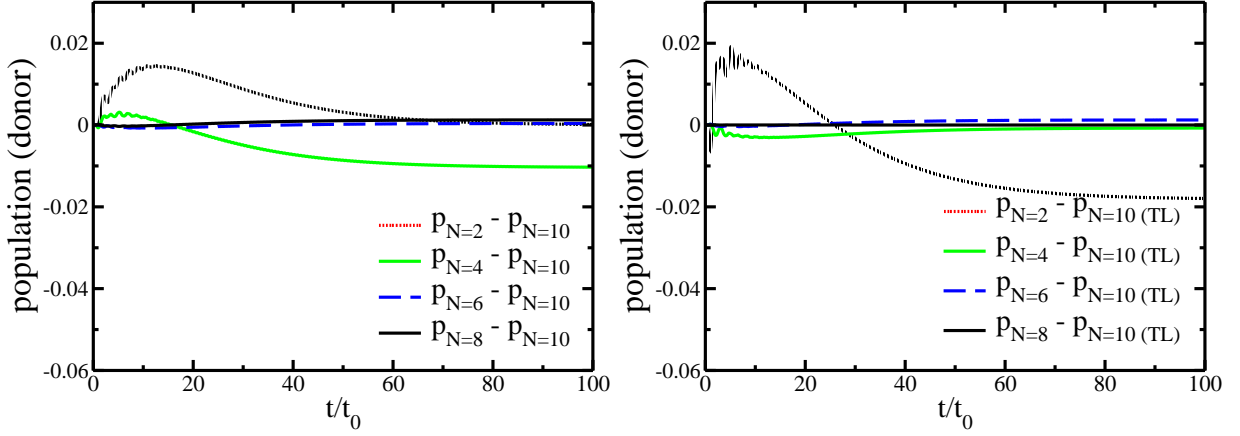
Figure 3.7: Difference plot for the electronic population of the donor with respect to 10th order (TL) in the system-bath interaction. The results were obtained using the same Drude spectral density as in Fig. 3.1 with TL (left) and TNL (right) truncation.

The effective Hamiltonians only take into account parts of the system-bath interaction and this in different ways. The equilibrium state which the system approaches therefore belongs to such an effective Hamiltonian and can have different values.

In Fig. 3.8 difference plots for the population dynamics of the 3rd excited vibronic level are given. The absolute value of the population of this state is very similar to that shown in Fig. 3.1 for a single oscillator and therefore not shown here. In case of a large Drude frequency the curves obtained with the TL truncation are almost zero and deviate only slightly for short times. However, the curves obtained with the TNL truncation show larger deviations, here especially the curve obtained with the second-order scheme differs significantly from the other curves around $t/t_0 = 1$. This behavior has already been found in Fig. 3.1 for the single oscillator. In total, however, all variations are still of the order 10^{-2} and both schemes yield agreeing results. Note, however the different time scales on which the vibronic and the electronic relaxation takes place. The vibronic system equilibrates ten times faster than the electronic system. The vanishing of the short time oscillations in Fig. 3.6 coincides with the time when the vibronic system reaches the equilibrium.
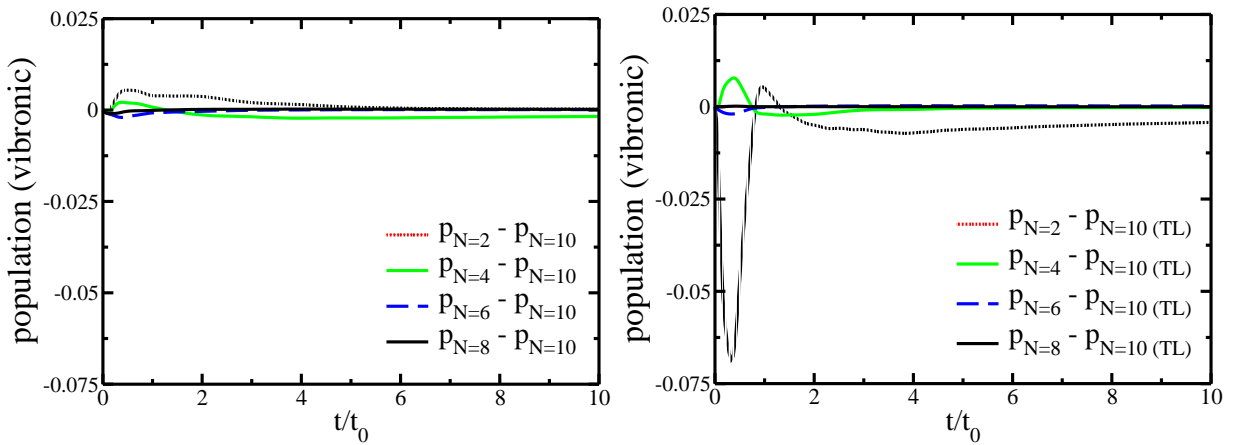

Figure 3.8: Same as in Fig. 3.7, but for the vibronic population of the 3rd excited vibronic state.

3.2.2 Large bath relaxation time

The results obtained with a larger bath correlation time are displayed in Figs. 3.9 and 3.10 for the electronic population of the donor state and the third excited of its vibronic sublevels, respectively. The population dynamics of the donor obtained with the TL truncation shows significant deviations in the lower orders, however seems to be converged in the 8th order of the system-bath interaction. Also within the TNL scheme deviations in the lower orders of the system-bath coupling can be observed, in contrast to the TL truncation method, the curves obtained with TNL scheme apparently have converged already in 4th order of the interaction.
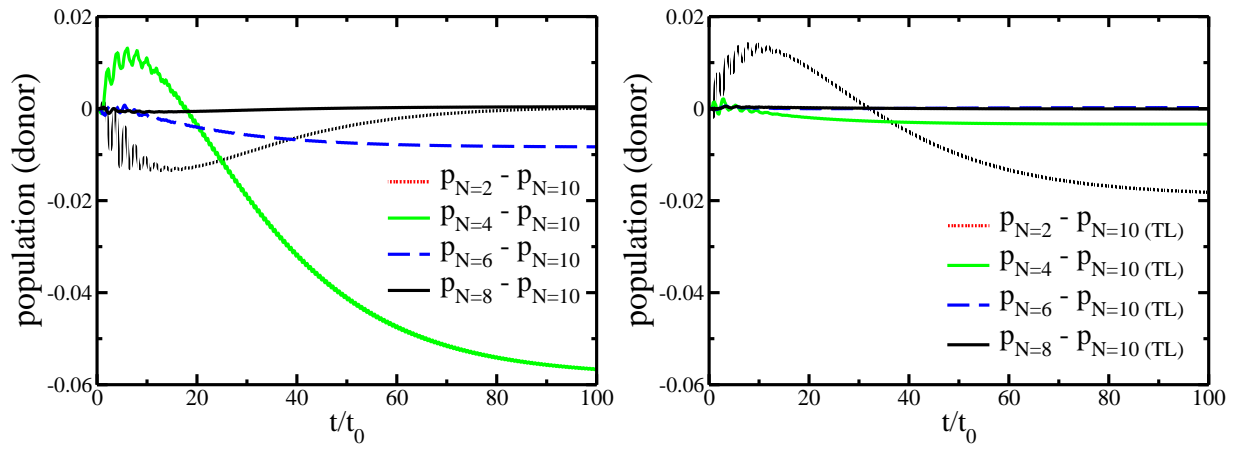

Figure 3.9: Same as in Fig. 3.7 but with the spectral density as in Fig. 3.3.

For comparison again the population of the third excited vibrational state of the donor is shown in Fig. 3.10. Within the TL truncation scheme the curves obtained within different orders of the system-bath interaction do not deviate much from each other. The most significant variations can be found around $t/t_0 = 1$. All curves except that obtained with the fourth-order scheme seem to reach the same equilibrium value. As in the previous section for the single harmonic oscillator the results obtained with the TNL truncation show large variations and converge only slowly. The variations are one order of magnitude larger that those displayed for the TL truncation. In both cases, however, the results near $t/t_0 = 1$ are possibly not yet converged since the difference in the various curves near this point decreases very slowly.

Apparently the question of which truncation scheme should be used for calculating certain observables if the condition (2.89) cannot be fulfilled is not easy to answer. In the cases shown above either the TL or the TNL truncation scheme yields better results depending on the observable which is calculated. However, other calculations with a different initial state suggest that such a clear statement cannot be made in every case. The convergence not only depends on the observable but also on the
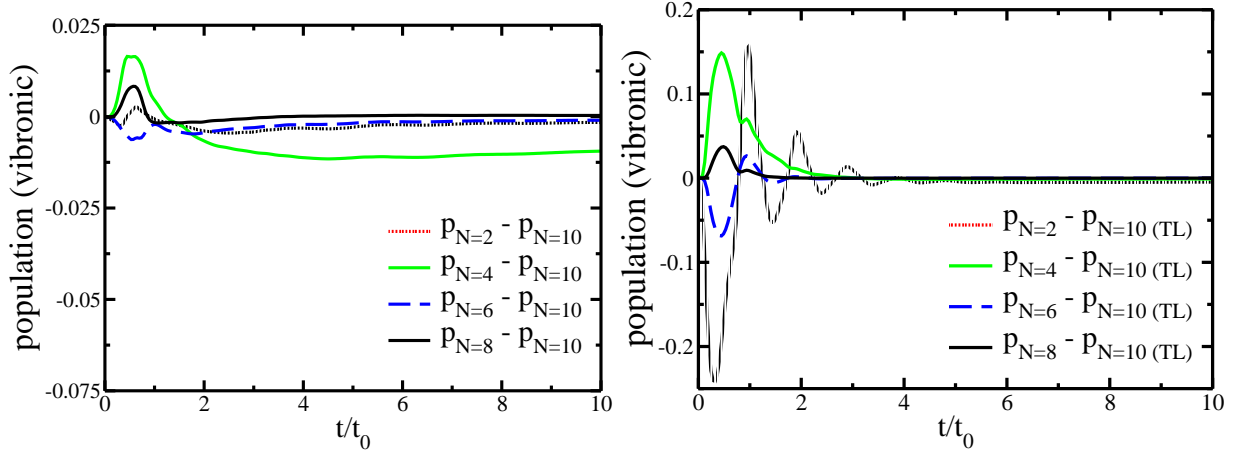
Figure 3.10: Same as in Fig. 3.8 but with the spectral density as in Fig. 3.3.

initial state and also on the system itself as indicated by the results displayed in the following chapters.

It could be observed that with growing orders in the system-bath interaction the hierarchical method converges towards the exact results. It can therefore serve as a tool for higher-order perturbative treatments of the reduced system dynamics if the damping is not too strong. It can be used to verify the validity of lower-order, e.g. second-order, perturbative treatments which are widely used when dissipative systems are considered.

4 Linear absorption spectra of LH2

4.1 Model system

In the present chapter different methods for obtaining the linear absorption spectra of the B850 ring of the LH2 systems of *Rs. molischianum* are compared. As mentioned in the introduction the B850 ring consists of 16 BChl *a* pigments that are arranged in a planar and circular pattern embedded in a protein structure. In Fig. 4.1 the structure of the LH2 complex is illustrated. For the numerical calculation of the
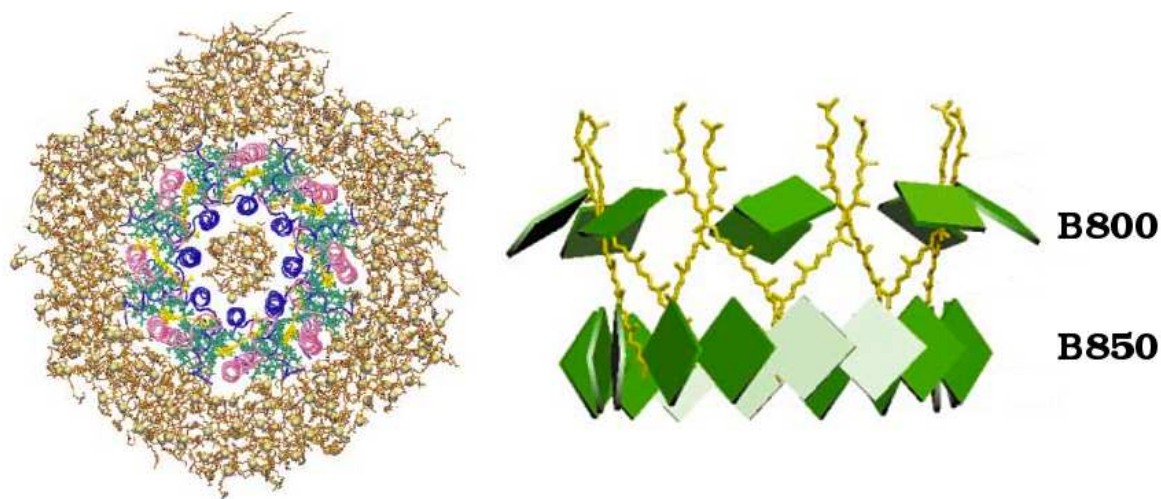

Figure 4.1: Schematic picture of the pigment-protein complex adapted from Ref. [18].
Left: LH2 of *Rs. molischianum* seen from the top. The chlorophyll pigments are marked green, the protein matrix is shown in blue and magenta. In addition carotenoids are coded yellow and surrounding lipids are colored brown.
Right: Arrangement of the pigments within the HL2 complex in side-view. The BChl molecules are displayed as green quads and the carotenoids as yellow strings.

linear absorption profile it will be assumed that the coupling to the electromagnetic field is only due to the electrons of the pigments that couple to the electric field of the radiation.

As a first approximation it is possible to describe the pigments as two-level systems since usually only the electronic ground state and the lowest excited state are populated. These two states are optically coupled via a transition dipole so that the pigments can be excited by an electromagnetic field. Besides other mechanisms the transition dipoles also cause a coupling between the various pigments due to dipole-dipole interaction.[4] Hence the electronic excitation of the pigment complex as a whole is no longer localized on a single chromophore and the delocalized eigenstates of excitation energy are also called excitons. If one chromophore is initially excited the

dipole-dipole interaction causes a transition from the ground to the excited state in a neighboring molecule while within the initially excited pigment a transition to the ground state occurs. This mechanism is called Förster transfer. Effectively, therefore, the population of the excited states has been transferred so that, for numerical treatment, one only needs to describe the coupled excited states of the pigments together with one common ground state.

In the present model it is assumed that only one exciton can exist throughout the ring if the intensity of the light is low. The incorporation of two-exciton states, however, is possible within the present framework.[16,92] The two- (or more-) exciton states have been neglected here since their contributions to the linear absorption are small compared to those of the single-exciton manifold. It is often argued that strong electromagnetic fields beyond the validity of the present linear approach are required to create two-exciton states and that the life-times of two-exciton states are small compared to those of the single-exciton states due to annihilation processes. For higher-order spectroscopy higher-order excitonic states have to be taken into account.[17]

As mentioned above, the pigments are embedded in a protein matrix which affects the properties of the excitonic system in several ways. Thermal fluctuations within this environment cause deformations of the ring system, lead to different environments of the single pigments or cause shifts in potential energy surfaces of the pigments and are also responsible for relaxation and dephasing processes.[2] The thermal fluctuations appear on very different time scales which in a rough approximation can be divided into three groups: (I) those that are much slower than the processes within the exciton manifold, such as slow deformations of the complete ring, (II) those that are much faster than the excitonic processes such as internal vibrations of the pigments or the protein matrix and (III) those processes that appear on the same time scale as the excitonic processes such as fast deformations of the ring structure or bending modes of parts of the protein matrix. Of course, the transitions between these classifications are smooth.[18]

However, in the present approach these three groups will only be segmented into two groups: quasi-static fluctuations that only vary slowly compared to the dynamics of the excitonic system and therefore are treated as time-independent variations $\delta\epsilon_i$ of the site energies ϵ_i within the pigment system. All other fluctuations are treated as dynamic disorder.

In the following the pigment system consisting of coupled two-level systems is treated as the relevant system (cf. section 2.3) while all other DOFs (the protein matrix, the internal DOFs of the pigments etc.) are treated as the bath. For *Rs. molischianum* with $M = 16$ pigments the system Hamiltonian reads

$$
\begin{aligned}
H_{\mathrm{S}} = \ & \epsilon_0 \left|0\right\rangle \left\langle 0\right| + \sum_{i=1}^{M} \left(\epsilon_i + \delta\epsilon_i\right) \left|i\right\rangle \left\langle i\right| \\
& + V \sum_{i=1}^{M-1} \left(\left|i+1\right\rangle \left\langle i\right| + \left|i\right\rangle \left\langle i+1\right|\right) + V \left(\left|1\right\rangle \left\langle M\right| + \left|M\right\rangle \left\langle 1\right|\right),
\end{aligned}
\tag{4.1}
$$

with $\left|0\right\rangle$ being the common ground state of the two-level systems and $\left|i\right\rangle$ being the excited state of the ith pigment. In the above case the dipole-dipole coupling strength between the pigments has been approximated by a constant term V and it has been assumed that due to the spatial distance of the pigments only nearest neighbors are affected by the coupling.

Since the remaining DOFs mainly describe vibrational motions of the surrounding proteins and the pigments itself, it is possible to describe these DOFs as a collection

of harmonic oscillators as discussed in section 2.5.1 with the Hamiltonian (2.26). In addition, due to the spatial distance of the pigments, their direct surroundings can be assumed to be independent from each other such that the bath can be split into a number of independent collections of harmonic oscillators. The structure of the protein matrix implies that the different parts of the bath are of the same type and also couple in the same way to the single pigments. Hence the coupling can be treated site-local. This becomes obvious in a semi-classical approach where the classical vibronic motion leads to fast fluctuations of the energy of the quantum mechanical excited electronic states of the single pigments.[18] In a first-order approximation these fluctuations are linear in the bath coordinates such that the site local coupling Hamiltonian (2.28) can be written as

$$H_{\mathrm{SB}} = \sum_{k=1}^{M} K_k \Phi_k = \sum_{k=1}^{M} a_k^+ a_k \sum_{\xi} c_{k\xi} x_{\xi}. \tag{4.2}$$

Here $a_k^+ = |k\rangle\langle 0|$ and $a_k = |0\rangle\langle k|$ are the creation and annihilation operators within the kth two-level system, respectively, and represent the system-part of the interaction. In site representation and excluding the ground state the matrix elements of the system parts of the interaction (4.2) are given by

$$\langle i| K_k |j\rangle = \delta_{ij}\delta_{ik}. \tag{4.3}$$

In the following and as mentioned above, the local bath approximation (2.58) is assumed to hold. Therefore the site indices in the bath parts are skipped in the following (cf. section 2.6.3) and the bath can be described by a single correlation function $C(t)$ or a single spectral density $J(\omega)$.

With the special form (4.3) of the interaction the renormalization term (2.32) has a rather simple form. Since $a_k^+ a_k$ is a projector onto the excited state of the kth pigment and the sum of all these projectors yields the identity operation in the excitonic system the renormalization can be expressed as

$$H_{\mathrm{ren}} = \lambda \sum_{k}^{M} |k\rangle\langle k|. \tag{4.4}$$

I.e. H_{ren} is scalar in the excitonic system and only yields a constant shift in the absorption spectra. Since the spectra will be shifted to match the experimental results the renormalization will be neglected in the following. The complete Hamiltonian of the model system for the B850 system therefore reads

$$H = H_{\mathrm{S}} + H_{\mathrm{SB}} + H_{\mathrm{B}} \tag{4.5}$$

with the definitions (4.1), (4.2) for the relevant system and the interaction with the bath and Eq. (2.26) for the bath Hamiltonian.

4.2 The linear absorption profile

As described in section 2.9 the linear absorption line-shape $I(\omega)$ is given by the Fourier transform of the dipole-dipole correlation function (2.109). Instead of propagating the density matrix, the dipole operator has to be propagated with the Hamiltonian (4.5). The dipole operator $\hat{\mu}$ in the present case is given by the transition dipoles

of the pigments which can be determined from the molecular structure of the BChl molecules.[18] Within the model of two-level systems the matrix elements of the dipole operator in site representation are given by

$$\langle 0| \, \hat{\mu} \, |j\rangle = \langle j| \, \hat{\mu} \, |0\rangle = \mathbf{d}_j \tag{4.6}$$

where $\mathbf{d}_j$ denotes the transition dipole vector between the ground and excited state of the jth pigment. The other matrix elements of the dipole operator are zero. Since the dipole operator connects only the electronic states of the pigments it is exclusively defined in the DOFs of the relevant system. For numerical evaluation of Eq. (2.106), therefore, the perturbative techniques discussed in chapter 2 can be used. The only difference here is that the reduced density matrix is replaced by the dipole operator such that based on the various second-order perturbative approaches different expressions for the linear absorption profile can be derived. At low temperatures such as room temperature only the electronic ground states of the pigments are populated so that the equilibrium density matrix W_{eq} in Eq. (2.106) can be expressed as

$$W_{\mathrm{eq}} = |0\rangle\langle 0|R_{\mathrm{eq}}. \tag{4.7}$$

Upon inserting Eqs. (4.6) and (4.7) in Eq. (2.107) the expression for the linear susceptibility becomes

$$
\begin{aligned}
\chi(t) \quad &\propto \quad -\mathrm{Im} \sum_{jk} \mathbf{d}_j \mathbf{d}_k \mathrm{tr} \left\{ U(t) \left(|j\rangle\langle 0| + |0\rangle\langle j| \right) |0\rangle\langle 0|R_{\mathrm{eq}}U^\dagger(t) \left(|k\rangle\langle 0| + |0\rangle\langle k| \right) \right\} \\
&\propto \quad -\mathrm{Im} \sum_{jk} \mathbf{d}_j \mathbf{d}_k \mathrm{tr} \left\{ U(t)|j\rangle\langle 0|R_{\mathrm{eq}}U^\dagger(t) \left(|k\rangle\langle 0| + |0\rangle\langle k| \right) \right\} \\
&\propto \quad -\mathrm{Im} \sum_{jk} \mathbf{d}_j \mathbf{d}_k \left[\mathrm{tr} \left\{ U(t)|j\rangle\langle 0|R_{\mathrm{eq}}U^\dagger(t)|k\rangle\langle 0| \right\} + \mathrm{tr} \left\{ U(t)|j\rangle\langle 0|R_{\mathrm{eq}}U^\dagger(t)|0\rangle\langle k| \right\} \right] \\
&\propto \quad -\mathrm{Im} \sum_{j} |\mathbf{d}_j|^2 \, \mathrm{tr} \left\{ U(t)|j\rangle\langle 0|R_{\mathrm{eq}}U^\dagger(t)|0\rangle\langle j| \right\}.
\end{aligned}
\tag{4.8}
$$

Here the last line has been obtained by noticing that the matrix element $\langle 0| \, U^\dagger(t) \, |k\rangle$ vanishes since by definition U does not induce any interaction between the ground and excited states and that the trace operation yields a δ_{jk} which cancels one of the sums. The expression within the trace can be interpreted as propagating a reduced density matrix with initial condition $\rho(0) = |j\rangle\langle 0|$ coupled to the reservoir $R(0) = R_{\mathrm{eq}}$ and later evaluating the matrix element $\rho_{j0}(t) = \langle j| \, \rho(t) \, |0\rangle$. Hence the various propagation schemes discussed in chapter 2 can be used.

It is often more convenient to evaluate the dipole correlation function (4.8) in energy representation where the linear susceptibility reads

$$\chi(t) \propto -\mathrm{Im} \sum_{\mu} |\mathbf{d}_\mu|^2 \, \mathrm{tr} \left\{ U(t)|\mu\rangle\langle 0|R_{\mathrm{eq}}U(t)^\dagger|0\rangle\langle \mu| \right\} \tag{4.9}$$

with the excitonic eigenstates $|\mu\rangle$ and the so-called transition dipole strength $|\mathbf{d}_\mu|^2$. The matrix element $\langle 0| \, U^\dagger(t) \, |0\rangle = \exp\left(i(\omega_0 + H_{\mathrm{B}})t\right)$ can be evaluated directly and χ can be written as

$$\chi(t) \propto \sum_{\mu} |\mathbf{d}_\mu|^2 \left(e^{i\omega_0 t} \mathrm{tr} \left\{ U(t)|\mu\rangle\langle \mu|R_{\mathrm{eq}}e^{iH_{\mathrm{B}}t} \right\} - e^{-i\omega_0 t} \mathrm{tr} \left\{ U^\dagger(t)|\mu\rangle\langle \mu|R_{\mathrm{eq}}e^{-iH_{\mathrm{B}}t} \right\} \right). \tag{4.10}$$

The two terms within the trace oscillate with positive and negative system frequencies and are called the resonant and the anti-resonant contribution, respectively. Since

in the Fourier domain one is only interested in the positive frequency range, the anti-resonant part containing the negative frequencies may be neglected.[2] Upon re-inserting $\langle 0 | U^\dagger(t) | 0 \rangle = \exp\left(i(\omega_0 + H_\mathrm{B})t\right)$ the expression for the linear susceptibility obeys the form

$$\chi(t) \propto \sum_\mu |\mathbf{d}_\mu|^2 \, \mathrm{tr}\left\{ U(t) | \mu \rangle \langle 0 | R_\mathrm{eq} U^\dagger(t) | 0 \rangle \langle \mu | \right\} \tag{4.11}$$

which might also be used to obtain the linear absorption spectrum. However, in this case care has to be taken if the spectrum is nonzero near $\omega = 0$ which is not the case in the present study. In the following a short review of existing methods for calculating the spectrum based on usual perturbative methods and two additional versions using the MRT based on a second-order cumulant expansion are given.

4.2.1 Second-order time-local theory

The second-order TL theory[93] is based on the perturbative treatment of the Hashitsume-Takahashi-Shibata identity (2.24) which has already been discussed in section 2.6.1. For the propagation of the dipole operator one can directly integrate the EOM (2.41) by only replacing the reduced density matrix ρ by the dipole operator $\hat{\mu}$. As already mentioned earlier the matrix elements of the operators Λ_k in Eq. (2.41) can be calculated in energy representation if the system Hamiltonian is time-independent. If this is not the case, EOMs for Λ_k can be derived as demonstrated in Ref. [76]. Utilizing the decomposition (2.66) of the bath correlation function the matrix elements of Λ_k can be expressed analytically as[76]

$$\langle \mu | \Lambda_k | \nu \rangle = \langle \mu | K_k | \nu \rangle \int_0^t dt' C(t') e^{-i\omega_{\mu\nu}t'} = \langle \mu | K_k | \nu \rangle \, \Theta(t, \omega_{\mu\nu}) \tag{4.12}$$

with the time-dependent function

$$\Theta(t, \omega_{\mu\nu}) = \sum_j^{n_\mathrm{r}} \alpha_j^\mathrm{r} \frac{1}{\gamma_j^\mathrm{r} - i\omega_{\mu\nu}} \left[e^{\left(\gamma_j^\mathrm{r} - i\omega_{\mu\nu}\right)t} - 1 \right] + i \sum_j^{n_\mathrm{i}} \alpha_j^\mathrm{i} \frac{1}{\gamma_j^\mathrm{i} - i\omega_{\mu\nu}} \left[e^{\left(\gamma_j^\mathrm{i} - i\omega_{\mu\nu}\right)t} - 1 \right] \tag{4.13}$$

and $\omega_{\mu\nu}$ being the transition frequency between the two eigenstates $|\mu\rangle$ and $|\nu\rangle$. At this point the advantage of the decomposition of the correlation function becomes obvious since Θ can be evaluated analytically to save numerical effort. It should be mentioned that, due to the local bath approximation (2.58), the sum in the definition (2.42) of Λ_k reduces to a single term. The Markovian form of the EOMs can be obtained by extending the integral leading to Eq. (4.13) to infinity[76] so that

$$\Theta(t \to \infty, \omega_{\mu\nu}) = -\sum_j^{n_\mathrm{r}} \frac{\alpha_j^\mathrm{r}}{\gamma_j^\mathrm{r} - i\omega_{\mu\nu}} - i \sum_j^{n_\mathrm{i}} \frac{\alpha_j^\mathrm{i}}{\gamma_j^\mathrm{i} - i\omega_{\mu\nu}}. \tag{4.14}$$

If in addition the imaginary part of Λ_k is neglected as discussed in section 2.6 one arrives at the well known Redfield EOMs.

In a totally symmetric ring without on-site disorder degenerate eigenstates exist, corresponding to wave functions traveling around the ring in positive and negative direction with the same energy. Due to the disorder the symmetry is broken and degenerate eigenstates are unlikely to appear so that the secular approximation according to Eqs. (2.52) and (2.53) can be applied to further reduce the numerical requirements.

4.2.2 Second-order TL Fourier method

It is interesting to note that due to the initial condition $\rho(0) = |j\rangle\langle 0|$ the second order TL EOM (2.41) simplifies to

$$\frac{\partial}{\partial t}\rho(t) = -i[H, \rho(t)] + \sum_k K_k \Lambda_k(t)\rho(t) \tag{4.15}$$

which describes the time evolution of the coherences between the ground state and the excitonic states. In eigenstate representation this equation reads

$$\rho_{\mu 0}(t) = -i\omega_{\mu 0}\rho_{\mu 0}(t) - \sum_{\nu\lambda} M_{\mu\nu\nu\lambda}\ \rho_{\lambda 0}(t) \int\limits_0^t d\tau\ C(\tau)e^{-i\omega_{\nu\lambda}\tau}. \tag{4.16}$$

Here the term

$$M_{\mu\nu\mu'\nu'} = \sum_k \langle\mu| K_k |\nu\rangle \langle\mu'| K_k |\nu'\rangle \tag{4.17}$$

has been defined for later convenience. Based on Eq. (4.16) Renger and Marcus proposed another method to calculate the approximate linear absorption spectrum of the B850 ring.[16] After applying the secular approximation (2.53) for the coherences Eq. (4.16) reduces to

$$\frac{\partial}{\partial t}\rho_{\mu 0}(t) = -i\omega_{\mu 0}\rho_{\mu 0}(t) - \sum_{\nu} M_{\mu\nu\nu\mu}\ \rho_{\mu 0}(t) \int\limits_0^t d\tau\ C(\tau)e^{-i\omega_{\nu\mu}\tau}. \tag{4.18}$$

This expression can be formally integrated as

$$\rho_{\mu 0}(t) = \exp\left[-i\omega_{\mu 0}t - \sum_{\nu} M_{\mu\nu\nu\mu} \int\limits_0^t d\tau\ (t-\tau)C(\tau)e^{-i\omega_{\nu\mu}\tau}\right]\rho_{\mu 0}(0). \tag{4.19}$$

Utilizing the decomposition (2.66) of the bath correlation function the integral in (4.19) can be evaluated as

$$
\begin{aligned}
M_{\mu\mu\mu\mu}\int\limits_0^t d\tau(t-\tau)C(\tau) &= M_{\mu\mu\mu\mu}\sum_j^{n_{\rm r}}\frac{\alpha_j^{\rm r}}{(\gamma_j^{\rm r})^2}\left(e^{\gamma_j^{\rm r}t} - 1 - \gamma_j^{\rm r}t\right) + iM_{\mu\mu\mu\mu}\sum_j^{n_{\rm i}}\frac{\alpha_j^{\rm i}}{(\gamma_j^{\rm i})^2}\left(e^{\gamma_j^{\rm i}t} - 1 - \gamma_j^{\rm i}t\right) \\
&= G_{\mu\mu\mu\mu}(t)
\end{aligned}
\tag{4.20}
$$

for the diagonal terms with $\mu = \nu$ and the off-diagonal terms with $\mu \neq \nu$ yield

$$\sum_{\nu\neq\mu} M_{\mu\nu\nu\mu}t\int\limits_0^t d\tau(t-\tau)C(t-\tau)e^{-i\omega_{\nu\mu}\tau} = \sum_{\nu\neq\mu} M_{\mu\nu\nu\mu}\int\limits_0^t d\tau\ \Theta(\tau, \omega_{\mu\nu}). \tag{4.21}$$

In their proposal Renger and Marcus suggested the application of the Markov approximation for the off-diagonal elements, i.e., setting

$$
\begin{aligned}
\sum_{\nu\neq\mu} M_{\mu\nu\nu\mu}t\int\limits_0^t d\tau(t-\tau)C(t-\tau)e^{-i\omega_{\nu\mu}\tau} &\approx \sum_{\nu\neq\mu} M_{\mu\nu\nu\mu}\int\limits_0^t d\tau\ \Theta(\tau\to\infty, \omega_{\mu\nu}) \\
&\approx \sum_{\nu\neq\mu}\Gamma_{\mu\nu\nu\mu}t
\end{aligned}
\tag{4.22}
$$

where $\Gamma_{\mu\nu\mu'\nu'}$ has been defined in Eq. 2.47. It is interesting to note that the real part of $\Gamma_{\mu\nu\nu\mu}$ contains the so-called population transfer rates

$$k_{\mu\nu} = 2\,\mathrm{Re}\,\Gamma_{\mu\nu\nu\mu} \tag{4.23}$$

out of state $|\mu\rangle$ into state $|\nu\rangle$ so that the sum in Eq. (4.22) contains the complete outflow of population from state $|\mu\rangle$. In addition, the imaginary part of $\Gamma_{\mu\nu\nu\mu}$ causes a frequency shift in the Fourier domain which is, however, canceled to some extent by the imaginary parts of G. The integrated EOM (4.19) then reads

$$\rho_{\mu0}(t) = \exp\left[-i\omega_{\mu0}t - G_{\mu\mu\mu\mu}(t) - \sum_{\nu\neq\mu}\Gamma_{\mu\nu\nu\mu}t\right]\rho_{\mu0}(0) \tag{4.24}$$

such that the absorption line shape (2.109) can be calculated as the Fourier transform of the resonant part of the linear susceptibility (4.11) according to

$$
\begin{aligned}
I(\omega) &\propto \mathrm{Re}\int_0^\infty dt\,e^{i\omega t}\chi(t)\\
&\propto \mathrm{Re}\sum_\mu|\mathbf{d}_\mu|^2\int_0^\infty dt\,\exp\left[i(\omega-\omega_{\mu0})t - G_{\mu\mu\mu\mu}(t) - \sum_{\nu\neq\mu}\Gamma_{\mu\nu\nu\mu}t\right].
\end{aligned}
\tag{4.25}
$$

This method will be called the TL Fourier method in the following. Upon neglecting the imaginary part of Γ this expression reads

$$I(\omega) \propto \mathrm{Re}\sum_\mu|\mathbf{d}_\mu|^2\int_0^\infty dt\,\exp\left[i(\omega-\omega_{\mu0})t - G_{\mu\mu\mu\mu}(t) - \frac{1}{2}\sum_{\nu\neq\mu}R_{\mu\mu\nu\nu}t\right] \tag{4.26}$$

where $R_{\mu\mu\nu\nu}$ is the Redfield tensor according to Eq. (2.46).

It is interesting to see that the line-shape formula (4.25) contains three different contributions. Without coupling to a thermal bath the absorption spectrum would be given as a number of delta functions at the transition frequencies $\omega_{\mu0}$. However, due to the coupling two additional terms appear leading to a broadening of the line shapes. The so-called line broadening functions $G_{\mu\mu\mu\mu}(t)$ describe the pure dephasing, i.e. a loss of coherence of the excited states because of the coupling to the bath, which leads to a broadening of the absorption line shape. The second additional contribution stems from the population transfer rates $\Gamma_{\mu\nu\nu\mu}$ which describe the transfer of population out of state $|\mu\rangle$ into state $|\nu\rangle$ such that the sum in Eq. (4.25) leads to a broadening of the line shape due to the limited life time of the excitonic states.

4.2.3 Second-order TNL theory

Analogous to the previous method also the second-order TNL theory based on the Nakajima-Zwanzig identity (2.23) can be applied to obtain the linear absorption line-shape. The respective EOM (2.54) can be directly applied for propagating the matrix elements of the dipole operator in Eq. (4.8). As mentioned above, this can be done with help of the decomposition of the bath correlation function (2.65) and the definition of auxiliary density matrices. However, as in the previous subsections the EOM of the reduced density matrix simplifies due to the initial conditions to

$$\frac{\partial}{\partial t}\rho_{\mu0}(t) = -i\omega_{\mu0}\rho_{\mu0}(t) - \sum_{\nu\lambda}M_{\mu\nu\nu\lambda}\int_0^t d\tau\,C(t-\tau)e^{-i\omega_{\nu0}(t-\tau)}\rho_{\lambda0}(\tau), \tag{4.27}$$

which further simplifies after invoking the secular approximation (2.53) for the coherences to

$$\frac{\partial}{\partial t}\rho_{\mu 0}(t) = -i\omega_{\mu 0}\rho_{\mu 0}(t) - \sum_\nu M_{\mu\nu\nu\mu} \int_0^t d\tau \; C(t-\tau)e^{-i\omega_{\nu 0}(t-\tau)}\rho_{\mu 0}(\tau). \qquad (4.28)$$

This expression is a convolution integral that can be evaluated by applying the Laplace transformation to both sides and using the convolution and differentiation theorems. The half-sided Fourier transform can be obtained from the Laplace transform by letting the real part s of the image variable $p = s + i\omega$ go to zero. The Laplace transformation yields

$$p \; \rho_{\mu 0}(p) - \rho_{\mu 0}(0) = -i\omega_{\mu 0}\rho_{\mu 0}(p) - \sum_\nu M_{\mu\nu\nu\mu}\rho_{\mu 0}(p) \int_0^\infty dt \; C(t)e^{-(p+i\omega_{\nu 0})t}. \qquad (4.29)$$

This equation can be easily solved for $\rho_{\mu 0}(p)$. The remaining integral

$$\int_0^\infty dt \; C(t)e^{-(p+i\omega_{\nu 0})t} = C(p + i\omega_\nu), \qquad (4.30)$$

can be evaluated in two different ways: either using the decomposition (2.66) of the bath correlation function or, as proposed by Renger and May,[14] by expressing $C(t)$ in the Fourier domain as $C(\omega')$. In the latter case care has to be taken when letting s tend to zero since this results in a Cauchy principal value integral for the imaginary part of $C(p + i\omega_\nu)$. Using $\rho_{\mu 0}(0) = 1$ and following the procedure proposed by Renger and May[14] the absorption line shape is given as

$$I(\omega) \propto \sum_\mu \frac{d_\mu C_\mu^{\mathrm{r}}(\omega)}{\left(\omega - \omega_{\mu 0} - C_\mu^{\mathrm{i}}(\omega)\right)^2 + \left(C_\mu^{\mathrm{r}}(\omega)\right)^2} \qquad (4.31)$$

where the abbreviations

$$C_\mu^{\mathrm{r}}(\omega) \;=\; \sum_\nu M_{\mu\nu\nu\mu} C^{\mathrm{r}}(\omega_{\nu 0} - \omega) = \sum_\nu M_{\mu\nu\nu\mu} \frac{J(\omega_{\nu 0} - \omega)}{e^{\beta(\omega_{\nu 0}-\omega)} - 1} \qquad (4.32)$$

$$C_\mu^{\mathrm{i}}(\omega) \;=\; \sum_\nu M_{\mu\nu\nu\mu} C^{\mathrm{i}}(\omega_{\nu 0} - \omega) = \sum_\nu M_{\mu\nu\nu\mu} \wp \int_{-\infty}^\infty \frac{d\omega'}{\pi} \; \frac{J(\omega')}{[e^{\beta\omega'} - 1]\,[\omega' - (\omega_{\nu 0} - \omega)]} \qquad (4.33)$$

have been defined. The symbol $\wp$ in Eq. (4.33) indicates the above mentioned principal value integral.

4.2.4 The hierarchical approach

As indicated in Eq. (4.11), it is not necessary to treat the complete density matrix but only the first column to obtain the linear absorption spectrum of the present model system. This is the case because the time evolution operator does not yield transfers to any other matrix elements if the initial state is chosen to be $\rho(0) = |\mu\rangle\langle 0|$. Inserting this initial state into the hierarchy (2.88) one notices that the commutators with the system part of interaction K_k reduce to simple matrix-vector multiplications. For numerical purposes it is therefore possible to establish a simpler hierarchy containing

only the first column vector of the auxiliary density matrices. The hierarchy (2.88) therefore simplifies to

$$
\begin{aligned}
\frac{d\rho^{(1)}_{\{I\}}(t)}{dt} &= \left(\sum_k^N \left(\sum_n^{n_{\mathrm{r}}} \gamma_n^{\mathrm{r}}\, I_{(k-1)(n_{\mathrm{r}}+n_{\mathrm{i}})+n} + \sum_n^{n_{\mathrm{i}}} \gamma_n^{\mathrm{i}}\, I_{(k-1)(n_{\mathrm{r}}+n_{\mathrm{i}})+n+n_{\mathrm{r}}} \right) - i\,(H_{\mathrm{S}} - \epsilon_0) \right) \rho^{(1)}_{\{I\}}(t) \\
&+ \sum_k^N K_k \sum_n^{n_{\mathrm{r}}+n_{\mathrm{i}}} \rho^{(1)}_{\{I;I_{(k-1)(n_{\mathrm{r}}+n_{\mathrm{i}})+n}+1\}} \\
&+ \sum_k^N K_k \sum_n^{n_{\mathrm{r}}} \alpha_n^{\mathrm{r}}\, I_{(k-1)(n_{\mathrm{r}}+n_{\mathrm{i}})+n}\, \rho^{(1)}_{\{I;I_{(k-1)(n_{\mathrm{r}}+n_{\mathrm{i}})+n}-1\}} \\
&+ \sum_k^N K_k \sum_n^{n_{\mathrm{i}}} \alpha_n^{\mathrm{i}}\, I_{(k-1)(n_{\mathrm{r}}+n_{\mathrm{i}})+n_{\mathrm{r}}+n}\, \rho^{(1)}_{\{I;I_{(k-1)(n_{\mathrm{r}}+n_{\mathrm{i}})+n_{\mathrm{r}}+n}-1\}}.
\end{aligned} \tag{4.34}
$$

Here the superscript (1) indicates that only the first column of the auxiliary density matrices is used. This scheme has the numerical advantage that matrix-matrix multiplications are replaced by matrix-vector multiplications and that the number of operations with the system-bath interaction is reduced to one half of the number of operations used in the original scheme.

4.2.5 Modified Redfield approach

In addition to the usual second-order schemes discussed above also, the MRT (cf. section 2.8) can be used to determine the linear absorption profile. After application of the secular approximation the resonant part (4.11) of the linear susceptibility reads

$$
\chi(t) \propto \sum_\mu |\mathbf{d}_\mu|^2 \ \mathrm{tr}\left\{ |0\rangle \langle \mu| e^{-iHt} R_{\mathrm{eq}} |\mu\rangle \langle 0| e^{iHt} \right\}. \tag{4.35}
$$

Here the cyclic invariance of the trace has been used to rearrange the operators. This expression can be approximately evaluated by using the splitting (2.92) of the total Hamiltonian. Changing to the interaction picture according to H_0 and expanding the the time-evolution operator up to second order in H' yields

$$
\begin{aligned}
\chi(t) &\propto \sum_\mu |\mathbf{d}_\mu|^2 \ \mathrm{tr}\left\{ |0\rangle \langle \mu| e^{-iH_0 t} \left(\vec{T} e^{-i\int_0^t d\tau H'(\tau)} \right) R_{\mathrm{eq}} |\mu\rangle \langle 0| \left(\overleftarrow{T} e^{i\int_0^t d\tau H'(\tau)} \right) e^{iH_0 t} \right\} \\
&\approx \sum_\mu |\mathbf{d}_\mu|^2 \ e^{-i\omega_{\mu 0} t + i\lambda_{\mu\mu\mu\mu} t} \\
&\quad \mathrm{tr}\left\{ e^{-iH_{\mathrm{B}}(\mu)t} \left(1 - \sum_{\nu \neq \mu} \int_0^t d\tau \int_0^\tau d\tau' H'(\tau) |\nu\rangle \langle \nu| H'(\tau') \right) |\mu\rangle \langle \mu| R_{\mathrm{eq}} e^{iH_{\mathrm{B}} t} \right\}.
\end{aligned} \tag{4.36}
$$

The terms under the trace can be evaluated using the second-order cumulant expansion technique with respect to the system bath interaction. Here the linear contributions of H' vanish and have been omitted. The first term to zeroth order in H' that only contains the diagonal elements of H_{SB} can be approximated as

$$
\mathrm{tr}\left\{ e^{-iH_{\mathrm{B}}(\mu)t} |\mu\rangle \langle \mu| R_{\mathrm{eq}} e^{iH_{\mathrm{B}} t} \right\} \approx 1 - G_{\mu\mu\mu\mu}(t) - i\lambda_{\mu\mu\mu\mu} t. \tag{4.37}
$$

The second term in Eq. (4.36) that also contains the off-diagonal elements of H_{SB} can be rewritten as

$$\mathrm{tr}\left\{ e^{-iH_B(\mu)t} \sum_{\nu\neq\mu} \int_0^t d\tau \int_0^\tau d\tau' H'(\tau) \left|\nu\right\rangle \left\langle\nu\right| H'(\tau') \left|\mu\right\rangle \left\langle\mu\right| R_{eq} e^{iH_B t} \right\}$$

$$= \sum_{\nu\neq\mu} \int_0^t d\tau \int_0^\tau d\tau' \, \mathrm{tr}\left\{ H'(\tau) \left|\nu\right\rangle \left\langle\nu\right| H'(\tau') \left|\mu\right\rangle \left\langle\mu\right| R_{eq} e^{iH_B t} e^{-iH_B(\mu)t} \right\} . \tag{4.38}$$

For weak diagonal coupling the following approximations can be performed: (I) $e^{iH_B t} e^{-iH_B(\mu)t} \approx 1$ and (II) $R_{eq} \approx R_{eq}^\mu$. Neglecting the imaginary parts Eq. (4.38) simplifies to

$$\sum_{\nu\neq\mu} \int_0^t d\tau \int_0^\tau d\tau' \, \mathrm{tr}\left\{ H'(\tau) \left|\nu\right\rangle \left\langle\nu\right| H'(\tau') \left|\mu\right\rangle \left\langle\mu\right| R_{eq} e^{iH_B t} e^{-iH_B(\mu)t} \right\}$$

$$\approx \mathrm{Re} \sum_{\nu\neq\mu} \int_0^t d\tau \int_0^\tau d\tau' \mathrm{tr}\left\{ \left|\nu\right\rangle \left\langle\nu\right| \exp\left(-iH_0\tau'\right) H' \left|\mu\right\rangle \left\langle\mu\right| R_{eq}^\mu \exp\left(iH_0\tau'\right) H' \right\}$$

$$\approx \frac{1}{2} \sum_{\nu\neq\mu} \int_0^t d\tau \, \overline{R}_{\nu\nu\mu\mu}(\tau) \tag{4.39}$$

which, except for a factor of one half, can be approximated by the time-dependent modified Redfield tensor[17,89] (cf. appendix B). After reassembling Eqs. (4.37) and (4.39) according to the cumulant expansion technique into an exponential function the linear susceptibility is given by

$$\chi(t) \approx \sum_\mu \left|\mathbf{d}_\mu\right|^2 \exp\left(-i\omega_{\mu0}t - G_{\mu\mu\mu\mu}(t) - \frac{1}{2} \sum_{\nu\neq\mu} \int_0^t d\tau \overline{R}_{\nu\nu\mu\mu}(\tau) \right) . \tag{4.40}$$

It is interesting to see that after invoking the Markov approximation the Redfield tensor becomes time-independent such that the integral changes into a multiplication with t and the linear susceptibility becomes

$$\chi(t) \approx \sum_\mu \left|\mathbf{d}_\mu\right|^2 \exp\left(-i\omega_{\mu0}t - g_{\mu\mu\mu\mu}(t) - \frac{1}{2} \sum_{\nu\neq\mu} \overline{R}_{\nu\nu\mu\mu}t \right) . \tag{4.41}$$

Note the structural similarities of the expressions (4.40) and (4.41) with the expressions (4.25) and (4.26) obtained with the standard second-order TL scheme. The pure dephasing contributions are the same but the standard Redfield tensor (2.46) has been replaced by the modified Redfield tensor (2.100). In the limit of vanishing diagonal coupling the equations obtained with the MRT and the TL theory are identical.

It should be mentioned that Ohta *et al.*[15] and others[94] also used a method they called MRT. However this method is, except from the imaginary parts of the population transfer rates, identical to the TL Fourier method[16] with Markov approximation as described in section 4.2.2. The confusion in the nomenclature most likely arises from the fact that parts of the line-shape formula used in Ref. [15] can be derived using the cumulant expansion technique which is also used to the derive the modified Redfield tensor.

4.3 Line broadening mechanisms

As discussed above, the formulas for the linear absorption spectrum basically contain two types of line broadening mechanisms which can especially be identified in Eqs. (4.25) and (4.40) or (4.41). These mechanisms are population transfer and pure dephasing. Within Redfield theory with secular approximation the damping of the reduced density matrix in energy representation is only determined by the population transfer rates for the diagonal parts and pure dephasing rates for the off-diagonal parts. This allows for the deduction of two characteristic times of the model system, the inverse life time

$$\frac{1}{T_{1,\mu}} = \sum_{\nu \neq \mu} k_{\mu\nu} \tag{4.42}$$

of an excitonic state μ and the inverse dephasing times $1/T_{2,\mu\nu}$, i.e. the inverse life time of the coherences. The latter can be determined by considering those terms of the Redfield tensor (2.46) that connect $\dot{\rho}_{\mu\nu}$ with $\rho_{\mu\nu}$ where $\mu \neq \nu$. This yields[95]

$$\begin{aligned} \frac{1}{T_{2,\mu\nu}} &= \sum_{\nu' \neq \mu} \tfrac{1}{2} k_{\mu\nu'} + \tfrac{1}{2} \sum_{\mu' \neq \nu} k_{\nu\mu'} + \mathrm{Re} \sum_k \left(\langle\mu| K_k |\mu\rangle - \langle\nu| K_k |\nu\rangle \right)^2 \Theta(t \to \infty, 0) \\ &= \frac{1}{2T_{1,\mu}} + \frac{1}{2T_{1,\nu}} + \frac{1}{T_{2,\mu\nu}^*}. \end{aligned} \tag{4.43}$$

The inverse life time of the coherence term between the two different states $|\mu\rangle$ and $|\nu\rangle$ is therefore given by the inverse life times of the respective populations and additional terms $1/T_{2,\mu\nu}^*$ also called the pure dephasing rates. When applying the Markov approximation the line broadening function turns to

$$\mathrm{Re}\, G_{\mu\mu\mu\mu}(t) \to \mathrm{Re}\, \Gamma_{\mu\mu\mu\mu} t = \frac{t}{T_{2,\mu0}^*} \tag{4.44}$$

which is proportional to the pure dephasing rate of the coherence element between the ground state and the excitonic state $|\mu\rangle$.

4.4 Results

In the following the optical line shapes obtained with the various methods discussed above are presented. In particular, the average line shape of 2000 disorder configurations of the Hamiltonian (4.1) and the line shape of one single realization are shown. For this four different spectral densities are used: three Ohmic spectral densities of the form

$$J(\omega) = \eta\omega \exp\left(-\omega/\omega_c\right) \tag{4.45}$$

with exponential cutoff determined by the cutoff frequency ω_c and a scaling parameter η and one spectral density obtained from the MD simulation published in Ref. [18]. Fig. 4.2 shows the different spectral densities that were used. The three ohmic spectral densities were chosen to demonstrate the influence of the bath correlation time which is determined by the cutoff frequency. The spectral density obtained with the MD simulation has maxima at several different frequencies leading to different correlation times. The effects induced by this spectral density therefore can, in a sense, be seen as a mixture of the three Ohmic spectral densities.

As in the previous chapters, also here the coupling strength has been kept constant according to Eq. (3.7) in all examples. The Ohmic spectral densities have been fitted
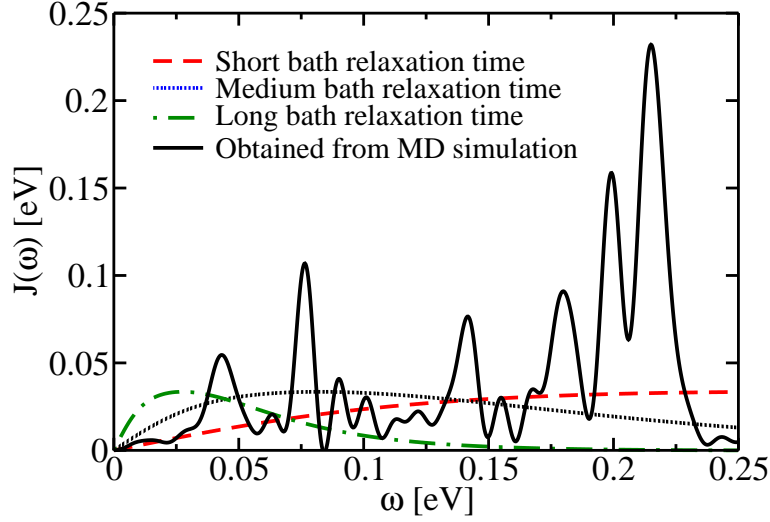
Figure 4.2: Different spectral densities used for calculating the absorption line shape

with three parameter sets p_j, Ω_j and Γ_j according to Eq. (2.62) where the parameters have been taken from Ref. [85]. The spectral density obtained from the MD simulation has been fitted with 21 parameter sets that were obtained with an optimization routine. Depending on the actual form of $J(\omega)$ 5 to 20 Matsubara frequencies had to be taken into account to reproduce the temperature dependency of the bath correlation function in time domain. In all calculations the temperature has been set to 300 K.

The values of the on-site energies $\epsilon_i = \epsilon$ in Eq. (4.1) (except for the ground state energy $\epsilon_0 = 0$) as well as the values of the transition dipoles have been taken from Ref. [18]. Here the transition dipoles were calculated as the time average of the dipoles obtained from the 400 fs MD simulation published in Ref. [18]. The precise value of ϵ, however, is of less importance since the spectra are shifted to match the experimental results anyway. The on-site disorder $\delta\epsilon_i$ of the site energies has been chosen randomly and Gaussian distributed with standard deviation $\sigma = 0.04$ eV. The particular realizations of the on-site disorder, however, are the same in all calculations. This is especially important for the single sample such that the only difference in results stems from the method of calculating the line shape and the different spectral densities. According to various values published in the literature[96, 97, 98] the coupling between neighboring pigments has been chosen to be 0.048 eV. The dipoles used in all calculations and the values of the on-site energies of the individual sample are given in table 4.1.

To allow for a better understanding of the spectra displayed below Fig. 4.3 shows the linear absorption spectrum of the ensemble average and the particular chosen sample obtained without coupling to a thermal bath. In this case the spectrum is obtained as a stick spectrum where the height of the sticks is weighted with the respective dipole strength. In Fig. 4.3 it is nicely visualized that the static disorder leads to a broadening of the ensemble line shape. In case of no disorder only one main peak is visible[5] belonging to both the second and third excitonic eigenstates which are degenerate and therefore appear as a single contribution. The dipole strength of all other states is almost zero. In case of the sample with on-site disorder the dipole strength is mainly distributed among the three lowest excitonic levels but also higher exciton states on the short wavelength side contribute to the spectrum. In the ensemble average (in this case over 10^6 realizations) the spectrum becomes a smooth

On-site	Dipoles [arbitrary units]		
energies [eV]	x	y	z
1.510	0.985	0.147	0.077
1.448	-0.946	-0.296	0.121
1.461	0.588	0.802	0.102
1.421	-0.426	-0.896	0.120
1.442	-0.040	0.993	0.104
1.407	0.329	-0.939	0.089
1.451	-0.750	0.649	0.116
1.433	0.817	-0.548	0.175
1.506	-0.930	-0.351	0.102
1.502	0.950	0.188	0.243
1.460	-0.655	-0.746	0.113
1.422	0.476	0.878	0.049
1.431	0.039	-0.998	0.048
1.363	-0.346	0.933	0.088
1.495	0.766	-0.633	0.107
1.430	-0.946	0.314	0.076

Table 4.1: Energies of the pigments of the single sample shown and dipoles used for all samples

and broad function in which the higher frequencies only contribute because of the disorder.
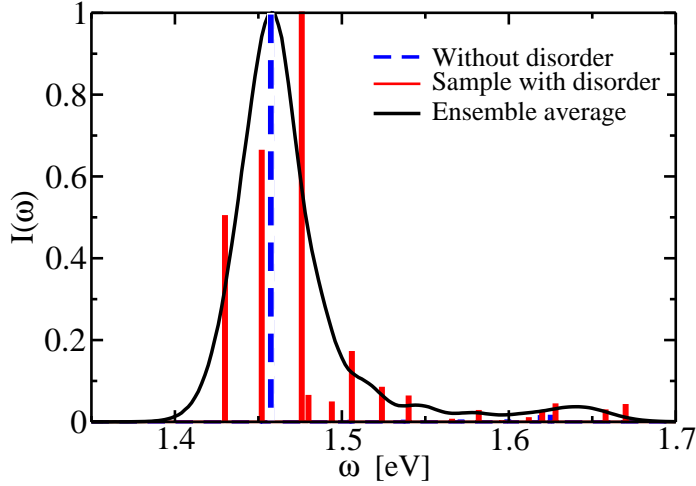
Figure 4.3: Absorption line shape obtained without damping.

4.4.1 Ohmic spectral density

Small bath relaxation time

The absorption line shapes obtained with the Ohmic spectral density for a short bath correlation time, i.e. $\omega_c = 0.272$ eV, are presented in Figs. 4.4 to 4.7. The normalization of the spectra of the single samples has been chosen such that

$$\int_0^t I(\omega)d\omega = \mathrm{const} \tag{4.46}$$

This is equivalent to providing the same $\chi(0)$ in all calculations. The ensemble spectra are normalized to a maximum height of unity, which enables a comparison with experimental data. Here a normalization according to an integral cannot be used since in the experimental spectrum a clear distinction between contributions of the B800 and B850 rings cannot be made.
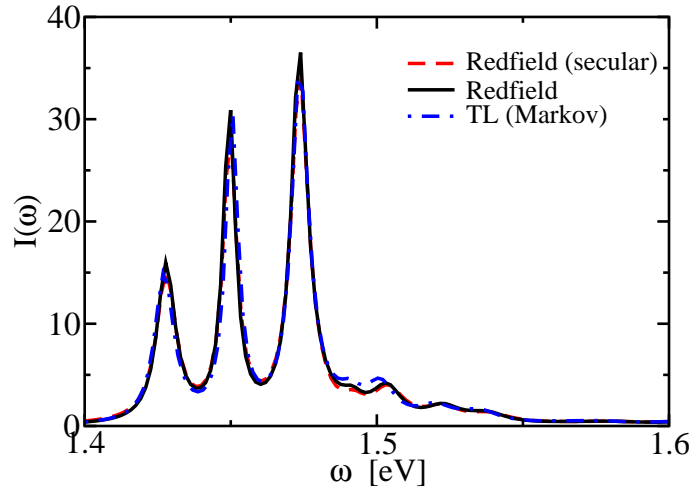
Figure 4.4: Line shape of the single sample of the B850 ring obtained with different Markovian methods for an Ohmic spectral density with $\omega_c = 0.272$ eV and $\eta = 0.34$.

In the following not all curves obtained with the various methods discussed above are shown since some of the methods yield very similar results as demonstrated in Fig. 4.4 where line shapes of one sample obtained with the second order Markovian methods are shown. Here the time evolution in Eq. (4.9) has been directly evaluated by propagating the reduced density matrix using Redfield theory with and without secular approximation and with the TL scheme with Markov approximation. These methods are described in section 2.6.1. One recognizes three main peaks in the lower frequency range and small additional contributions at higher frequencies as also observed in Fig. 4.3 for the single sample without damping. While in the stick spectrum the peaks correspond to delta-like functions, in Fig. 4.4 the peaks are broadened due to the influence of the bath. The curves in this figure, however, do not differ significantly. Only the Markovian TL method yields small additional contributions around $\omega = 1.5$ eV while otherwise the curves lie almost on top of each other. A similar behavior has also been observed for the other realizations. In the remaining figures,

therefore, the curves obtained with Redfield theory with and without secular approximation will not be shown and only the curve obtained with the Markovian TL method including the Lamb shift will be displayed representatively for all second-order Markovian methods.

In Fig. 4.5 the direct second-order TL and TNL schemes (2.41) and (2.54) are compared with the respective Fourier schemes (4.31) and (4.25). Due to the normalization according to Eq. (4.46) the maximum heights of the spectra are different. Here the peaks of the spectra obtained with the TNL methods are narrower than the peaks obtained with the TL methods. Broadening of the line shape due to damping therefore results in a reduction of the maximum height of the spectra. If the spectra were normalized to a maximum height of unity one would observe larger deviations in the minima between the peaks,
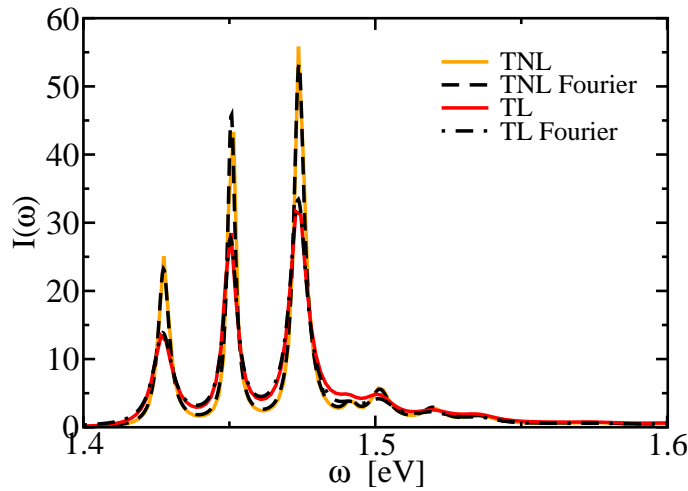

Figure 4.5: Same parameters as in Fig. 4.4 but a comparison of the non-Markovian TL and TNL methods with the respective Fourier variants.

The main difference between the direct and the Fourier methods is that the latter involve the secular approximation. In addition, the absorption formula of the TL Fourier method contains both, elements with and without Markov approximation, which can lead to different results compared to the usual TL formalism. This is demonstrated below for long bath correlation times where these effects are larger. The curves obtained with the TL Fourier method do not differ significantly from those obtained with the direct TL algorithm as shown in Fig. 4.5. Here both schemes only differ slightly around $\omega = 1.5$ eV. The results obtained with the TL Fourier method will not be shown in comparison with other methods for small and medium bath correlation times. The curves obtained with the TNL and TNL Fourier scheme lie almost on top of each other. In the other samples, only very small deviations have been observed so that in the remaining figures only the curve obtained with the TNL Fourier method will be shown. Both examples and the curves presented in Fig. 4.4, however, indicate that for the present model the secular approximation does not have a significant influence on the absorption line-shape.

In Fig. 4.6 the line shapes obtained with the non-Markovian second-order schemes

as well as those obtained with the MRT method (4.41) and with the TDMRT scheme (4.40) are displayed for a single sample. Here and in the following the imaginary parts of the pure dephasing within the MRT and TDMRT have been neglected as well since neglecting only the imaginary parts of one, the population transfer rates or the pure dephasing leads to artificial shifts in the relative peak positions. It can be seen that in all cases the three main peaks are clearly resolved. The line shapes obtained
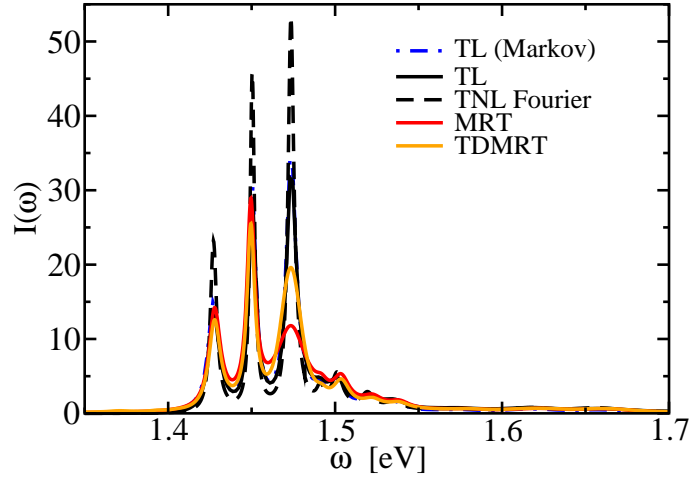

Figure 4.6: Same as Fig. 4.4 but for non-Markovian methods.

with the Markovian and non-Markovian TL method lie almost on top of each other except for some small deviations around $\omega = 1.5$ eV and slightly different maxima of the peaks. In contrast, the line shape obtained with the TNL method differs from the previous ones to some extent. Especially the minima between the peaks are lower and the absolute heights of the peaks are almost twice as large compared to the spectra obtained with the TL methods. A different behavior can be observed for the the line shapes obtained with the MRT and TDMRT methods. Strong damping leads to a broadening of the third peak which does, in contrast to the other spectra, not determine the maximum height of the line shapes. The first and the second peaks, however, are of comparable height and shape as those obtained with the TL methods. Interestingly the third peak of the spectrum calculated with the TDMRT method is higher than that obtained with its Markovian form. An explanation of this effect is the absence of damping at the initial moment in the TDMRT case. Here the damping slowly builds up with increasing time while, within the MRT formula, the full damping terms already contribute from the beginning. The strong broadening in this case also leads to additional contributions at the positions of the first and second peaks such that these peaks appear slightly higher than those obtained with the TDMRT method. On the high frequency side these effects are weaker due to the relatively small height of the peaks and stronger damping in this region.

In the ensemble average displayed in Fig. 4.7 all methods yield agreeing results and the single curves lie almost on top of each other. The main difference compared to the single realization shown above is that the ensemble line shapes are less structured. The ensemble line shapes are of almost Lorentzian shape with additional contributions at higher frequencies and are very similar to the ensemble line shape shown in
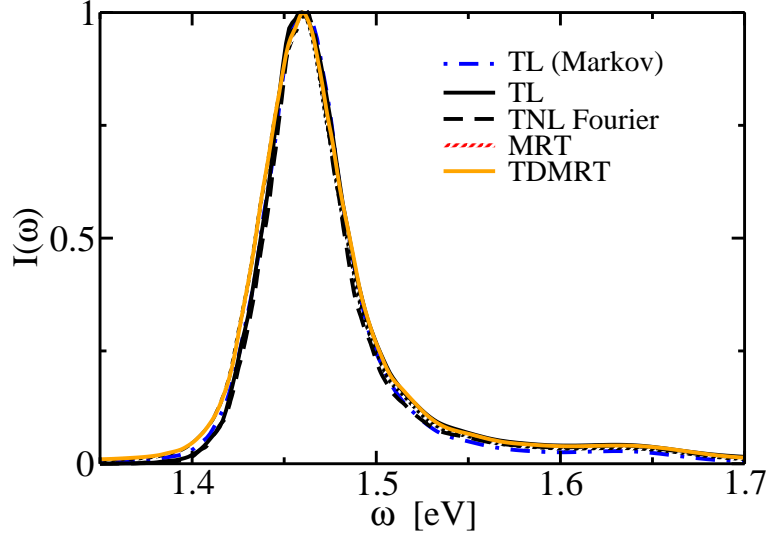
Figure 4.7: Same as Fig. 4.6 but in the ensemble average.

Fig. 4.3, though slightly broader, which can be explained by the broadening of the single realizations. The disorder leads to broadening in the ensemble average due to the superposition of the peaks of the single realizations that are mainly distributed around the maximum of the ensemble line shape shown in Fig. 4.7. The contributions at higher frequencies also stem from additional contributions due to the disorder as already described above. Hence, the width of the ensemble line shape in this case is dominated by disorder and not by dissipation.

Medium bath relaxation time

In Fig. 4.8 the line shapes obtained for a larger bath correlation time, i.e. $\omega_c = 0.081$ eV are depicted for the single realization. The increase of the bath correlation time causes larger broadening effects of the individual peaks compared to the previous example. The broadening effects also lead to a reduction of the absolute height of the spectra compared to those displayed in Fig. 4.6. In the line shape calculated with the TNL method all three peaks, especially the first one, are still resolved while this is hardly the case in the other line shapes where the first peak becomes a shoulder of the second. The TNL method yields very different results compared to the others. The maximum value as well as the differences between the minima and maxima of the TNL line shape are much larger compared to the spectra obtained with the other methods.

Also the deviations between the Markovian and the non-Markovian TL schemes are slightly increased, in particular the Markovian TL method yields a slightly broader line shape, especially on the low frequency side, than the non-Markovian variant. This can also be explained with a build up of damping with increasing time. The line shape obtained with the TDMRT has changed significantly compared to the previous case. The third peak now determines the maximum height while this is not the case for the MRT line shape. For the first two peaks the TDMRT method yields comparable results as the TL approach, while the maximum heights of these two peaks obtained with the MRT method are again slightly higher. In the ensemble average displayed in Fig. 4.9 the differences are still small. All curves are of comparable width but due
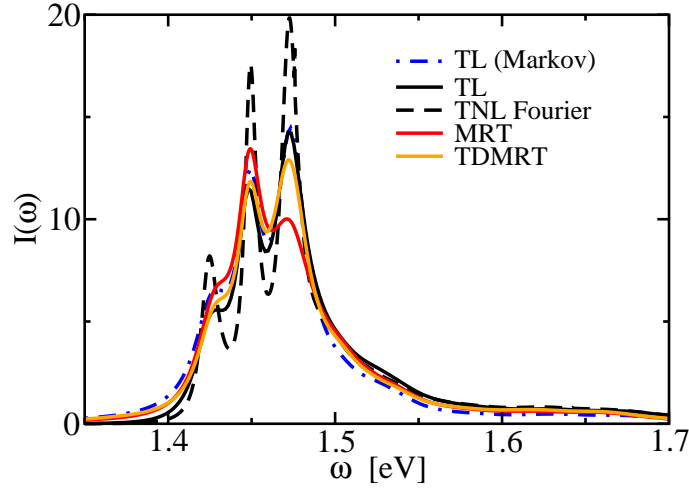
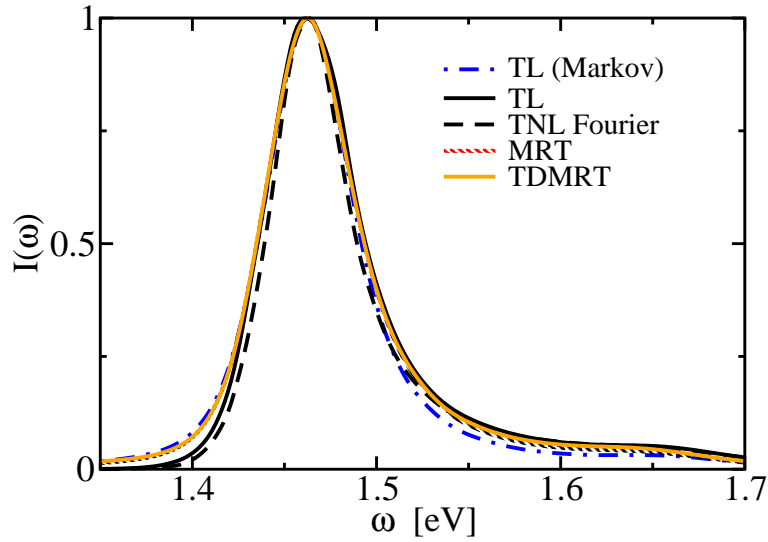Figure 4.8: Same as Fig. 4.6 but for $\omega_c = 0.081$ eV and $\eta = 1.12$.

Figure 4.9: Same as Fig. 4.7 but for $\omega_c = 0.081$ eV and $\eta = 1.12$.

to stronger damping slightly broader than in Fig. 4.7. Small effects, however, can be observed. The width of the TNL curve is slightly smaller than that of the others and the TDMRT and MRT methods yield the broadest line shapes.

Large bath relaxation time

The line shapes of the individual sample obtained for the large bath correlation time are presented in Fig. 4.10. Here the cut-off frequency has been reduced to $\omega_c = 0.027$ eV which results in a clear broadening of the spectra due to stronger damping. This causes a further reduction of the maximum height of the spectra. Except for the line shape obtained with the TNL method the single peaks are no longer resolved, i.e., the

broadening due to damping becomes comparable to the broadening due to the disorder. The difference between the TNL line shape and those obtained with the other methods is even larger than in the previous case. On the other hand the TL, MRT and TDMRT approaches now yield comparable results with only small differences, mainly around the maximum and the low frequency edge of the spectra. The line shape obtained with Markovian TL method differs significantly from all others especially for low frequencies where the damping leads to a broadening of the spectrum and due to the normalization a smaller maximum value. For higher frequencies the Markovian TL method yields comparable results to the TL, MRT and TDMRT approaches.
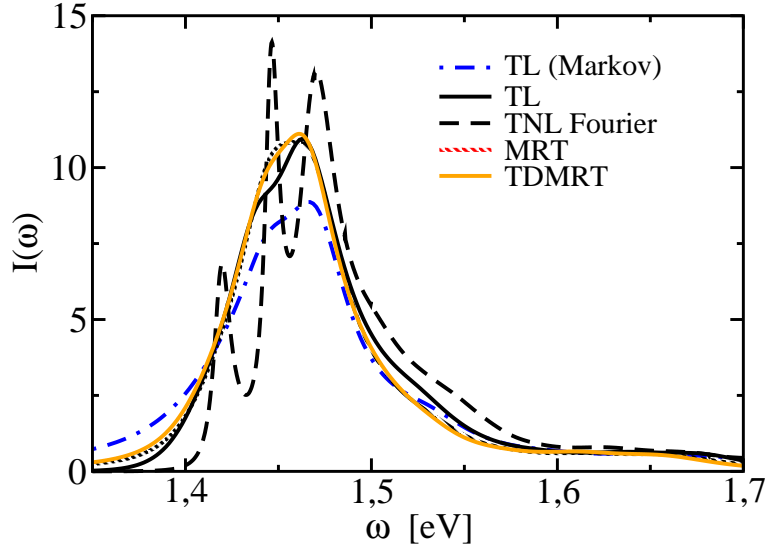

Figure 4.10: Same as Fig. 4.6 but for $\omega_c = 0.027$ eV and $\eta = 3.37$.

Within this parameter set the broadening of the ensemble line shape displayed in Fig. 4.11 is no longer dominated by the static disorder but by the effects of damping. This can be seen especially for the spectrum obtained with the Markovian TL method which is much broader than all others. Also here the TL, MRT and TDMRT approaches yield comparable results while the width of the line shape obtained with the TNL method is again the smallest. Due to the large variances of the line shapes, however, it is likely that second-order perturbation theory is not sufficient and higher-order perturbative methods should be used in this case.

As mentioned above the line shape formula of the TL-Fourier method contains both, elements with and without Markov approximation (cf. Eqs. (4.20) and (4.22)) which can lead to differences in the spectra compared to the direct TL method. One example of these effects is shown in Fig. 4.12. Here the most obvious variation is that within the TL method the right hand peak of the spectrum is larger than that of the line shape obtained with the TL-Fourier method. This difference, however, can be reduced, if all terms within the TL-Fourier method are treated consistently either with or without the Markov approximation.

4.4.2 Spectral density from MD simulation

The line shapes obtained with the different Ohmic spectral densities with varied cutoff frequencies show the influence of the particular form of the spectral densities.
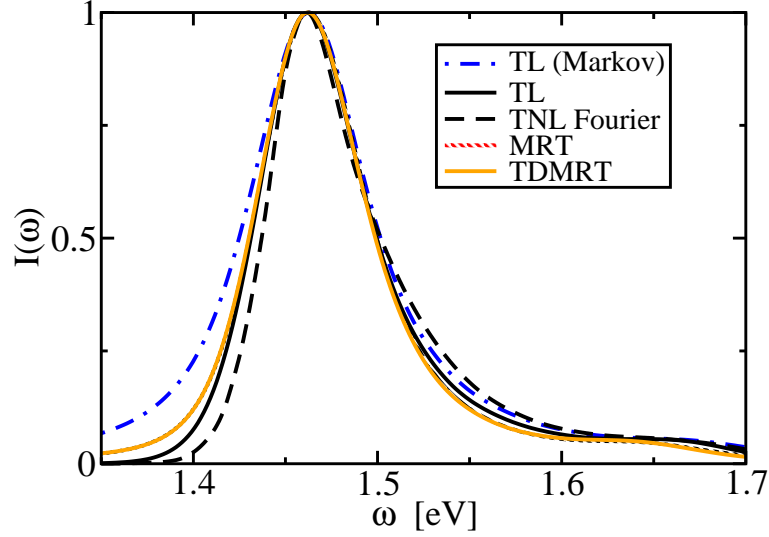
Figure 4.11: Same as Fig. 4.7 but for $\omega_c = 0.027$ eV and $\eta = 3.37$.
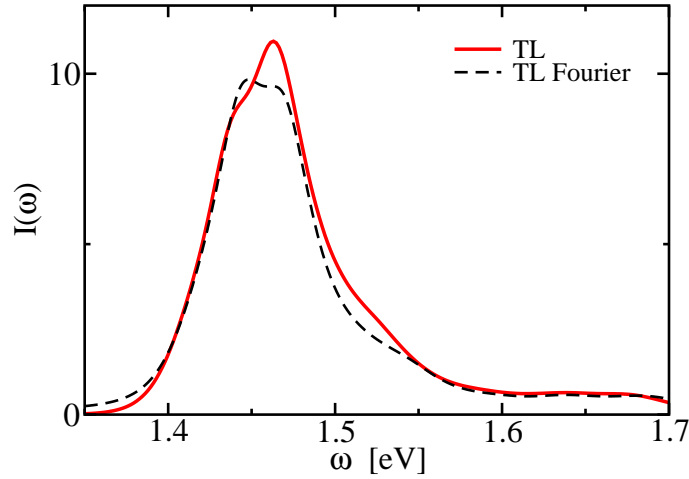

Figure 4.12: Comparison of TL and TL-Fourier method.

The spectral density from the MD simulation also shown in Fig. 4.3 contains maxima at different frequencies, corresponding to different bath correlation times. For this spectral density, therefore, a mixture of the line shapes discussed above can be expected.

As in the case for the Ohmic spectral density with short bath correlation time the three main peaks of the single sample displayed in Fig. 4.13 are clearly resolved with all methods. However, there is a variety of deviations within the different line shapes. The line shape obtained with the TNL method deviates significantly from the other line shapes. The maximum height of the curve obtained with the TNL method is about twice as large as the maximum heights of the other line shapes. The Markov approximation within the TL method has some impact on the spectrum compared to
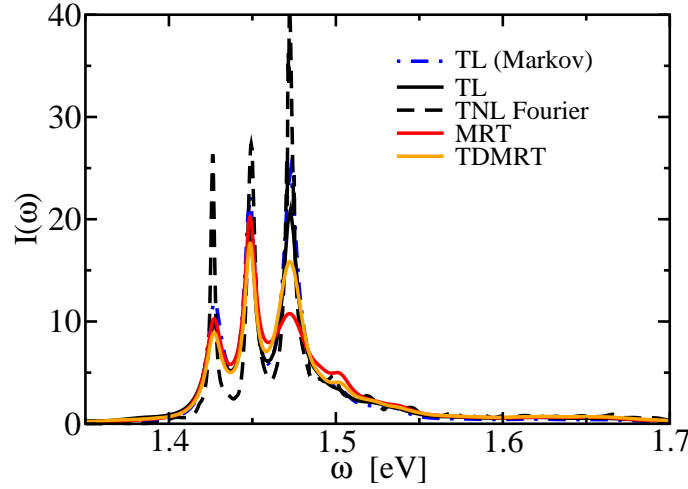
Figure 4.13: Line shapes of one sample using a spectral density obtained from the MD simulation.

its non-Markovian variant, but the deviation is rather small. The individual peaks of both spectra are slightly broader than those of the line shape calculated with the TNL method. The TDMRT and MRT methods yield further broadening due to strong damping, especially of the third peak which does, in contrast to the other curves, in both cases not determine the maximum height of the spectra. As in Fig. 4.6 the particular peak obtained with the TDMRT method is much higher than that obtained with the MRT approach.

Although the line shapes of the individual samples differ significantly depending on the method of calculation, there are only small variations within the ensemble line shapes shown in Fig. 4.14, i.e., the broadening is clearly dominated by static disorder and not by damping. As mentioned above, the experimental data displayed in Fig. 4.14 have been taken from Ref. [99] and show the peaks belonging to the B850 and B800 rings, respectively. The ensemble line shapes show good agreement with the experimental results for the B850 ring. There are, however, additional contributions at the low energy shoulder of the experimental data which are not obtained within the present calculations.

The spectral density obtained with the MD simulation has been criticized concerning the low frequency contributions. Since the spectral density was obtained from a 400 fs calculation it is possible that these contributions are underestimated.[94] In turn this would mean that the bath correlation times are longer than those used in the present calculations and the spectra would be rather comparable to those shown in Fig. 4.11. In this case the low frequency shoulder would be better approximated by damping effects. Since the width of the ensemble average in Fig. 4.11 is much larger than that of the experimental data, this would also mean that the static disorder is overestimated in the present case. Another possibility for this discrepancy could be the rough approximations made in the present model of coupled two-level systems which are linearly coupled to the bath.

It should be emphasized that the single samples in the present calculations do not
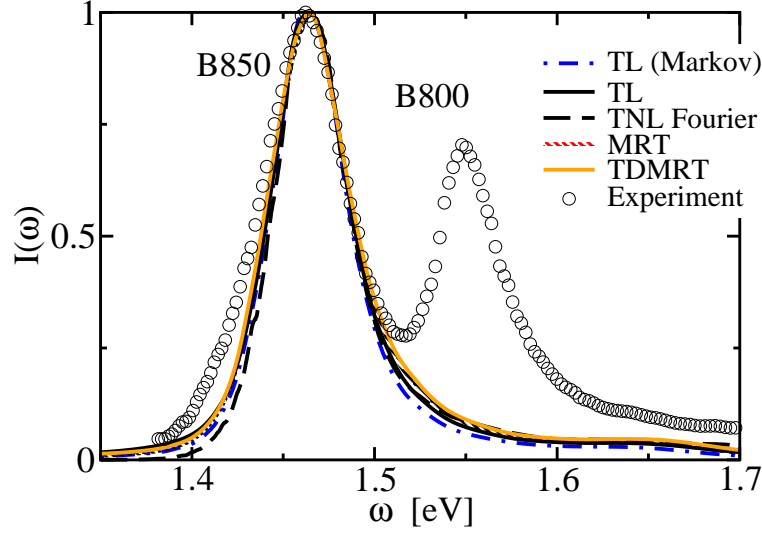
Figure 4.14: Comparison of the absorption line shapes of the B850 ring obtained using the spectral density from an MD simulation with experimental results.

represent single-molecule experiments though both are related on a very basic level. Several additional features such as dynamic disorder or the polarization of the light have been neglected in the present calculations. It should also be mentioned that such narrow peaks as observed for the single samples in Fig. 4.13 have not been observed in single-molecule experiments not even at low temperatures. This could be an additional argument for the underestimation of low frequency contributions of the spectral density as discussed above.

It should also be questioned whether or not the homogeneous broadening is underestimated by the second-order perturbative schemes discussed above. The experimental relaxation times T_1 are in the 10 fs to 100 fs range.[100] In the present calculations using standard Redfield theory with secular approximation the T_1 times lie within this range with a maximum at 15 fs. However, the life times of the lower excitonic states which mainly contribute to the absorption spectrum in this case are mainly beyond 50 fs. The dephasing times T_2 of the coherences, i.e. the matrix elements coupling the ground state to the excitonic states, however, are in the 15 fs to 200 fs range with a maximum at 30 fs.

An additional indication of the underestimation of low frequency contributions of the spectral density could be the strong damping observed within the MRT and TDMRT methods. In principle this could be verified by the hierarchical approach for absorption spectra (4.34) discussed above. Unfortunately the numerical demands increase very rapidly, especially concerning memory, due to the large number of exponentials of the correlation function and interaction operators. It is only possible to treat the system-bath coupling to fourth order within the TL scheme in the present case as displayed for a single sample in Fig. 4.4.2. Here the spectra of second-order TL and TNL methods which are the same (except from the secular approximation in the TNL case) as presented in Fig. 4.13 are displayed in comparison with that of the fourth-order TL scheme. The second and the fourth-order TL scheme only differ slightly, however, the three individual peaks obtained with the fourth-order scheme are slightly more broadened and the minima between them are slightly higher compared to those of the line shape obtained with the second-order scheme. It is hard to say whether the
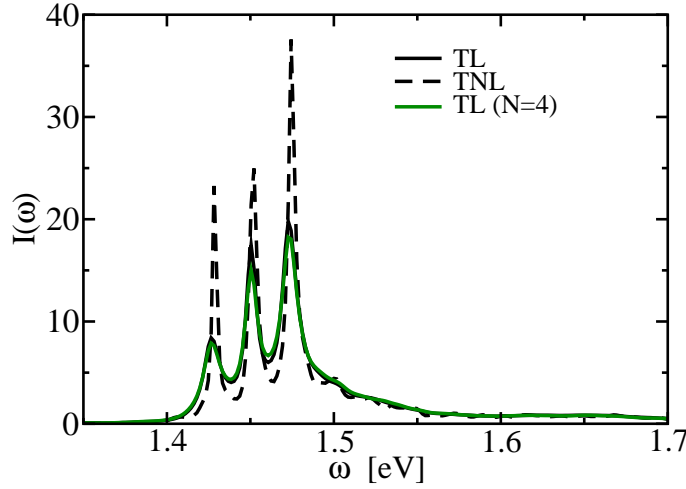
Figure 4.15: One sample calculated using the hierarchical method to fourth order in the system-bath coupling

fourth-order TL line shape is more accurate since results from higher orders of the hierarchy are not available. Taking into account the experience with larger deviations of the fourth-order TL scheme in the last chapter (cf. for instance Fig. 3.9) the result presented in Fig. 4.4.2 can only serve as an indication but not a proof that higher orders of the system-bath interaction only lead to minor corrections of the spectrum.

On the other hand, it is possible that the modified Redfield tensor yields too strong damping compared to the other methods. Due to the disorder the coefficients of the exponential terms within the modified Redfield tensor are varied so that even small changes can have a significant impact on selected tensor elements. Also the fourth-order contributions can dominate the second order terms in the last line of Eq. 2.100. This effects the inverse life times of the states such that single states are stronger (or sometimes less) damped. This explains why the third peak of the single sample line shape is selectively stronger damped when the MRT or TDMRT method is used while the other peaks remain almost unchanged compared to the other methods. This is due to the fact that that the modified Redfield tensor describes a different system since the equilibrium state of the bath is shifted in coordinate space. This shift depends on the excitonic state of the system and is therefore also different for each disorder configuration. Within the standard model all bath modes are shifted independent from the system state (cf. section 2.5.3) leading to a scalar renormalization Hamiltonian for the present model. This, however, is not the case within the MRT and will be further discussed in chapter 5.

To demonstrate the impact of the shift one can calculate the modified Redfield tensor with the equilibrium density matrix of the unshifted bath coordinate. In this case the population transfer rates are given as

$$
\begin{aligned}
\tilde{R}_{\nu\nu\mu\mu}(t) \;=\; & \mathrm{Re} \int_0^t d\tau \exp\left(-i\omega_{\nu\mu}\tau - G_{\nu\nu\nu\nu}(\tau) - G^\star_{\mu\mu\mu\mu}(\tau) + G_{\mu\mu\nu\nu}(\tau) + G^\star_{\nu\nu\mu\mu}(\tau)\right) \\
& \times \left[\ddot{G}_{\nu\mu\nu\mu}(\tau) + \left(\dot{G}_{\nu\mu\nu\nu}(\tau) - \dot{G}_{\nu\mu\mu\mu}(\tau)\right)\left(\dot{G}_{\mu\mu\mu\nu}(\tau) - \dot{G}^\star_{\nu\mu\nu\nu}(\tau)\right) \right].
\end{aligned}
\tag{4.47}
$$

The derivation of this expression can be done in analogy to the shifted tensor as given in appendix B. One can recognize that the terms within the exponential have the same
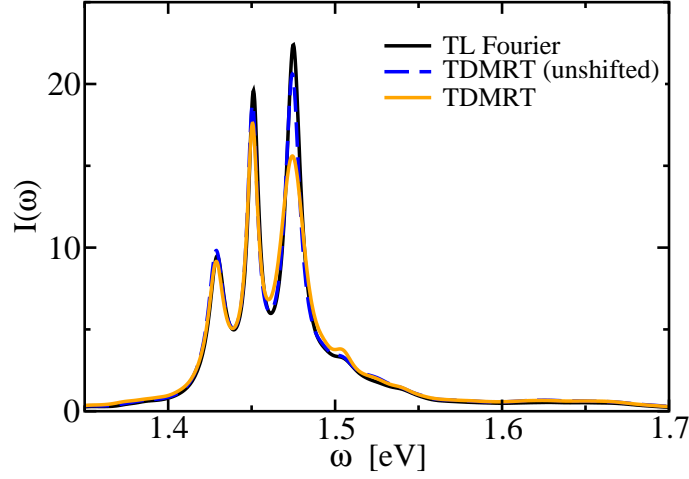

Figure 4.16: One sample calculated using the TDMRT with and without shifted bath as well as the TL-Fourier method.

structure as the Feynman-Vernon form of the influence functional.[88] This indicates that the diagonal part of the interaction is treated exactly. The other parts multiplied to the exponential are of second and fourth order in H'. The most obvious difference to the modified Redfield tensor (2.100) is that no terms in λ (the renormalization) but in the complex conjugate of G appear. In Fig. 4.16 line shape of the individual sample obtained with the shifted and unshifted version of the MRT and the TL-Fourier method (which can be understood as the same kind of method but with the time-dependent standard Redfield tensor) are compared. It can be clearly seen that the line shapes obtained with the TDMRT with unshifted bath and with the TL Fourier methods are in good agreement. The single peaks are of almost the same height and width. Compared to the TDMRT method with the shifted bath there is no stronger damping of the third peak. This indicates that the stronger damping of the third peak observed above is due to the effects of the shifted bath. It is interesting to see, that also the 4th-order TL scheme yields comparable results as the TDMRT with unshifted bath. This is an indication that the TL method yields the most reliable line shapes among second-order methods within the present model.

5 Exciton dynamics

The population dynamics of excitonic systems such as pigments systems is of special interest in chapter 4 since the population transfer rates strongly influence the absorption line shape. Various methods have been developed to model the population dynamics of such a system. Unfortunately the system discussed in chapter 4 is too large to be treated to higher orders in the system-bath coupling with the hierarchical method 2.88. In the present chapter, therefore, a similar but smaller pigment system will be discussed.

The model for the pigment system under consideration is the same as in chapter 4 so that all expressions and parameters can also be used here with the only difference that the system consists of $M = 4$ instead of $M = 16$ pigments. In addition the on-site disorder of the single pigment energies has been omitted here.

In this chapter the modified Redfield tensor for population transfer and the population transfer obtained with the hierarchical method will be compared in more detail. This will also help to validate the usage of the population transfer rates in the absorption formulas (4.40) and (4.41). The population dynamics will be calculated with the initial excitonic state being the fourth eigenstate of the system Hamiltonian. This is a rather artificial state, however, since the TDMRT and MRT are only rate equations and no coherences can be treated one is restricted to an initial state which only contains populations in energy representation. In the following the results obtained for two different spectral densities with short and long bath correlation times, respectively, are displayed.

5.1 Short bath relaxation time

In Fig. 5.1 the population dynamics of the fourth excitonic state is presented obtained for a spectral density with short bath correlation times, i.e., $\omega_c = 0.272$ eV. The curves obtained with the MRT and TDMRT rate equations are shown in the left panel of Fig. 5.1 for comparison with the results calculated using the hierarchical method. In the left panel of Fig. 5.1, the hierarchy has been truncated using the TL scheme to order $N = 2, 4$ and 6 in the system-bath coupling while in the right panel, the TNL truncation has been used except for the 6th-order where the TL truncation was used since storing another level of the hierarchy in the computer was not feasible. The population dynamics obtained with the modified Redfield tensor (4.47) with unshifted bath are not shown in the following. The results obtained with this method are, exept for small corrections of the equilibrium populations, comparable to those obtained with the MRT and TDMRT methods with shifted bath.

The various methods yield comparable results in all cases. The initially populated 4th excitonic state decays to the thermal equilibrium population which is almost reached after 100 fs. Only the equilibrium populations are slightly different for the various methods, especially those obtained with the hierarchical method approach different

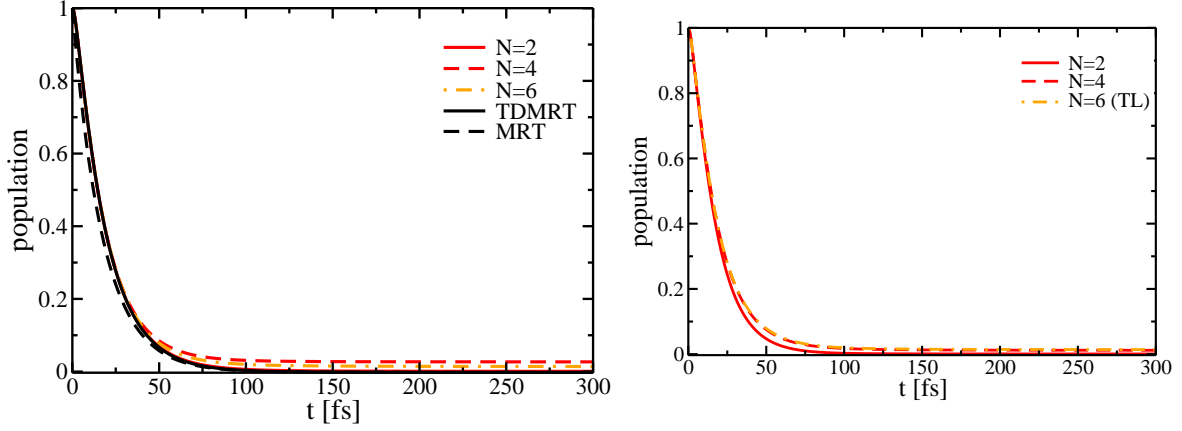values. This is again due to variations within the effective Hamiltonians as discussed in section 3.2.1.

Figure 5.1: Population dynamics of the 4th excitonic state obtained with the hierarchical method and the MRT and TDMRT approach for an Ohmic spectral density using $\omega_c = 0.272$ eV and $\eta = 0.34$. **Left:** TL truncation of the hierarchy. **Right:** TNL truncation of the hierarchy in 2nd and 4th order and TL truncation in 6th order of the system bath coupling.

For the ground state population shown in Fig. 5.2 the situation is slightly different. While both the MRT and TDMRT scheme as well as the TL and TNL to second-order in the system-bath coupling yield agreeing results, the higher-order curves obtained with the hierarchical approach differ from the latter mainly in the equilibrium populations which are almost reached after 200 fs. In particular the fourth-order TL curve differs from all others. The qualitative behavior, however, is almost the same in all cases. The populations obtained with the 4th-order TNL and the 6th-order TL method are quite similar. However, the hierarchy has possibly not yet converged such that a definite evaluation of these results cannot be made. Provided that the hierarchy method has almost converged in the 6th order (as indicated by the small difference between the 4th-order TNL and the 6th-order TL curve) it seems, that except for the equilibrium population, all methods give qualitatively comparable results.

5.2 Large bath relaxation time

In Fig. 5.3 a spectral density with large bath correlation time has been used. Here it was possible to calculate the population dynamics up to 8th order in the system-bath coupling since only a few Matsubara frequencies had to be taken into account. In the left panel of Fig. 5.3 the ground state population obtained with the modified Redfield approaches and the TL truncated hierarchy are shown. Again the MRT, TDMRT and the second-order TL scheme yield agreeing results. The curve obtained with the 4th-order TL scheme, however, assumes negative values for long times. This
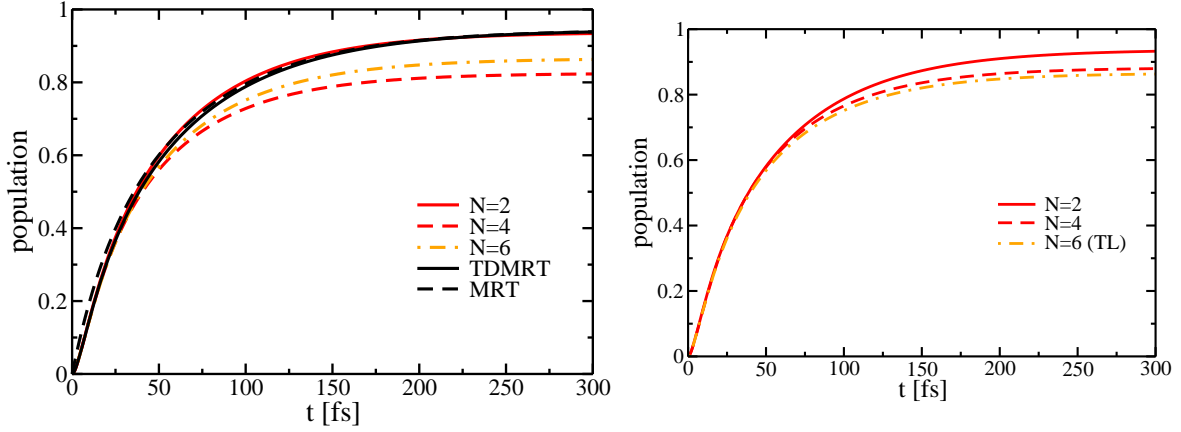
Figure 5.2: Same as Fig. 5.1 but for the ground state.

result does not have a physical meaning and is from the numerical point of view an indication that the system-bath coupling is too strong to be treated to low orders. The second-order scheme in this case yields positive equilibrium populations since $C(\omega_{\mu\nu}) = C(\omega_{\nu\mu}) \coth(\beta\omega_{\mu\nu}/2)$ which causes the equilibrium populations to be those of the unperturbed system Hamiltonian. The 6th- and 8th-order curves decay slightly slower than the other graphs with somewhat different equilibrium values.
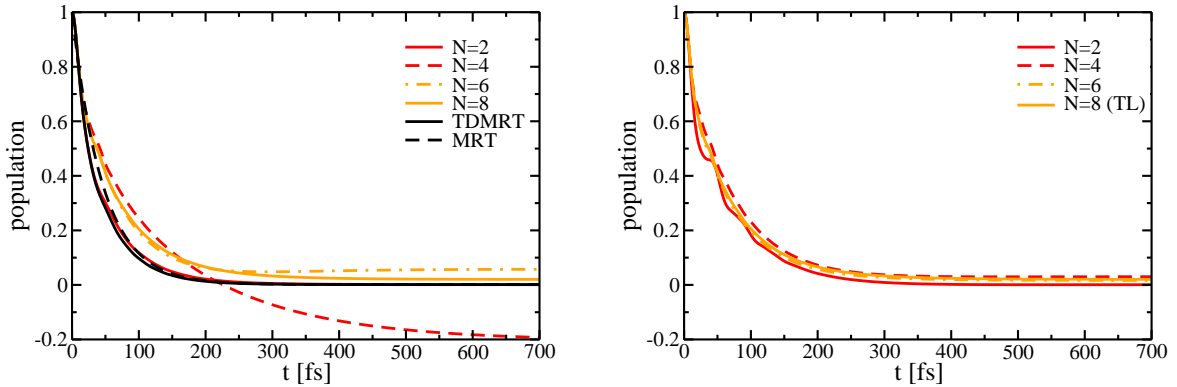
Figure 5.3: Same as Fig. 5.1 but with $\omega_c = 0.027$ eV and $\eta = 3.37$.

In the right panel of Fig. 5.3 the population dynamics obtained with the MRT, TDMRT and the TNL truncated hierarchy (except from the 8th-order curve where the TL truncation has been used) are displayed. All orders obtained with the hierarchal method give comparable results and the hierarchy seems to be converged in the 8th order. The MRT and TDMRT curves do not differ significantly from each other but decay faster than the other curves.

The ground state populations for the same initial state are presented in Fig. 5.4. Here it can be clearly seen that the population obtained with the MRT and TDMRT methods increases much faster than those obtained with the hierarchical method. The relaxation process observed within the second-order TL scheme displayed in the left panel

of Fig. 5.4 is slower than within MRT and TDMRT approaches but faster than those obtained with the higher orders of the hierarchy. Again the 4th-oder curve does not have a physical meaning since the population exceeds unity. The 6th- and 8th-order curves, however, display comparable population dynamics with slightly different equilibrium population. This equilibrium population deviates significantly from those of the MRT, TDMRT and second-order curves. Also the equilibrium states of the second-order scheme and both modified Redfield approaches deviate slightly. The difference in the equilibrium states is due to the shifted bath used to calculate the modified Redfield tensor. Taking into account further orders of the system bath coupling in this case leads to a slower relaxation process than obtained with the second-order TL scheme.

In contrast, the short time behavior of the curves obtained with the TNL (and the 8th-order TL) truncation of the hierarchy shown in the right panel of Fig. 5.4 is in good agreement until about 200 fs. Thereafter the populations approach different equilibrium states. The hierarchy in this case appears to be converged in the 8th order as a comparison with the 6th-order curve implies. Again, all curves obtained with the hierarchical method display a longer relaxation process than obtained with the modified Redfield approaches.
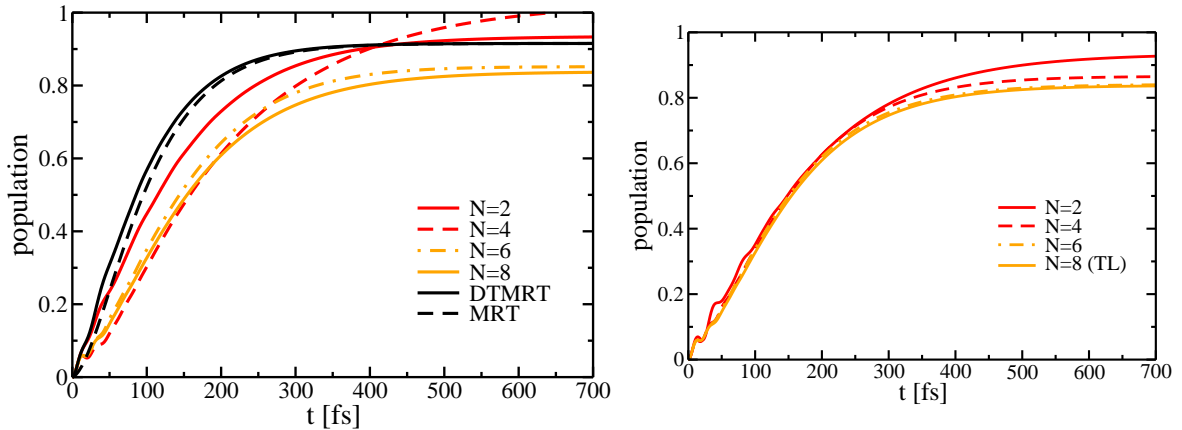

Figure 5.4: Same as Fig. 5.3 but for the ground state.

The reason for the different population dynamics for short times observed within the modified Redfield approaches and the hierarchical methods could be due to two reasons: (I) the different bath state and/or (II) an underestimation of higher orders in H' in case of the modified Redfield approaches. The influence of the shift of the bath, however, seems to be rather small since a similar curve can be obtained with the MRT with unshifted bath. In this case the equilibrium popolation is slightly smaller than the equilibrium position obtained with the MRT with shifted bath. It is therefore most likely that the difference in the short time behavior stems mainly from the second argument. In terms of the standard Redfield tensor the modified Redfield tensor contains all, population transfer elements ($\ddot{G}_{\mu\nu\nu\mu}$), terms that are responsible for dephasing ($G_{\mu\mu\mu\mu}$) and population-coherence transfer parts ($\dot{G}_{\mu\nu\mu\mu}$). However, due to the cumulant expansion technique the exponentials of matrix elements of H' have been calculated and not the matrix elements of the exponential of H' (cf. appendix

B). For stronger damping as in the case for large bath correlation functions this can lead to large differences in the population dynamics although the diagonal part of the system-bath interaction is treated exactly.[17] For weak damping as in the case for short bath correlation times the modified Redfield tensor yields agreeing results with the usual TL scheme for the present case. This is to be expected since in the limit of vanishing damping both methods are equivalent. But this agreement is also due to the symmetry of the system in the present case. If on-site disorder would have been added as in the previous chapter the damping would have to be further reduced in order to reach the limit where both the second-order TL scheme and the modified Redfield approaches are in agreement.

It is interesting to note that, except for the effects of the shifted bath, the broadening of the absorption spectra seems to be predicted with adequate precision while, compared to the hierarchical method, the population transfer seems to be overestimated. In the latter case higher order effects seem to yield additional transport mechanisms that transfer population back to the original state so that the net change of the population is decreased. This, however, does not affect the inverse life time of the excitonic states since it is defined only by the outflow of population.

6 Stochastic wave packet propagation

In chapters 3 and 5 a hierarchical approach based on the stochastic decoupling of the dynamics of the relevant system and the bath has been used to solve the deterministic EOM of the relevant system. In this case the derivation of a deterministic EOM was possible due the assumption that the bath consists of a collection of harmonic oscillators which are linearly and weakly coupled to the system. Only this allowed for the analytical evaluation of the trace over the bath DOFs and the use of bath correlations functions of the form (2.56). For an anharmonic bath and/or nonlinear coupling to the system an analytical evaluation of the trace over the bath becomes much more difficult or even impossible. In this case a direct stochastic propagation of the states of the individual DOFs can be performed. It is, however, only possible to treat a few DOFs at one moment in time and calculate the ensemble average later.

In the present chapter stochastic fields are used to decouple the EOM of a multi-dimensional state vector $|\Psi\rangle$ evolving on a potential energy surface instead of separating the system and bath DOFs of a statistical operator as in the previous chapters. The EOM of an M-dimensional state vector is given by the time-dependent Schrödinger equation

$$\frac{\partial}{\partial t}|\Psi(t)\rangle = -iH|\Psi(t)\rangle = -i\left[\sum_{j=1}^{M} H_j + V\right]|\Psi(t)\rangle. \tag{6.1}$$

As in the previous chapters the Hamiltonian H of the complete system is assumed to be time-independent to simplify notation. In Eq. (6.1) the Hamiltonian has been split into a number of single mode Hamiltonians H_j which are exclusively defined in the jth DOF and an additional term V that is responsible for the coupling. In general V is defined in all DOFs without any requirements for its particular form but it can always be split into a sum of products of which the factors are exclusively defined in a single DOF. This allows for the stochastic separation of V. As often done for the description of physical and chemical systems such as discretized thermal baths[101] or atomic clusters[44] it will be assumed in the following that V can be written as a sum of pair interactions

$$V = \sum_{j=1}^{M-1} \sum_{k>j}^{M} V_{jk} V_{kj}. \tag{6.2}$$

Here V_{jk} denotes that part of the pair coupling term defined in the jth DOF which has to be multiplied by V_{kj} defined in the kth DOF.

Starting with a Hartree ansatz for the complete wave function $|\Psi\rangle$ at the initial time $t = 0$, i.e.,

$$|\Psi(0)\rangle = \prod_{j=1}^{M} |\Phi_j(0)\rangle \tag{6.3}$$

with the single mode wave functions $|\Phi_j\rangle$ it is, analogous to the method used in section 2.7.2, possible to make an ansatz for decoupled but stochastically driven single mode

wave functions that, in the ensemble average, reproduce the complete wave function $|\Psi\rangle$. One possible ansatz is[102]

$$|d\Phi_j(t)\rangle = D_j |\Phi_j(t)\rangle \, dt + \sum_{k \neq j} S_{jk} |\Phi_j(t)\rangle \, d\nu_{jk}. \tag{6.4}$$

Here a differential of a single mode wave function is given by a deterministic part governed by the operator D_j and a stochastic part governed by the operators S_{jk} which both are exclusively defined in the jth DOF[102] and will have to be specified later. The stochastic fields $d\nu_{jk}$ obey the rules given in Eq. (2.68) such that the Itó formula (2.70) can be applied to evaluate the differential of the product state (6.3). Differently from the ansatz discussed in section 2.7.2 here only one stochastic field for each coupling term has been used.

Applying the Itó formula to the product state and applying the ensemble mean operation, an EOM for the product form is obtained as

$$d\,E\left\{\prod_j |\Phi_j\rangle\right\} = \left[\sum_j D_j + \sum_j \sum_{k>j} S_{jk} S_{kj}\right] E\left\{\prod_l |\Phi_l\rangle\right\} dt \tag{6.5}$$

which has the same structure as the original Schrödinger equation (6.1) when using the ansatz (6.2) for the pair potentials. To reproduce the Schrödinger equation (6.1) the operators S_{jk} therefore must be of such a form that the product $S_{jk} S_{kj}$ yields a term $-iV_{jk}V_{kj}$ which can be achieved by defining

$$S_{jk} = \sqrt{-i}\,V_{jk} + \alpha_{jk}, \tag{6.6}$$

where α_{jk} is an arbitrary scalar parameter. Inserting this definition into Eq. (6.5) yields

$$d\,E\left\{\prod_j |\Phi_j\rangle\right\} = \left[\sum_j D_j + \sum_j \sum_{k>j} (-iV_{jk}V_{kj} + \alpha_{jk}\alpha_{kj}) + \sum_j \sum_{k\neq j} \sqrt{-i}\,V_{jk}\alpha_{kj}\right] E\left\{\prod_l |\Phi_l\rangle\right\} dt. \tag{6.7}$$

Comparison with Eq. (6.1) leads to the immediate identification

$$D_j = -iH_j - \sqrt{-i}\sum_{k\neq j} V_{jk}\alpha_{kj} - \sum_{k>j} \alpha_{jk}\alpha_{kj} \tag{6.8}$$

such that upon inserting this expression into Eq. (6.5) all terms except those containing H_j cancel. With the definitions (6.6) and (6.8) for the S and D operators the stochastic EOM (6.4) of the single mode wave functions becomes

$$\begin{aligned} d\,|\Phi_j\rangle \;=\; & \left[-iH_j - \sqrt{-i}\sum_{k\neq j} V_{jk}\alpha_{kj} - \sum_{k>j} \alpha_{jk}\alpha_{kj}\right] |\Phi_j\rangle \, dt \\ & + \sum_{k\neq j}\left(\sqrt{-i}\,V_{jk} + \alpha_{jk}\right)|\Phi_j\rangle \, d\nu_{jk}\ . \end{aligned} \tag{6.9}$$

This equation constitutes the basis of the following considerations. Using the ansatz (6.3) it becomes possible to unravel the original Schrödinger equation so that the mean of the stochastic product state is identical with the state vector evaluated using Eq. (6.1). Hence it becomes possible to evaluate a number of one-dimensional wave functions in order to reproduce a multi-dimensional state vector. It should be emphasized that one is not limited to a factorizing initial state as in Eq. (6.3) in the sense that each general state vector can be expanded in a sum of product states as also used in the MCTDH approach.[54, 55]

6.1 Jump algorithm

There are several methods known for the numerical evaluation of stochastic EOMs that are driven by continuous stochastic processes such as Wiener processes.[87] However, in the present case a different type of stochastic process, the so-called jump process, is used. It will be assumed that most of the time the wave function follows a deterministic evolution interupted by discrete jumps that occur with a jump rate P_{jk}. Such a stochastic process can be realized by[102]

$$d\nu_{jk} = \frac{dn_{jk} - P_{jk}dt}{\sqrt{P_{jk}}} \tag{6.10}$$

where dn_{jk} is either one when a jump occurs or zero when the wave function follows deterministic evolution. The probability that a jump occurs, i.e., dn_{jk} being one during a time interval of length dt, is equal to $P_{jk}dt$ such that the expectation value of $d\nu_{jk}$ is zero. The expectation value of $(d\nu_{jk})^2$ is given by

$$
\begin{aligned}
E\left\{(d\nu_{jk})^2\right\} &= E\left\{\frac{(dn_{jk} - P_{jk}dt)^2}{P_{jk}}\right\} \\
&= E\left\{\frac{(dn_{jk})^2 - 2P_{jk}dtdn_{jk} + P_{jk}^2dt^2}{P_{jk}}\right\} \\
&= E\left\{\frac{dn_{jk}}{P_{jk}}\right\} + \mathcal{O}\left(dt^2\right) \\
&= dt + \mathcal{O}\left(dt^2\right) \ .
\end{aligned}
\tag{6.11}
$$

Here it has been used that $dn_{jk}^2 = dn_{jk}$. This has the consequence that the expectation value of higher orders in $d\nu_{jk}$ is of order dt as well. However, in the present case only quadratic orders of $d\nu_{jk}$ are used. It should be mentioned that with the definition (6.10) $d\nu_{jk}$ is not a Wiener process any more and care has to be taken when applying the Itó formula to evaluate the differentials of the product state.

Inserting the definition (6.10) for $d\nu_{jk}$ the EOM of the single mode wave function is given as

$$
\begin{aligned}
d|\Phi_j\rangle &= \left[-iH_j - \sqrt{-i}\sum_{k\neq j}V_{jk}\left(\alpha_{kj} + \sqrt{P_{jk}}\right) - \sum_{k>j}\alpha_{jk}\alpha_{kj} - \sum_{k\neq j}\sqrt{P_{jk}}\alpha_{kj}\right]|\Phi_j\rangle\, dt \\
&\quad + \sum_{k\neq j}\frac{\sqrt{-i}V_{jk} + \alpha_{jk}}{\sqrt{P_{jk}}}|\Phi_j\rangle dn_{jk} \ .
\end{aligned}
\tag{6.12}
$$

Using the relation

$$|\Phi_j(t+dt)\rangle = |\Phi_j(t)\rangle + d|\Phi_j(t)\rangle \tag{6.13}$$

all those terms that are of order dt on the right hand side of Eq. (6.13) can be neglected if a jump occurs. Since α_{jk} and P_{jk} are arbitrary parameters they can be chosen such that the wave function is completely replaced when a jump occurs. This is possible by using $P_{jk} = P_{kj}$ and defining

$$\alpha_{jk} = -\sqrt{P_{jk}} \tag{6.14}$$

such that the EOMs of the single mode wave functions become

$$|d\Phi_j\rangle = \left[-iH_j + \frac{1}{2}\sum_{k\neq j}P_{jk}\right]|\Phi_j\rangle\,dt + \sum_{k\neq j}\left(\sqrt{\frac{-i}{P_{jk}}}V_{jk} - 1\right)|\Phi_j\rangle\,dn_{jk}\,. \qquad (6.15)$$

Due to this definition of the free parameters α an additional term containing the jump rates appears in the deterministic part of the EOM. Since the jump rates are real and positive this leads to an exponential growth of the wave functions which might generate numerical instabilities. In Eq. (6.15) each single-mode wave function in principle grows with a different rate but since the product state is to be evaluated the growth can be equally distributed among all wave functions. Of course it is possible to choose the free parameters α differently from definition (6.14). However, in this case the growth is transfered to the jump process which then does not replace the wave function but adds additional contributions so that the norm of the wave function is not conserved. As will be discussed later the jump rates are however still free parameters which can be used to control the norm when a jump occurs.

6.2 Reconstruction of the original EOM

As mentioned above the stochastic jump processes are no Wiener processes and the Itó formula has to be used with care. In order to verify the correctness of the above given equations it has to be shown that, on average, the product state of the single mode wave functions propagated with the stochastic EOMs (6.15) reproduces the original Schrödinger equation (6.1). For this the evolution of the product state at time t is split into two parts, a deterministic part that occurs with a probability of $1 - \overline{p}dt$ and a jump part occurring with a probability $\overline{p}dt$. Here $\overline{p} = 1/2\,\sum_j\sum_{k\neq j}P_{jk}$ is the overall rate for any jump to occur. In detail one has to verify

$$d\,|\Psi\rangle = (1 - \overline{p}dt)d\,|\Psi\rangle_{\mathrm{det}} + 1/2\,\sum_j\sum_{k\neq j}P_{jk}dt\,d\,|\Psi\rangle_{\mathrm{jump},j,k} \qquad (6.16)$$

where $d\,|\Psi\rangle_{\mathrm{det}}$ denotes the differential of the product state during deterministic evolution, i.e.,

$$d\,|\Psi\rangle_{\mathrm{det}} = \left(1 - \frac{1}{2}\sum_j\sum_{k\neq j}P_{jk}dt\right)\left[\sum_j -iH_j + \frac{1}{2}\sum_j\sum_{k\neq j}P_{jk}\right]\prod_l|\Phi_l\rangle\,dt \qquad (6.17)$$

and $|d\Psi\rangle_{\mathrm{jump},j,k}$ the differential of the wave function when a jump affecting the modes j and k occurs, i.e.,

$$|d\Psi\rangle_{\mathrm{jump},j,k} = \left[\left(\sqrt{\frac{-i}{P_{jk}}}V_{jk} - 1\right) + \left(\sqrt{\frac{-i}{P_{kj}}}V_{kj} - 1\right)\right.$$
$$\left. + \left(\sqrt{\frac{-i}{P_{jk}}}V_{jk} - 1\right)\left(\sqrt{\frac{-i}{P_{kj}}}V_{kj} - 1\right)\right]\prod_l|\Phi_l\rangle\,. \qquad (6.18)$$

Re-inserting Eqs. (6.17) and (6.18) into Eq. (6.16) and neglecting all higher orders in dt yields

$$
\begin{aligned}
d\left|\Psi\right\rangle &= \left[\sum_j -iH_j + \frac{1}{2}\sum_j\sum_{k\neq j} P_{jk}\right]\prod_l |\Phi_l\rangle\, dt + \frac{1}{2}\sum_j\sum_{k\neq j} P_{jk}dt\left[\frac{-i}{P_{jk}}V_{jk}V_{kj} - 1\right]\prod_l |\Phi_l\rangle \\
&= -i\left[\sum_j H_j + \sum_j\sum_{k>j} V_j^k V_k^j\right]\prod_l |\Phi_l\rangle\, dt\,,
\end{aligned}
\tag{6.19}
$$

which is the original Schrödinger equation. It should be emphasized that this reproduction does not depend on the choice of the jump rates as long as the rates are nonzero. For vanishing jump rates the reproduction would yield a Schrödinger equation without the coupling terms.

6.3 Determination of the jump rates

At this point the jump rates P_{jk} are still free parameters. Since the jump rates also appear in the operators they can be used to adjust the norm of the state vector. As the norm of the wave function grows upon integration it is possible to reset the norm to unity, i.e. the condition

$$
P_{jk}^2 = \left\langle \Phi_j \middle| V_{jk}^\dagger V_{jk} \middle| \Phi_j \right\rangle \left\langle \Phi_k \middle| V_{kj}^\dagger V_{kj} \middle| \Phi_k \right\rangle
\tag{6.20}
$$

has to be fullfilled. However, this method turned out to be numerically unstable because large jump probabilities can appear that lead to a fast growth of the norm of the samples. Another possibility is to choose the jump rates such that the norm is conserved when a jump occurs. This is achieved by the condition

$$
P_{jk}^2 = \frac{\left\langle \Phi_j \middle| V_{jk}^\dagger V_{jk} \middle| \Phi_j \right\rangle \left\langle \Phi_k \middle| V_{kj}^\dagger V_{kj} \middle| \Phi_k \right\rangle}{\langle \Phi_j | \Phi_j \rangle \langle \Phi_k | \Phi_k \rangle}.
\tag{6.21}
$$

This choice will result in a moderate but monotone growth of the norm and still leads to instabilities as discussed in the following section.

6.4 Numerical limitations

6.4.1 Exponential growth of the norm

In the previous section it was shown that in the limit of infinitely many realizations the original Schrödinger equation is reproduced. For practical purposes, however, the ensemble average has to be approximated with a limited number of realizations. Usually a few thousand samples are sufficient to obtain satisfying results as for example shown within similar approaches for unraveling quantum master equations.[63, 103] In the present approach, however, an exponential growth of the norm is caused by the jump rates. Since the jump rates are determined dynamically at runtime and individually for each realization all samples contribute to the ensemble mean with much different weights. It is likely that, for longer times, very few realizations dominate

the ensemble mean such that the number of samples needed for a certain accuracy approximately grows exponentially with time. It is possible to avoid the appearance of the jump rates in the deterministic part in the EOM by introducing additional jump processes. In this case, however, the norm of the single realizations cannot be controlled when a jump occurs and again an exponential increase of the norm of the single realizations can be observed.

6.4.2 Instability on jump

From Eq. (6.15) it can be seen that the wave function is completely replaced by the original wave function modified by the interaction term. Depending on the particular operator eigenstates with high energy could be populated, which might cause numerical instabilities. If the wave function is, for example, represented on a discrete grid in coordinate representation and the interaction term is a potential that increases at the outer regions, the wave functions will reach the edges of the grid leading to numerical problems. To overcome this problem additional projection operators can be introduced that project the wave function back to the center of the grid. This has been achieved by adding a zero to the original Schrödinger equation (6.1) such that

$$\frac{\partial}{\partial t}\ket{\Psi} = \left[-i\sum_j^M H_j - i\sum_j\sum_{k>j} V_j^k V_k^j + \sum_s Q_s Q_{s+1} - \sum_s Q_s Q_{s+1} \right] \ket{\Psi}. \qquad (6.22)$$

Here the index s denotes an odd positive integer $s = 1, 3, 5, \ldots$ such that the product of the projection operators Q_s and Q_{s+1} connects two modes. In the particular realization (6.22) each mode is affected by one projection operator but other arrangements such as a double sum over projection operators $\sum_r \sum_{s>r} Q_{r,s} Q_{s,r}$ are possible as long as all modes that can become unstable are affected. As in Eq. (6.6) for the interaction operators, one can define jump operators for the projectors as

$$Y_s = Q_s + \beta_s , \qquad Z_s = iQ_s + \gamma_s \qquad (6.23)$$

and the respective stochastic processes

$$d\tilde{\nu}_{s,1} = d\tilde{\nu}_{s+1,1} = \frac{d\tilde{n}_{s,1} - \tilde{P}_{s,1}dt}{\sqrt{\tilde{P}_{s,1}}} , \qquad d\tilde{\nu}_{s,2} = d\tilde{\nu}_{s+1,2} = \frac{d\tilde{n}_{s,2} - \tilde{P}_{s,2}dt}{\sqrt{\tilde{P}_{s,2}}} \qquad (6.24)$$

for each pair of Q_s and Q_{s+1} as well as iQ_s and iQ_{s+1} with the additional jump rates $\tilde{P}_{s,1}$ and $\tilde{P}_{s,2}$, respectively, such that the stochastic EOMs for the single-mode wave functions become

$$d\ket{\Phi_j} = \left[-iH_j + \frac{1}{2}\sum_{k\neq j} P_{jk} + \frac{1}{2}\left(\tilde{P}_{j,1} + \tilde{P}_{j,2} \right) \right] \ket{\Phi_j} dt + \sum_{k\neq j} \left(\sqrt{\frac{-i}{P_{jk}}} V_{jk} - 1 \right) \ket{\Phi_j} dn_{jk}$$

$$+ \left(\frac{Q_j}{\sqrt{\tilde{P}_{j,1}}} - 1 \right) \ket{\Phi_j} d\tilde{n}_{j,1} + \left(\frac{iQ_j}{\sqrt{\tilde{P}_{j,2}}} - 1 \right) \ket{\Phi_j} d\tilde{n}_{j,2} . \qquad (6.25)$$

The choice of the projection operators Q_s is completely free and opens not only the possibility to control the population of the eigenstates but also to control the norm after a projecting jump occurs independently from the respective jump rate. The jump rates themselves are free as well and can for instance be chosen according to the number of jumps involving the interaction that occurred since the last jump involving a projection. It also becomes possible to reset the norm of all single-mode wave functions since only the norm of the product state is of interest.

6.4.3 Propagation time and jump probabilities

In order to prevent the occurrence of more than one jump at a propagation step of length dt it has to be assured that the probability of any jump to occur is much less than the probability of deterministic evolution, i.e.,

$$\left(\sum_j \sum_{k \neq j} P_{jk} + \sum_s \left(\tilde{P}_{s,1} + \tilde{P}_{s,2} \right) \right) dt \ll 1 \qquad (6.26)$$

For systems with a large number of DOFs the time step therefore might have to be adjusted to a very small value which creates a numerical bottleneck. This also might lead to a fast exponential growth the norm of the single realizations and cause large amounts of noise in the ensemble mean of a finite number of realizations. According to Eqs. (6.20) and (6.21) large expectation values of the interaction operators lead to large jump rates and in turn create numerical instabilities since in most cases the energy of the system will grow when a jump occurs.

6.5 Results for two dimensions

The algorithm derived above is applied to two test systems that consist of two coupled harmonic oscillators coupled with different interaction terms. The Schrödinger equation of the test systems reads

$$\frac{\partial}{\partial t} |\Psi\rangle = -i \left[H_1 + H_2 + V_{1,2} V_{2,1} \right] |\Psi\rangle \qquad (6.27)$$

with

$$H_j = \frac{1}{2} \left(\frac{p_j^2}{m_j} + m_j \omega_j^2 x_j^2 \right) \qquad (6.28)$$

being the Hamiltonian of a one-dimensional harmonic oscillator with momentum p_j, coordinate x_j, mass m_j and frequency ω_j. In the following m_j and ω_j are set to unity. Since only one coupling term is present in Eq. (6.27) the second index identifying the associated operators in the other DOF will be skipped in the following, i.e., $V_{1,2} \to V_1$, $V_{2,1} \to V_2$. The particular realization of the coupling terms V_1 and V_2 will be defined later. For numerical stability additional projection operators according to Eq. (6.22) projecting to the ground state $|0_j\rangle$ of the jth single-mode harmonic oscillator are introduced, i.e.

$$Q_1 = \Lambda |0_1\rangle \langle 0_1| \quad \text{and} \quad Q_2 = \Lambda |0_2\rangle \langle 0_2| . \qquad (6.29)$$

Here Λ is a real number that is determined such that the norm of the product wave function is equal to unity after one of the jumps involving Q_1 or Q_2 occurs. With these definitions the EOM of the single-mode wave function (6.25) becomes

$$\begin{aligned}
d |\Phi_j\rangle &= \left[-iH_j + \frac{1}{2} \left(P + \tilde{P}_1 + \tilde{P}_2 \right) \right] |\Phi_j\rangle \, dt + \left(\sqrt{\frac{-i}{P}} V_j - 1 \right) |\Phi_j\rangle \, dn \\
&\quad + \left(\frac{Q_j}{\sqrt{\tilde{P}_1}} - 1 \right) |\Phi_i\rangle \, d\tilde{n}_1 + \left(\frac{iQ_j}{\sqrt{\tilde{P}_2}} - 1 \right) |\Phi_j\rangle \, d\tilde{n}_2 .
\end{aligned} \qquad (6.30)$$

where $P = P_{12}$ is the rate of the jumps involving the potential and $\tilde{P}_1$ and $\tilde{P}_2$ denote the rates of the two projecting jumps. The jump rate involving the interaction terms has been chosen as

$$P = \sqrt{\frac{\left\langle \Phi_1 | V_1^\dagger V_1 | \Phi_1 \right\rangle \left\langle \Phi_2 | V_2^\dagger V_2 | \Phi_2 \right\rangle}{\langle \Phi_1 | \Phi_1 \rangle \langle \Phi_2 | \Phi_2 \rangle}} \qquad (6.31)$$

which guarantees that the norm of the samples stays constant during a jump. The rates for the additional jumps were chosen as $\tilde{P}_1 = \tilde{P}_2 = P$. In Figs. 6.1 and 6.2 the real part of the auto-correlation function

$$C(t) = \langle \psi(0) | \Psi(t) \rangle = E\left\{ \langle \Phi_1(0) | \Phi_1(t) \rangle \langle \Phi_2(0) | \Phi_2(t) \rangle \right\} \qquad (6.32)$$

is shown as a measure for the accuracy of the algorithm. For this the stochastic EOMs of the single-mode wave functions have been evaluated in the time interval $t = 0$ to 5 a.u. which covers almost one oscillation period of one uncoupled harmonic oscillator. For comparison the exact result is displayed together with the expectation value of the correlation function approximated with different numbers of realizations.
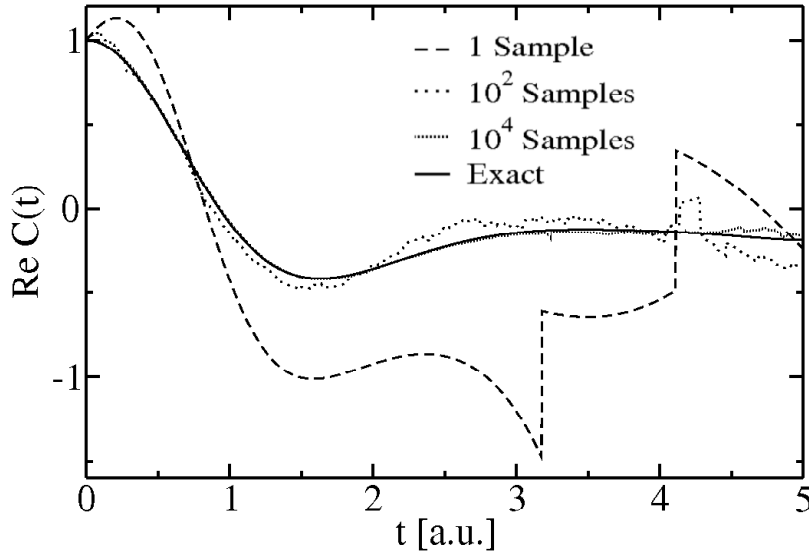

Figure 6.1: Auto-correlation function of a state vector evolving in two coupled harmonic potential surfaces modeled with different numbers of realizations. The coupling is $V_1 = x_1/2$ and $V_2 = x_2/2$.

In both cases the state vector has been represented on a grid with 32 points in each DOF representing the interval $[-15\, a_0, 15\, a_0]$ in coordinate domain. Here a_0 denotes the Bohr radius. For the initial state vector a real Gaussian wave function centered at $(x_{1,0}, x_{2,0})$ with variance σ, i.e.,

$$\begin{aligned} |\Psi(x_1, x_2, 0)\rangle &= |\Phi_1(x_1, 0)\rangle |\Phi_2(x_2, 0)\rangle \\ &\equiv \frac{1}{\pi} \exp\left(-\frac{1}{2\sigma}(x_1 - x_{1,0})^2 \right) \exp\left(-\frac{1}{2\sigma}(x_2 - x_{2,0})^2 \right) \end{aligned} \qquad (6.33)$$

with $x_{1,0} = 1\, a_0$, $x_{2,0} = -1\, a_0$ and $\sigma = 1\, a_0^2$ has been used and propagated during the deterministic evolution with the so-called split operator technique with $dt = 10^{-4}$ a.u.[45,48]
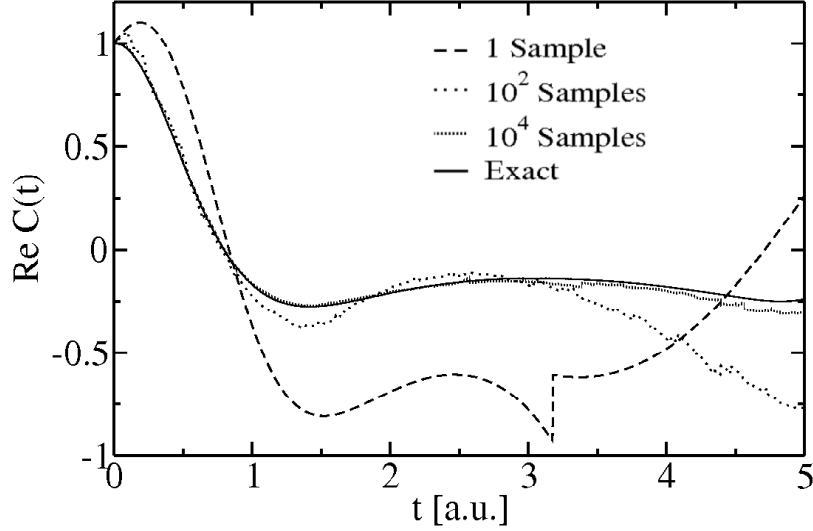
Figure 6.2: Same as Fig. 6.1 but with $V_1 = x_1/2$ and $V_2 = x_2^2/4$.

In Fig. 6.1 the correlation function obtained from a system of two coupled harmonic oscillators is shown with the interaction potential

$$V_1 = \frac{x_1}{2} \quad \text{and} \quad V_2 = \frac{x_2}{2} \; . \tag{6.34}$$

The same initial wave function was used to obtain the correlation function displayed in Fig. 6.2 but the coupling was chosen as

$$V_1 = \frac{x_1}{2} \quad \text{and} \quad V_2 = \frac{x_2^2}{4} \; . \tag{6.35}$$

In both cases the accuracy of the approximated correlation function increases with increasing number of realizations included to evaluate the ensemble mean. The growth of the norm of some of the single realizations to large values leads to large amounts of noise in the ensemble mean. For this reason those samples where $|C(t)| > 500$ have not been taken into account to obtain the results displayed in Figs. 6.1 and 6.2. In both cases less than 1 sample out of 1000 have been omitted. Although in principle omitting selected realizations will lead to a loss of accuracy in the limit of infinitely many realizations, the deficit of this procedure is by far outbalanced for a limited number of samples. Figs. 6.1 and 6.2 also illustrate that with increasing propagation time more and more noise enters the results leading to growing inaccuracy while for short times the correlation function is rendered very accurately. The growing noise is due to the exponential growth of the norm and hence the growing weight of the respective realizations in the ensemble average.

In addition in Fig. 6.3 the contours of the real parts of the exact wave function and the approximated wave function captured at different times are shown. In this case the wave function has been approximated with 10^4 realizations and discretized on a grid of 64×64 points to achieve a better resolution. As also observed for the correlation functions the wave function is reproduced very accurately at short times ($t = 1$ a.u.) although small artifacts of the stochastic processes are visible which become larger with increasing time ($t = 1.5$ a.u.). At even larger times ($t = 2$ a.u.) significant deviations from the exact wave function can be observed. Although parts of the exact wave function can be recognized in the approximation, more samples are needed to achieve a better accuracy in this case.
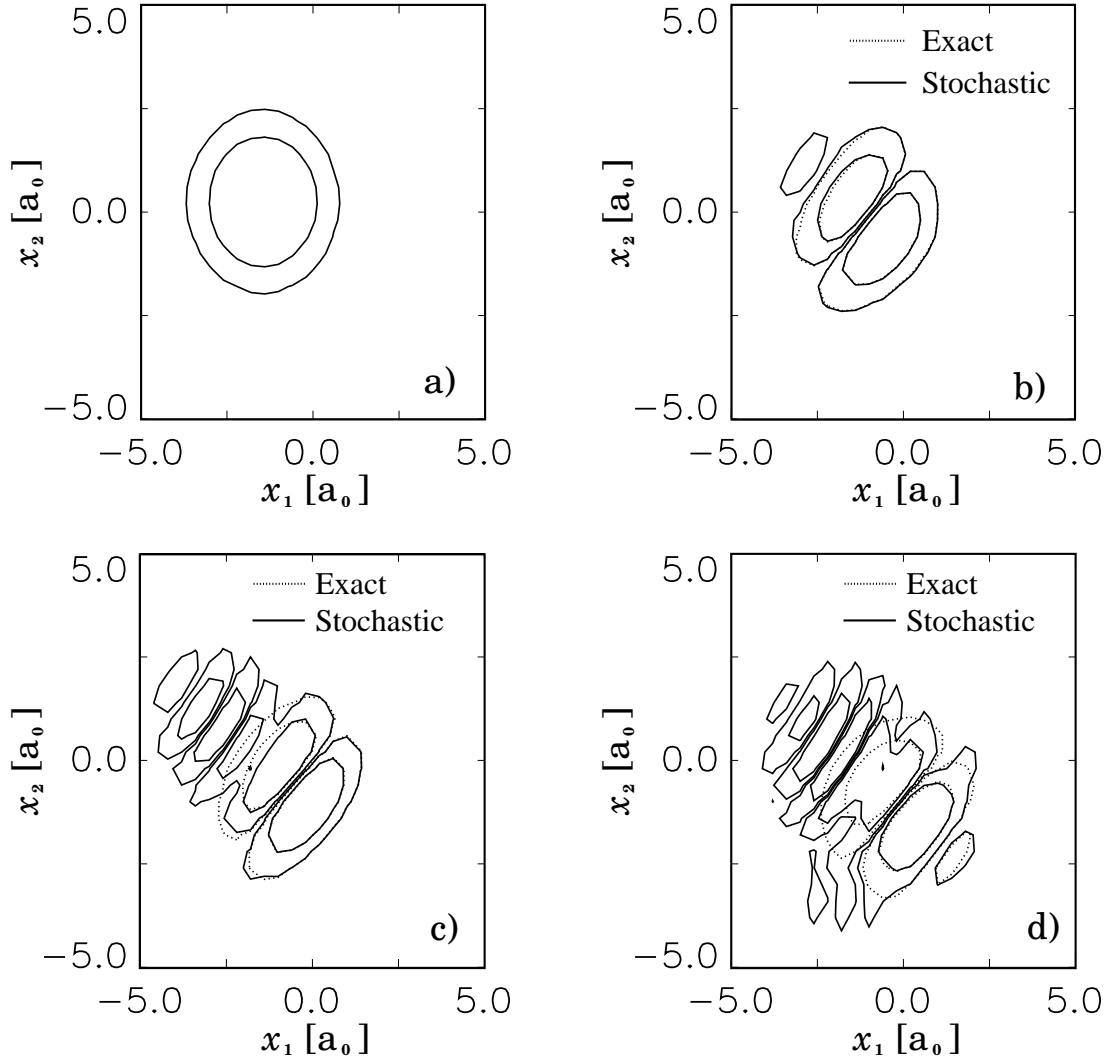
Figure 6.3: Contour plot of the real parts of the exact and approximate wave function captured at **a)** $t = 0$ a.u. **b)** $t = 1$ a.u. **c)** $t = 1.5$ a.u. **d)** $t = 2$ a.u.

6.6 Results for four dimensions

In this section the previous model is extended to four coupled harmonic oscillators with the single-mode Hamiltonians (6.28). As before m_j and ω_j are set to unity and the interaction is defined as

$$V_{jk}V_{kj} = \frac{1}{4}x_j x_k. \tag{6.36}$$

Also in this case additional projection operators according to Eq. (6.23) have been introduced to stabilize the system after repeated jumps as described in section 6.4.2. Figs. 6.4 and 6.5 display the real part of the auto-correlation function obtained with initially two real Gaussian wave packets with variance $1 a_0^2$ in each DOF, centered at $(x_{1,0}, x_{2,0}, x_{3,0}, x_{4,0}) = (1, -1, 1, -1) a_0$ and $(x_{1,0}, x_{2,0}, x_{3,0}, x_{4,0}) = (-0.5, 0.8, -0.1, 0.1) a_0$, respectively. In both cases the wave function has been discretized on a grid of 32 points for each DOF representing the coordinate space in the interval $[-15 a_0, 15 a_0]$. The main difference between these two wave functions is that due to the different position the
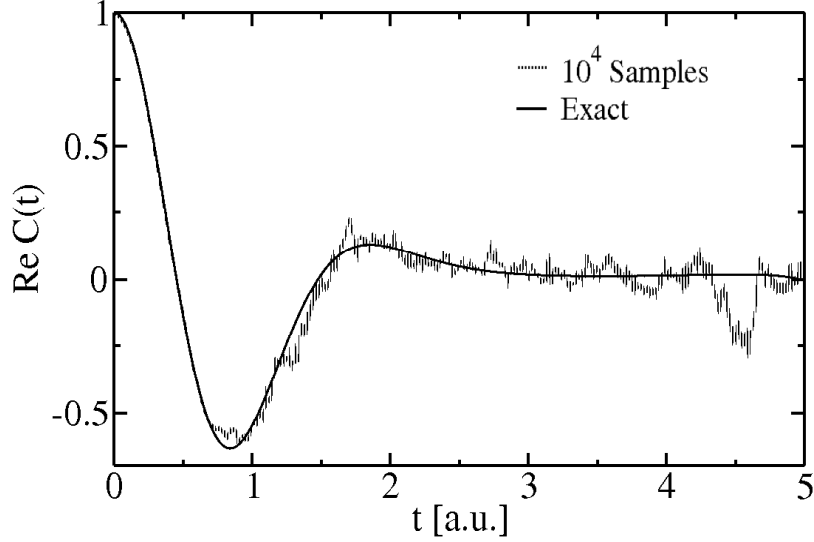
Figure 6.4: Correlation function of a four-dimensional initially Gaussian wave function centered at $(1, -1, 1, -1) \, a_0$.

expectation value of the interaction terms is smaller in the first case. In addition, for the second wave function the overlap with the ground state of the uncoupled system is larger which leads to a larger rate for jumps involving the projectors while in the first case more jumps involving the potential will occur. This effect can be clearly seen in Figs. 6.4 and 6.5. The approximated correlation function in Fig. 6.4 already deviates significantly from the exact correlation function at times $t < 1$ a.u. while this is not the case for the correlation function shown in Fig. 6.5. For very short times, however,

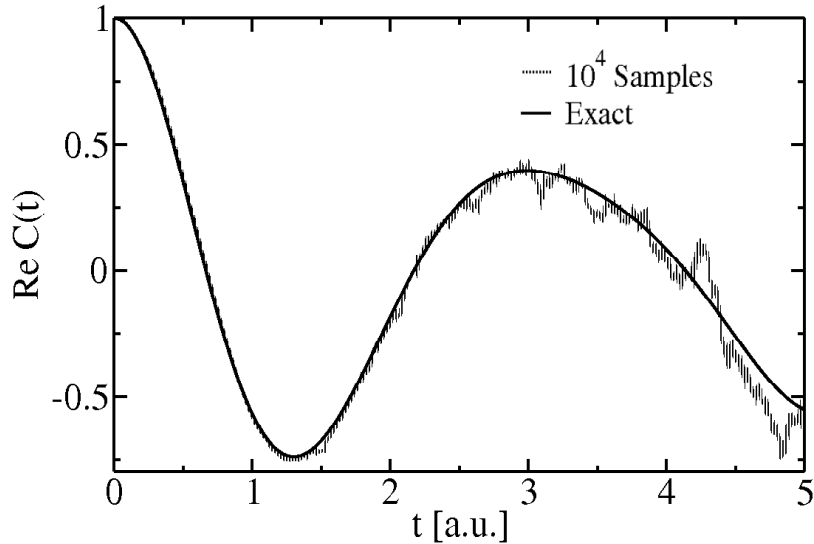Figure 6.5: Same as Fig. 6.4 but initially centered at $(-0.5, 0.8, -0.1, 0.1) \, a_0$.

in both examples the approximate correlation function yields good agreement with the exact result. Due to the larger value of the jump rates, however, the propagation time step had to be chosen as $dt = 5 \cdot 10^{-5}$ in order to prevent simultaneous jumps involving several interaction terms. As in the two-dimensional case all realizations

with $|C(t)| > 500$ which were about 2% of all samples in both cases have not been taken into account. Differently from the procedure in the previous section, the rates for the projecting jumps $\tilde{P}_{jk}$ have been set proportional to $(n_{jk} + 1)^2$ where n_{jk} is the number of jumps involving potential operators (6.36) defined in the jth and kth mode that occurred since the last projection.

In all examples discussed above, the amount of noise is growing with increasing time. This is mainly caused by the growth of the norm of the single realizations. The growth of the norm amplifies the noise introduced by each realization. For long times and a finite number of realizations the nose dominates the signal. Omitting the jump rates in the deterministic part of Eq. (6.15) would lead to an exponential decrease of the expectation values, e.g. of the correlation function (6.32), with time. The exponential growth of the norm can therefore be interpreted as a compensation for the loss of information about the initial state that occurs due to the introduction of the stochastic processes. Unfortunately this compensation leads to numerical instabilities.

In Ref. [63] a similar but stable algorithm for unraveling quantum master equations with wave functions is developed. The formal form of the EOMs for the wave functions proposed by Kondov *et al.* is very similar to the EOMs used within the algorithm discussed above. However, the deterministic part of the EOMs in Ref. [63] contains operators that are responsible for damping and a decrease of the norm of the single realizations. The jump rates within the algorithm proposed by Kondov *et al.* can be determined such that the reduction of the norm of the single realizations is compensated almost completely. This not only leads to damping of the high energy states that cause numerical problems in the present approach. The existence of damping can also be interpreted as a loss of information about the initial state. But once the system has reached thermal equilibrium, the information about the initial state is of no importance any more. I.e., a complete compensation for the loss of information about the initial state is not necessary if the system approaches a final state which is independent from the initial state. The information has to be conserved only for a finite time until the equilibrium state has almost been reached. Hence, it seems that the absence of such a finite time scale is one reason for the slow convergence of the algorithm discussed above for long times.

7 Summary and outlook

7.1 Electron transfer

In section 3.1 the dynamics of the population of the third excited state of a damped harmonic oscillator as well as the expectation value of the squared coordinate operator have been discussed for different orders in the system-bath coupling and two different spectral density functions corresponding to small and large bath correlation times. The calculations were performed with a hierarchical method with different truncation methods as proposed by Shao, Xu, Tanimura and others[33,34,35,36] as discussed in Section 2.7.

For small bath correlation times the differences in the various orders of perturbation theory and the different truncation schemes are rather small. It can be assumed that the scheme has almost converged in second order of the system-bath interaction since taking into account higher orders only leads to minor corrections of the results. The reason for this behavior is the strong damping in the higher orders of the hierarchy so that for both, the results for the population dynamics as well as for the expectation value of the squared coordinate operator, mainly second order contributions have to be taken into account. For the same reason also the method of truncation is of less importance.

In the second example the bath correlation time has been enlarged. In this case the influence of the auxiliary density matrices becomes more important. Also the method of truncation plays a more important role for the convergence. It could be observed that for the population of the eigenstates of the system Hamiltonian the results obtained with the TL truncation converge much faster than those obtained with the TNL truncation where strong oscillations can be observed for low orders in the system-bath interaction. This is vice versa for the convergence of $\langle q^2 \rangle$. Here the results obtained with TNL truncation converge much faster. This is especially interesting since the calculation of $\langle q^2 \rangle$ in energy representation involves the populations of the eigenstates as well as offdiagonal matrix elements. Within the TL truncation where the diagonal elements converge fast the error therefore stems from the coherences. A general reason for the different convergence behavior cannot be given at this point. In the present case, the strong oscillations observed for the population dynamics obtained with the second-order TNL method can possibly be explained by the rather artificial initial state and the structure of the coupling operator q in energy representation. This is indicated by the frequency of the oscillations which is almost the same as the transition frequency between neighboring eigenstates. Within the TL scheme, these oscillations are suppressed. A reduction of the oscillations can also be observed when a general initial state is used.

In section 3.2 the model system has been extended to two coupled and damped harmonic oscillators which are arranged along a common reaction coordinate. Such a system is often used to model donor-acceptor systems for charge transfer processes. Within this model the electronic population of the donor and the population of the

initially excited third vibronic state of the donor have been calculated. This was done to different orders in the system-bath interaction with the hierarchical method for two spectral densities and TL as well as TNL truncation.

As in the previous case for a single harmonic oscillator and small bath relaxation time the expectation value of both the population of the third excited vibrational state as well as the electronic population of the donor seem to be converged already to low orders in the system-bath interaction. Also the method of truncation seems to play a minor role in this case.

For larger bath relaxation time the impact of the higher order terms of the hierarchy increases. The dynamics of the population of the third excited vibrational state of the donor shows strong oscillations within the lower orders of the TNL truncation method and is very similar to the behavior observed for the singe oscillator. The population dynamics slowly converge to those calculated using the TL truncation method which seem to yield more reliable results in this case. It is interesting to see that the convergence behavior of the electronic population dynamics concerning the method of truncation is vice versa. It seems to be converged already in fourth order in the system-bath coupling when the TNL truncation method is used while it has converged not until the sixth order in the system-bath interaction with the TL truncation method.

The reliability of the results obtained with the hierarchical algorithm discussed in section 2.7 therefore strongly depends on the method of truncation and the value which is to be calculated if the algorithm has not yet converged. It may also depend on the system under consideration[38] as well as its initial state. A general rule which method performs superior for a given problem cannot be stated at this point. In any case, the hierarchy seems to be converged when both, the TL and the TNL truncation yield the same results or if the condition (2.89) is fulfilled. If the usual second-order perturbation theory is to be used it can be tested whether the second order TL or the TNL scheme yields more precise results by taking into account higher levels of the hierarchy.

Unfortunately the numerical scaling of the hierarchical method is rather poor such that only small systems and a few orders in the system-bath coupling can be taken into account. For stronger damping additional levels will have to be taken into account such that the required memory quickly reaches the limits of computational capacity and the hierarchy may possibly not converge.[37] In this case other methods seem to be the better choice.

The numerical bottleneck created by the large number of exponential terms within the bath correlation form can hardly be overcome for complex spectral densities and low temperatures. Both circumstances are, however, met in most experiments. In the high temperature limit and with simple spectral densities such as the Drude spectral density opens the hierarchy the possibility to treat a small system to large orders in the system-bath coupling.[32]

7.2 Linear absorption of LH2

In chapter 4 the linear absorption spectrum of the B850 pigment ring of the LH2 system of *Rhs. molischianum* has been calculated based on a model system of coupled two-level systems interacting with a thermal bath of harmonic oscillators. For

this purpose various methods, time-dependent as well as time-independent methods, with and without Markov and secular approximation based on second-order perturbation theory in the system-bath coupling have been used. In addition two methods based on the modified Redfield approach which treat the diagonal part of the system-bath interaction exactly have been developed and applied to calculate the absorption spectra of the B850 ring.

All line shape formulas have been tested on three different Ohmic spectral densities and one obtained from an MD simulation.[18] The Ohmic spectral densities where used to study the influence of different bath correlation times on the absorption spectra and provided the possibility of comparison with the spectral density taken from the MD simulation. The latter involves a mixture of the different time scales seen within the Ohmic spectral densities. Also, to emulate the influence of long-time quasistatic fluctuations of the bath on the pigment system, static disorder has been added to the pigment energies. The line shapes of one single realization as well as of the ensemble average of the disorder configurations have been discussed in section 4.4. In case of the MD spectral density, the ensemble average has also been compared with experimental data.[99]

In case of the Ohmic spectral densities it could be shown that the variation of the bath correlation has a significant influence on the line shapes. Since all line shape formulas contain integrations over the past of the bath correlation functions those 'memory from the past' terms gain influence with increasing bath correlation time, leading to larger broadening of the absorption spectra. Especially the methods using the Markov approximation yield significant differences compared to those without Markov approximation. This is due to the the fact that the full damping strength already exists in the initial moment and does not build up with time as within the other methods. The line shapes obtained with the methods based on the modified Redfield approach show stronger damping than those obtained with the methods based on usual second order perturbation theory. The stronger damping can be assigned to effects of the shifted bath used to derive the MRT and TDMRT methods as comparison with the line shape obtained with the TDMRT with unshifted bath in section 4.4.1 for the spectral density obtained from the MD simulation implies. Especially the static disorder leads to a random variation of the damping of single excitonic states. This has a minor influence on the ensemble line shape but a significant impact on the single sample line shapes. Whether these effects caused by the state-dependent shifted bath are realistic or do not describe the pigment system correctly has to be verified by other methods such as MD simulations or by experiments.

With the calculations using the spectral density obtained from an MD simulation it could be shown that the line shape of the individual samples depends on the method of calculation. Especially the line shape obtained with the second-order TNL scheme differs significantly from those obtained with the other methods. The line shape of one sample has also been calculated within 4th order perturbation theory based on the hierarchical method discussed in chapter 2 and shows only small differences to the line shape obtained with the second order TL formalism. This is also the case for the line shape obtained with the TDMRT method with unshifted bath. For the present spectral density therefore the TL formalism seems to yield the most reliable results among the second-order schemes.

There are indications that the spectral density used in the present case is not suitable to describe the spectral properties of the vibrational DOFs of the pigment complex, especially concerning the low frequency contributions.[94] If these contributions are un-

derestimated in the present study, this has certainly consequences for the absorption line shapes as shown for the Ohmic spectral densities above. In this case higher order perturbative techniques should be used to calculate the absorption spectra. This also will have consequences for modeling the results of single-molecule spectroscopy within a perturbative treatment. The relaxation times calculated with the standard Redfield theory are in the correct range compared to experimental data, however, those that mainly influence the spectrum were found in the long time region of this range.

In the ensemble average the differences observed for the single line shapes are hardly visible any more. All methods of calculation yield comparable results which are in good agreement with the experimental results. Single molecule experiments, however, suggest a larger influence of the relaxation-induced broadening on the absorption line shape. This could also reduce a discrepancy between the calculated spectra and the experimental data at the low frequency edge in the present case. It should be emphasized, that the individual samples used in the present study, are not suited to model single molecule experiments since several features of the molecules, such as dynamic disorder on long time scales and the polarization of the light have been neglected. Recently Jang and Silbey[104] have developed a theory for single-molecule line shapes for multichromophoric systems based on a TL master equation and applied it to a model for the B850 ring.[105] The question was raised whether the TL or the TNL master equations are more suitable to describe single-molecule experiments such as in Refs. [106] and [107]. A comparison with the 4th-order TL method and the TDMRT approach with unshifted bath suggest that the TL method yields the most reliable results among the second-order perturbative approaches.

7.3 Exciton dynamics

In chapter 5 a similar but smaller pigment system than in chapter 4 has been studied. Here a ring consisting of 4 chromophores without static disorder instead of 16 with static disorder has been used to calculate the population dynamics of the excitonic system. This was done using the Markovian and the non-Markovian variant of the modified Redfield tensor which treats the diagonal part of the system-bath interaction exactly and a hierarchical set of EOMs that treats the system-bath interaction to different orders. In order to study the influence of the bath correlation time two Ohmic spectral densities with different cutoff frequencies have been used.

For short bath correlation times it was observed that the MRT, TDMRT and the second order TL theory yield comparable results for the population dynamics. Taking into account higher orders of the system-bath interaction within the hierarchical method leads to small corrections of the equilibrium populations, especially for the ground state. However, the qualitative behavior of the population dynamics did not change. Besides, it was observed, that the TNL truncation of the hierarchy yields faster convergence. However, as in the case for the electron transfer model discussed in chapter 3, this might also depend on the initial state used here.

For large bath correlation times, it was again observed that the MRT, TDMRT and the second order TL theory are in good agreement for the dynamics of the initially populated highest excitonic state. The curve obtained with fourth order TL truncation of the hierarchy does not have a physical meaning since it assumed negative values. This is an indication that the system-bath interaction is too strong to be treated

with this method. Taking into account further orders of the system-bath interaction yields a slow convergence of the hierarchical scheme. Interestingly the relaxation of the system is slowed down when further orders of the system-bath coupling are taken into account. Also in this case the TNL truncation seems to yield a faster convergence of the hierarchy. This may have consequences for convergence of the absorption spectrum discussed in 4. However, the convergence of the hierarchical scheme strongly depends on the observable as discussed in chapter 3 and might be different for line shapes and population dynamics.

For the ground state the increase of population obtained with the MRT and TDMRT methods is much larger than obtained with the other methods. Also here the relaxation process of the system is slowed down when higher orders of the system-bath interaction are taken into account. The curves obtained with the TNL method give comparable results for small times but assume different equilibrium states. The hierarchy seems to be converged in 8th order in the system bath interaction.

The reasons for the different behavior of the modified Redfield approaches compared to the hierarchy can be due to two reasons. On the one hand, the bath state within the modified Redfield approaches is shifted compared to the bath state used within the hierarchical approach. However, this shift is not too large and plays a minor role within the present model as calculations based on an unshifted bath can show. The shift of the bath modes leads to a different equilibrium state but does not significantly change the qualitative behavior of the population dynamics. More importantly, within the MRT and TDMRT methods the population dynamics is calculated using rate equations. Here a variety of contributions of the system-bath interaction is neglected. Within the cumulant expansion technique the cumulants of matrix elements of the system-bath interaction are evaluated instead of matrix elements of the time evolution operator. For strong damping that has probably quite some impact on the population transfer rates.

7.4 Stochastic wave packet propagation

In chapter 6 a stochastic algorithm for propagating multi-dimensional wave packets has been developed and tested using a test system of two and four coupled harmonic oscillators, respectively. The algorithm starts with a separation of the complete multi-dimensional system into a number of one-dimensional subsystems. The multi-dimensional wave function is represented as a product state of the single mode wave functions of these sub systems. To unravel the coupling of the various one-dimensional subsystems stochastic jump processes are introduced in the EOMs of the single modes in such a way that the Schrödinger equation of the combined system is reproduced in the ensemble average.

It was shown that such an algorithm can in principle serve as a tool for multi-dimensional wave packet propagation. In the ensemble average the correlation functions and the wave functions are in good agreement with the exact solutions of the Schrödinger equation for short times though for longer times the convergence of the algorithm decreases rapidly and growing amounts of noise enter the results. The main reason for this is that the norm of single realizations of wave functions is not conserved but grows exponentially with a different rate for each individual sample. As a consequence some of the realizations dominate the ensemble such that the stochastic noise of these few samples is still present in the ensemble average.

A second major problem is the numerical instability introduced by the stochastic processes. When a jump occurs high energy states can be populated. In the present case this caused the wave function to reach the edges of the grid on which it is discretized. This problem, however, could be partly controlled with additional jump operations that project the wave function back to the center of the grid. For small interactions therefore the algorithm should show better convergence, since both, the growth of the norm of the samples as well as the population of high energy states is reduced in this case.

Another reason for numerical instabilities can be found in the time evolution of the combined system. In contrast to the time evolution of reduced density matrices which approach thermal equilibrium for long times, there exists no stationary final state for wave functions.

7.5 Outlook

In this section possible extensions and modifications of the methods discussed in the previous chapters are suggested. Several properties have been neglected or simplified within the present models such that the inclusion of additional features could lead to a deeper insight into the dynamics of the underlying systems.

As indicated in the introduction most of the methods discussed in this work are in general not limited to time-independent Hamiltonians. This opens the possibility to study the reduced system dynamics under the influence of external fields such as a laser field or slow variations of the external environment. This is especially of interest when single molecule experiments are to be modeled for systems such as the B850 ring. Unfortunately the complex structure of the spectral density restricts the application of the hierarchy method as discussed in chapter 4. Possibly here a temperature dependent fit of $J(\omega)n(\omega)$ in terms of Lorentzians can reduce the number of auxiliary density matrices within the hierarchy. In this case the Matsubara frequencies can be incorporated in the other terms which could be especially useful when low temperature experiments are modeled.

In addition the inclusion of the B800 ring could lead to changes in the linear absorption line shape of the LH2 systems. It is to be expected that due to the weak coupling between the two rings the respective line shapes will stay almost separated. But especially the correct modeling of the relative heights of the minimum and the two maxima of the experimental spectra displayed in Fig. 4.14 can give useful hints for the correct amounts of disorder and damping used within the model system. Also the inclusion of higher excitonic states might change the spectra but especially allow for modeling higher order spectroscopy.[17]

For modeling charge transfer processes it would be interesting to also model the initial charge injection, for example by laser excitation as done in Ref. [26] or from a fermionic electron bath as in Ref. [22]. Here it would also be interesting to study the influence of higher orders in the coupling to the fermionic electron bath in connection with the damping due to the bosonic vibrational bath.

Within the algorithm for stochastic wave packet propagation discussed in chapter 6 the main problem is the growth of the norm of the single realizations. In contrast to the original scheme for unraveling the evolution of a density matrix coupled to a thermal bath as proposed by Kondov *et al.*[63] the present scheme diverges for long

times. A possible solution to this problem could be the introduction of a limited time scale as in Ref. [63]. Since the evolution of the wave function without damping is not limited, a final state such as the equilibrium state in case of the reduced density matrix, will not be reached. The exponential increase of the norm in the present case in a sense compensates for the loss of information for the coherent motion caused by the stochastic processes. The introduction of damping as for example known for the MCTDH method[54,55] might reduce this problem since in this case a stationary state will be approached. In addition the introduction of damping will possibly lead to a reduction of the population of high energy states which created numerical problems in the present algorithm.

A Projection operator technique

Using the time-independent projectors $\mathcal{P}$ and $\mathcal{Q}$ the EOM of the relevant part can be expressed as

$$
\begin{aligned}
\tfrac{\partial}{\partial t}\mathcal{P}W(t) &= \mathcal{P}\tfrac{\partial}{\partial t}W(t) \\
&= -i\mathcal{P}\mathcal{L}W(t) \\
&= -i\mathcal{P}\mathcal{L}\left(\mathcal{P}+\mathcal{Q}\right)W(t) \\
&= -i\mathcal{P}\mathcal{L}\mathcal{P}W(t) - i\mathcal{P}\mathcal{L}\mathcal{Q}W(t).
\end{aligned}
\tag{A.1}
$$

This EOM contains the projected system part $(\mathcal{P}W(t))$ as well as the bath part $(\mathcal{Q}W(t))$ which has to be specified further. In analogy to Eq. (A.1) one can find an EOM for the bath part

$$
\frac{\partial}{\partial t}\mathcal{Q}W(t) = -i\mathcal{Q}\mathcal{L}\mathcal{P}W(t) - i\mathcal{Q}\mathcal{L}\mathcal{Q}W(t).
\tag{A.2}
$$

This equation is a linear but inhomogeneous differential equation in $\mathcal{Q}W(t)$ and can be formally integrated using a similar method as the 'variation of parameters' for ordinary differential equations. One first solves the homogeneous differential equation

$$
\frac{\partial}{\partial t}\left(\mathcal{Q}W\right)_{\mathrm{h}}(t) = -i\mathcal{Q}\mathcal{L}\left(\mathcal{Q}W\right)_{\mathrm{h}}(t).
\tag{A.3}
$$

as

$$
\begin{aligned}
\left(\mathcal{Q}W\right)_{\mathrm{h}}(t) &= \overrightarrow{T}\exp\left(-i\int\limits_{t_0}^{t}d\tau\,\mathcal{Q}\mathcal{L}(\tau)\right)\mathcal{Q}W(t_0) \\
&= \mathcal{U}_{\mathcal{Q}}(t,t_0)\mathcal{Q}W(t_0)
\end{aligned}
\tag{A.4}
$$

where $\overrightarrow{T}$ is the time ordering operator which is needed if $\mathcal{L}$ is time-dependent and $\mathcal{U}_{\mathcal{Q}}(t,t_0)$ denotes the time evolution superoperator with respect to $\mathcal{Q}\mathcal{L}$ from time t_0 to time t. As in chapter 2 $\mathcal{L}$ will be assumed to be time independent in the following such that the integral in Eq. (A.4) results in a multiplication with $(t-t_0)$. To solve the inhomogeneous differential equation one can make the ansatz

$$
\left(\mathcal{Q}W\right)_{\mathrm{i}}(t) = \mathcal{U}_{\mathcal{Q}}(t,t_0)\mathcal{A}(t)\mathcal{Q}W(t_0),
\tag{A.5}
$$

where $\mathcal{A}(t)$ is a (super-)operator that will have to be defined in the following. The time derivative of ansatz (A.5) reads

$$
\begin{aligned}
\tfrac{\partial}{\partial t}\left(\mathcal{Q}W\right)_{\mathrm{i}}(t) &= -i\mathcal{Q}\mathcal{L}\mathcal{U}_{\mathcal{Q}}(t,t_0)\mathcal{A}(t)\mathcal{Q}W(t_0) + \mathcal{U}_{\mathcal{Q}}(t,t_0)\left(\tfrac{\partial}{\partial t}\mathcal{A}(t)\right)\mathcal{Q}W(t_0) \\
&= -i\mathcal{Q}\mathcal{L}\left(\mathcal{Q}W\right)_{\mathrm{i}}(t) + \mathcal{U}_{\mathcal{Q}}(t,t_0)\left(\tfrac{\partial}{\partial t}\mathcal{A}(t)\right)\mathcal{Q}W(t_0).
\end{aligned}
\tag{A.6}
$$

Direct comparison with Eq. (A.2) leads to the identification

$$
\mathcal{U}_{\mathcal{Q}}(t,t_0)\left(\frac{\partial}{\partial t}\mathcal{A}(t)\right)\mathcal{Q}W(t_0) = -i\mathcal{Q}\mathcal{L}\mathcal{P}W(t).
\tag{A.7}
$$

Multiplying the inverse time evolution operator from the left leads to

$$
\left(\frac{\partial}{\partial t}\mathcal{A}(t)\right)\mathcal{Q}W(t_0) = -i\mathcal{U}_{\mathcal{Q}}^{-1}(t,t_0)\mathcal{Q}\mathcal{L}\mathcal{P}W(t),
\tag{A.8}
$$

which can be formally integrated as

$$(\mathcal{A}(t) - \mathcal{A}(t_0)) \mathcal{Q}W(t_0) = -i \int_{t_0}^{t} d\tau \mathcal{U}_{\mathcal{Q}}^{-1}(\tau, t_0) \mathcal{Q}\mathcal{L}\mathcal{P}W(\tau). \tag{A.9}$$

Solving this equation for $\mathcal{A}(t)\mathcal{Q}W(t_0)$ and substituting into Eq. (A.5) yields

$$\begin{aligned}
(\mathcal{Q}W)_{\mathrm{i}}(t) &= -i\mathcal{U}_{\mathcal{Q}}(t, t_0) \int_{t_0}^{t} d\tau \mathcal{U}_{\mathcal{Q}}^{-1}(\tau, t_0) \mathcal{Q}\mathcal{L}\mathcal{P}W(\tau) + \mathcal{U}_{\mathcal{Q}}(t, t_0)\mathcal{A}(t_0)\mathcal{Q}W(t_0) \\
&= -i \int_{t_0}^{t} d\tau \mathcal{U}_{\mathcal{Q}}(t, \tau) \mathcal{Q}\mathcal{L}\mathcal{P}W(\tau) + \mathcal{U}_{\mathcal{Q}}(t, t_0)\mathcal{A}(t_0)\mathcal{Q}W(t_0).
\end{aligned} \tag{A.10}$$

The general solution of Eq. (A.2) is constructed by a linear combination of the homogeneous and the inhomogeneous solution Eqs. (A.4) and (A.10), respectively, i.e.,

$$\mathcal{Q}W(t) = B_{\mathrm{h}} (\mathcal{Q}W)_{\mathrm{h}}(t) + B_{\mathrm{i}} (\mathcal{Q}W)_{\mathrm{i}}(t) \tag{A.11}$$

where B_{h} and B_{i} are scalar coefficients. Since the inhomogeneous part in the differential equation (A.2) can only be deduced from the particular solution (A.10) the coefficient B_{i} has to be one. In addition, assuming $\mathcal{Q}W(t_0)$ to be known as initial condition, leads to the constraint that $\mathcal{A}(t_0)$ has so be scalar and $\mathcal{A}(t_0) + B_{\mathrm{h}} = 1$ which can be verified upon setting $t = t_0$ in Eqs. (A.4) and (A.10). The formal integrated differential equation (A.2) reads

$$\mathcal{Q}W(t) = \mathcal{U}_{\mathcal{Q}}(t, t_0)\mathcal{Q}W(t_0) - i \int_{t_0}^{t} d\tau \mathcal{U}_{\mathcal{Q}}(t, \tau) \mathcal{Q}\mathcal{L}\mathcal{P}W(\tau). \tag{A.12}$$

This solution contains two parts, the projected initial bath part that undergoes free evolution according to the time evolution operator $\mathcal{U}_{\mathcal{Q}}$ and a projected system part which is integrated over the past.

A.1 The Nakajima-Zwanzig identity

Having formally solved the differential equation for $\mathcal{Q}W(t)$ the result (A.12) can be inserted in the differential equation (A.1) for $\mathcal{P}W(t)$ leading the well known Nakajima-Zwanzig identity (2.23). The three parts on the right hand side of this EOM can be interpreted as follows: the first term covers the coherent motion of the projected system part while the middle part are so-called *memory from the past* terms which are responsible for the dissipation. They cover the influence of the bath on the system. Due to the implicit treatment of the bath state the information of its effects to the system motion has to be taken into account by an integral over the past times of the system state so that the EOM of the system is nonlocal in time. The last part in Eq. (2.23) covers the so-called initial correlations, i.e., the initial entanglements of system and bath, which are not treated explicitly in the projected part $\mathcal{P}W(t)$ but, of course, influence its motion.

A.2 The Hashitsume-Takahashi-Shibata identity

In addition to the TNL Nakajima-Zwanzig identity it is possible to derive a TL EOM for the projection $\mathcal{P}W(t)$ on the relevant system. Starting with Eq. (A.12) one can express the state $W(\tau)$ in the integral in terms of a time evolution operator $\mathcal{U}$ that propagates the state $W(t)$ back to time τ and use the projection operators to solve for $\mathcal{P}W(t)$:

$$
\begin{aligned}
\mathcal{Q}W(t) &= \mathcal{U}_{\mathcal{Q}}(t,t_0)\mathcal{Q}W(t_0) - i\int_{t_0}^{t} d\tau \mathcal{U}_{\mathcal{Q}}(t,\tau)\mathcal{Q}\mathcal{L}\mathcal{P}W(\tau)) \\
&= \mathcal{U}_{\mathcal{Q}}(t,t_0)\mathcal{Q}W(t_0) - i\int_{t_0}^{t} d\tau \mathcal{U}_{\mathcal{Q}}(t,\tau)\mathcal{Q}\mathcal{L}\mathcal{P}\mathcal{U}(\tau,t)\left(\mathcal{P}+\mathcal{Q}\right)W(t)),
\end{aligned}
\tag{A.13}
$$

where

$$
\mathcal{U}(\tau,t) = \exp\left(-i\mathcal{L}(\tau-t)\right)
\tag{A.14}
$$

is the time evolution operator of the combined system with respect to the full Liouville operator $\mathcal{L}$. To simplify notation one often introduces the superoperator

$$
\mathcal{D}(t) = i\int_{t_0}^{t} d\tau \mathcal{U}_{\mathcal{Q}}(t,\tau)\mathcal{Q}\mathcal{L}\mathcal{P}\mathcal{U}(\tau,t),
\tag{A.15}
$$

such that Eq. (A.13) simplifies to

$$
\mathcal{Q}W(t) = \mathcal{U}_{\mathcal{Q}}(t,t_0)\mathcal{Q}W(t_0) - \mathcal{D}(t)\mathcal{P}W(t) - \mathcal{D}(t)\mathcal{Q}W(t).
\tag{A.16}
$$

Solving this equation for $\mathcal{Q}W(t)$ yields

$$
\mathcal{Q}W(t) = [\mathcal{D}(t)+1]^{-1}\left(\mathcal{U}_{\mathcal{Q}}(t,t_0)\mathcal{Q}W(t_0) - \mathcal{D}(t)\mathcal{P}W(t)\right).
\tag{A.17}
$$

Inserting this into Eq. (A.1) yields

$$
\frac{\partial}{\partial t}\mathcal{P}W(t) = -i\mathcal{P}\mathcal{L}\left(\mathcal{P}W(t) + [\mathcal{D}(t)+1]^{-1}\left(\mathcal{U}_{\mathcal{Q}}(t,t_0)\mathcal{Q}W(t_0) - \mathcal{D}(t)\mathcal{P}W(t)\right)\right)
\tag{A.18}
$$

which can be further simplified to

$$
\frac{\partial}{\partial t}\mathcal{P}W(t) = -i\mathcal{P}\mathcal{L}\left[\mathcal{D}(t)+1\right]^{-1}\left(\mathcal{P}W(t) + \mathcal{U}_{\mathcal{Q}}(t,t_0)\mathcal{Q}W(t_0)\right).
\tag{A.19}
$$

Equation (A.19) is the well known Hashitsume-Shibata-Takahashi identity.

B Evaluation of the modified Redfield tensor

The second order expression of the modified Redfield tensor

$$
\begin{aligned}
\overline{R}_{\mu\mu\nu\nu}(t) &= 2\operatorname{Re}\operatorname{tr}\left\{|\mu\rangle\langle\mu|U_0(t)H'|\nu\rangle\langle\nu|R_{\mathrm{eq}}^{\nu}U_0^{\dagger}(t)H'\right\} \\
&= \frac{2}{Z_{\nu}}\operatorname{Re}\operatorname{tr}_{\mathrm{B}}\left\{\exp\left(iH_0^{\nu\nu}t\right)H'_{\nu\mu}\exp\left(-iH_0^{\mu\mu}t\right)H'_{\mu\nu}\exp\left(-\beta H_{\mathrm{B}}(\nu)\right)\right\}
\end{aligned}
\tag{B.1}
$$

can be evaluated by a second-order cumulant expansion of the exponentials under the trace. To achieve a fully exponential representation the two matrix elements of H' in Eq. (B.1) which are not part of an exponential, are rewritten as the derivative of exponentials with respect to parameters α and α', respectively, evaluated at $\alpha, \alpha' = 0$, so that

$$
\overline{R}_{\mu\mu\nu\nu}(t) = 2\operatorname{Re}\left.\frac{\partial^2}{\partial\alpha\partial\alpha'}\overline{R}_{\mu\nu}(t,\alpha,\alpha')\right|_{\alpha,\alpha'=0}
\tag{B.2}
$$

with

$$
\overline{R}_{\mu\nu}(t,\alpha,\alpha') = \frac{1}{Z_{\nu}}\operatorname{tr}_{\mathrm{B}}\left\{\exp\left(iH_0^{\nu\nu}t\right)\exp\left(i\alpha H'_{\nu\mu}\right)\exp\left(-iH_0^{\mu\mu}t\right)\exp\left(-i\alpha' H'_{\mu\nu}\right)\exp\left(-\beta H_{\mathrm{B}}(\nu)\right)\right\}.
\tag{B.3}
$$

and $Z_{\nu} = \operatorname{tr}\left\{\exp(-\beta H_{\mathrm{B}}(\nu))\right\}$. Assuming that the local bath approximation holds and using $\langle\mu|K_k|\nu\rangle = a_{\mu\nu}(k)$ and Eq. (2.67) to obtain λ Eq. (B.3) yields

$$
\begin{aligned}
\overline{R}_{\mu\nu}(t,\alpha,\alpha') &= \exp\left(-i\omega_{\mu\nu}t - \sum_k\left(a_{\mu\mu}^2(k) - a_{\nu\nu}^2(k)\right)\lambda t\right) \\
&\quad \frac{1}{Z_{\nu}}\operatorname{tr}_{\mathrm{B}}\left\{\exp\left(i\sum_k H_{\mathrm{B}}^k(\nu)\right)\exp\left(i\alpha\sum_k a_{\nu\mu}(k)\Phi_k\right)\exp\left(-i\sum_k H_{\mathrm{B}}^k(\mu)t\right)\right. \\
&\quad \left.\exp\left(-i\alpha'\sum_k a_{\mu\nu}(k)\Phi_k\right)\exp\left(-\beta\sum_k H_{\mathrm{B}}^k(\nu)\right)\right\}.
\end{aligned}
\tag{B.4}
$$

The sums in the exponents can be written as a product of traces over the separate bath DOFs, so that

$$
\overline{R}_{\mu\nu}(t,\alpha,\alpha') = \exp\left(-i\omega_{\mu\nu}t - \sum_k\left(a_{\mu\mu}^2(k) - a_{\nu\nu}^2(k)\right)\lambda t\right)\prod_k \overline{R}_{\mu\nu}^k(t,\alpha,\alpha')
\tag{B.5}
$$

with

$$
\begin{aligned}
\overline{R}_{\mu\nu}^k(t,\alpha,\alpha') &= \frac{1}{Z_{\nu}^k}\operatorname{tr}_{\mathrm{B}}^k\left\{\exp\left(iH_{\mathrm{B}}^k(\nu)\right)\exp\left(i\alpha a_{\nu\mu}(k)\Phi_k\right)\exp\left(-iH_{\mathrm{B}}^k(\mu)t\right)\right. \\
&\quad \left.\exp\left(-i\alpha' a_{\mu\nu}(k)\Phi_k\right)\exp\left(-\beta H_{\mathrm{B}}^k(\nu)\right)\right\}
\end{aligned}
\tag{B.6}
$$

and $Z_{\nu}^k = \operatorname{tr}\left\{\exp\left(-\beta H_{\mathrm{B}}^k(\nu)\right)\right\}$. The problem in Eq. (B.6) is that the Hamiltonians in the exponent are shifted according to different system eigenstates μ and ν and that Φ_k is unshifted. Using the relations

$$
\Phi_k(\nu) = \Phi_k + 2a_{\nu\nu}(k)\lambda
\tag{B.7}
$$

and

$$H_{\mathrm{B}}^k(\mu) = H_{\mathrm{B}}^k(\nu) + \phi_k(\nu) \left(a_{\mu\mu}(k) - a_{\nu\nu}(k) \right) + \left(a_{\mu\mu}(k) - a_{\nu\nu}(k) \right)^2 \lambda \tag{B.8}$$

the operators in Eq. (B.6) can be expressed in terms of ν-shifted operators so that

$$
\begin{aligned}
\overline{R}_{\mu\nu}^n(t,\alpha,\alpha') &= \exp\left(-2ia_{\nu\nu}(k)a_{\nu\mu}(k)\left(\alpha - \alpha'\right) - i\left(a_{\mu\mu}(k) - a_{\nu\nu}(k)\right)^2 \right) \lambda t \\
&\quad \mathrm{tr}_{\mathrm{B}}^k \Big\{ \exp\left(iH_{\mathrm{B}}^k(\nu)\right) \exp\left(i\alpha a_{\nu\mu}(k)\Phi_k(\nu)\right) \\
&\quad \exp\left(-i\left(H_{\mathrm{B}}^k(\nu) + \phi_k(\nu)\left(a_{\mu\mu}(k) - a_{\nu\nu}(k)\right)t\right)\right) \\
&\quad \exp\left(-i\alpha' a_{\mu\nu}(k)\Phi_k(\nu)\right) \tfrac{1}{Z_\nu^k} \exp\left(-\beta H_{\mathrm{B}}^k(\nu)\right) \Big\}.
\end{aligned}
\tag{B.9}
$$

In the next step the cumulant expansion is prepared by changing to the interaction picture with respect to $H_{\mathrm{B}}^k(\nu)$, expanding all exponentials up to second order and keeping only those terms which are in second or lower order in $\Phi_k(\nu)$. One finds that all terms linear in $\Phi_k(\nu)$ vanish and only the quadratic terms contribute to the cumulants such that

$$
\begin{aligned}
\overline{R}_{\mu\nu}^n(t,\alpha,\alpha') &\approx \exp\Big(-2ia_{\nu\nu}(k)a_{\nu\mu}(k)\left(\alpha - \alpha'\right)\lambda \\
&\quad -i\left(a_{\mu\mu}(k) - a_{\nu\nu}(k)\right)^2 \lambda t - \tfrac{1}{2}a_{\nu\mu}^2(k)\ddot{G}(0)\left(\alpha^2 + \alpha'^2\right) \\
&\quad +\alpha\alpha' a_{\nu\mu}^2 \ddot{G}(t) - \left(\alpha - \alpha'\right)a_{\nu\mu}(k)\left(a_{\mu\mu}(k) - a_{\nu\nu}(k)\right)\dot{G}(t) \\
&\quad - \left(a_{\mu\mu}(k) - a_{\nu\nu}(k)\right)^2 G(t) \Big)
\end{aligned}
\tag{B.10}
$$

with $G(t) = \int_0^t d\tau \int_0^\tau d\tau' C(\tau')$. Inserting this result into Eqs. (B.2) and (B.5) leads after carrying out the differentiation with respect to α and α' to the modified Redfield tensor

$$
\begin{aligned}
\overline{R}_{\mu\mu\nu\nu}(t) &= 2\,\mathrm{Re}\,\exp\left(-i\left(\omega_{\mu\nu} + 2\lambda_{\nu\nu\nu\nu} - 2\lambda_{\mu\mu\nu\nu}\right)t - G_{\mu\mu\mu\mu}(t) - G_{\nu\nu\nu\nu}(t) + 2G_{\mu\mu\nu\nu}(t) \right) \\
&\quad \times \left[\ddot{G}_{\mu\nu\mu\nu}(t) - \left(\dot{G}_{\mu\nu\mu\mu}(t) - \dot{G}_{\mu\nu\nu\nu}(t) + 2i\lambda_{\nu\nu\nu\mu} \right)^2 \right].
\end{aligned}
\tag{B.11}
$$

Here it was assumed that the matrix elements of K_k are real and $\langle\mu| K_k |\nu\rangle = \langle\nu| K_k |\mu\rangle$, i.e, $a_{\mu\nu}(k) = a_{\nu\mu}(k)$ so that some of the terms in Eq. (B.10) can be combined.

C Evaluation of the stochastic bath evolution

The derivation of an analytical expression of the trace over the stochastic bath density operator R can be done similar to the evaluation of the Feynman-Vernon influence functional.[88] Starting from the stochastic differential equation (2.72) for the bath operator one can find the formal solution as

$$\hat{R}(t) = U_+ \left(\{\nu\}, t \right) \, \hat{R}(0) \, U_- \left(\{\nu\}, t \right) \tag{C.1}$$

where the stochastic time evolution operators $U_\pm$ are defined as

$$U_\pm(t) = \overrightarrow{T} \exp \left(\mp i H_{\mathrm{B}} t + \frac{1}{2} \sum_k \Phi_k [\nu]_k^\pm (t) \right). \tag{C.2}$$

with

$$[\nu]_k^\pm (t) = \nu_{1,k}(t) - i\nu_{2,k}(t) \mp i\nu_{3,k}(t) \pm \nu_{4,k}(t). \tag{C.3}$$

Here the time-ordering operator is necessary due to the time-dependent fluctuating fields. A change into the interaction picture yields

$$
\begin{aligned}
U_+(t) &= U_{\mathrm{B}}(t) \, \tilde{U}_+(t) \\
U_-(t) &= \tilde{U}_-(t) \, U_{\mathrm{B}}^\dagger(t)
\end{aligned}
\tag{C.4}
$$

with

$$\tilde{U}_\pm(t) = \overrightarrow{T} \exp \left(\frac{1}{2} \sum_k \int_0^t \Phi_k(\tau) \, d[\nu]_k^\pm (\tau) \right) \tag{C.5}$$

and

$$\Phi_k(t) = e^{iH_{\mathrm{B}} t} \Phi_k e^{-iH_{\mathrm{B}} t} \tag{C.6}$$

being the bath part of the interaction Hamiltonian which evolves according to the interaction picture. For a bath of harmonic oscillators with linear coupling to the system as defined in Eq. (2.26), Eq. (C.6) can be rewritten as

$$\Phi_k(t) = \sum_\xi c_{k\xi} \left(x_\xi \cos \left(\omega_\xi t \right) + \frac{p_\xi}{m_\xi \omega_\xi} \sin \left(\omega_\xi t \right) \right). \tag{C.7}$$

Since the single harmonic oscillators of the bath are uncoupled one can write the time evolution operator of the bath as a product of the time evolution operators of the single oscillators:

$$\tilde{U}_\pm(t) = \prod_\xi \tilde{U}_\pm^\xi(t) \tag{C.8}$$

with the independent stochastic time evolution operators

$$\tilde{U}_\pm^\xi(t) = \overrightarrow{T} \exp \left(\frac{1}{2} \sum_k \int_0^t c_{k\xi} \left(x_\xi \cos \left(\omega_\xi \tau \right) + \frac{p_\xi}{m_\xi \omega_\xi} \sin \left(\omega_\xi \tau \right) \right) d[\nu]_k^\pm (\tau) \right) \tag{C.9}$$

for each DOF of the bath. These operators, however, contain terms linear in the coordinate operator x_ξ and the momentum operator p_ξ, respectively. To evaluate the trace (2.78) one can make the ansatz

$$\tilde{U}_+^\xi(t) = e^{A_+^\xi(t)} e^{x_\xi B_+^\xi(t)} e^{p_\xi C_+^\xi(t)}, \tag{C.10}$$

such that both, the momentum and the coordinate operator appear in separate exponentials with time dependent and stochastic coefficients $A_+^\xi(t)$, $B_+^\xi(t)$ and $C_+^\xi(t)$. This ansatz, based on the Baker-Champel-Hausdorff formula, is possible since the commutator of momentum and coordinate operator is scalar.

For the coefficients one can make the ansatz

$$A_+^\xi(t) \;=\; \sum_k \int_0^t a_{k+}^\xi(\tau)\, d[\nu]_k^+(\tau) \tag{C.11}$$

$$B_+^\xi(t) \;=\; \sum_k \int_0^t b_{k+}^\xi(\tau)\, d[\nu]_k^+(\tau) \tag{C.12}$$

$$C_+^\xi(t) \;=\; \sum_k \int_0^t c_{k+}^\xi(\tau)\, d[\nu]_k^+(\tau) \tag{C.13}$$

where $a_{k+}^\xi(t)$, $b_{k+}^\xi(t)$ and $c_{k+}^\xi(t)$ still have to be specified. This can be done by comparing the stochastic differentials of the original expression (C.9) and ansatz (C.10) which leads to

$$
\begin{aligned}
d\tilde{U}_+^\xi(t) \;&=\; \frac{1}{2} \sum_k c_{k\xi} \left(x_\xi \cos(\omega_\xi t) + \frac{p_\xi}{m_\xi \omega_\xi} \sin(\omega_\xi \tau) \right) \tilde{U}_+^\xi(t)\, d[\nu]_k^+(t) \\
&=\; \sum_k \left(a_{k+}^\xi(t) + i c_{k+}^\xi(t) B_+^\xi(t) + x_\xi b_{k+}^\xi(t) + p_\xi c_{k+}^\xi(t) \right) \tilde{U}_+^\xi(t)\, d[\nu]_k^+(t). \quad \text{(C.14)}
\end{aligned}
$$

To arrive at the second expression the commutator relation

$$[p_\xi, e^{\alpha x_\xi}] = -i\alpha e^{\alpha x_\xi} \tag{C.15}$$

has been applied to rearrange the exponentials. Direct comparison of the coefficients of x_ξ and p_ξ yields

$$a_{k+}^\xi(t) \;=\; -\frac{i}{4} \sum_j \frac{c_{k\xi} c_{j\xi}}{m_\xi \omega_\xi} \sin(\omega_\xi t) \int_0^t \cos(\omega_\xi \tau)\, d[\nu]_j^+(\tau) \tag{C.16}$$

$$b_{k+}^\xi(t) \;=\; \frac{1}{2} c_{k\xi} \cos(\omega_\xi t), \tag{C.17}$$

$$c_{k+}^\xi(t) \;=\; \frac{c_{k\xi}}{2m_\xi \omega_\xi} \sin(\omega_\xi t), \tag{C.18}$$

In the same way one can make an ansatz for $\tilde{U}_-^\xi(t)$ as

$$\tilde{U}_-^\xi(t) = e^{p_\xi C_-^\xi(t)} e^{x_\xi B_-^\xi(t)} e^{A_-^\xi(t)}, \tag{C.19}$$

with

$$A^\xi_-(t) \;=\; \sum_k \int_0^t a^\xi_{k-}(\tau)\,d[\nu]^-_k(\tau) \tag{C.20}$$

$$B^\xi_-(t) \;=\; \sum_k \int_0^t b^\xi_{k-}(\tau)\,d[\nu]^-_k(\tau) \tag{C.21}$$

$$C^\xi_-(t) \;=\; \sum_k \int_0^t c^\xi_{k-}(\tau)\,d[\nu]^-_k(\tau) \tag{C.22}$$

and find that

$$a^\xi_{k-}(t) \;=\; \frac{i}{4}\sum_j \frac{c_{k\xi}c_{j\xi}}{m_\xi \omega_\xi}\sin(\omega_\xi t)\int_0^t \cos(\omega_\xi \tau)\,d[\nu]^-_j(\tau) \tag{C.23}$$

$$b^\xi_{k-}(t) \;=\; \frac{1}{2}c_{k\xi}\cos(\omega_\xi t)\,, \tag{C.24}$$

$$c^\xi_{k-}(t) \;=\; \frac{c_{k\xi}}{2m_\xi \omega_\xi}\sin(\omega_\xi t)\,. \tag{C.25}$$

The trace over the stochastic bath density matrix can be performed separately for each bath oscillator

$$\mathrm{tr}\left\{\tilde U_+(t)R_{\mathrm{eq}}\tilde U_-(t)\right\} = \prod_\xi \mathrm{tr}\left\{R^\xi_{\mathrm{eq}}\tilde U^\xi_-(t)\tilde U^\xi_+(t)\right\} \tag{C.26}$$

where R^ξ_{eq} is the equilibrium density matrix of the ξth harmonic oscillator. The trace over a single oscillator can be evaluated in the coordinate representation

$$
\begin{aligned}
\mathrm{tr}\left\{R^\xi_{\mathrm{eq}}\tilde U^\xi_-(t)\tilde U^\xi_+(t)\right\} \;=&\; \int_{-\infty}^\infty dx_\xi \left\langle x_\xi\right| R^\xi_{\mathrm{eq}}\exp\left(p_\xi C^\xi_-\right)\exp\left(x_\xi\left(B^\xi_- + B^\xi_+\right)\right)\exp\left(p_\xi C^\xi_+\right)\left|x_\xi\right\rangle \\
&\times \exp\left(A^\xi_+ + A^\xi_-\right)
\end{aligned}
\tag{C.27}
$$

where the equilibrium matrix reads in coordinate representation[88]

$$\left\langle x_\xi\right| R^\xi_{\mathrm{eq}}\left|x'_\xi\right\rangle = \frac{1}{Z_\xi}\sqrt{\frac{m_\xi \omega_\xi}{2\pi \sinh(\beta\omega_\xi)}}\exp\left(-\frac{m_\xi \omega_\xi}{2\sinh(\beta\omega_\xi)}\left[\left(x_\xi^2 + x'^2_\xi\right)\cosh(\beta\omega_\xi) - 2x_\xi x'_\xi\right]\right) \tag{C.28}$$

with the partition function $Z_\xi = 2\sinh(\beta\omega_\xi/2)$. The integral (C.27) can be evaluated by using the coordinate shift properties of the exponentials of the momentum operator

$$\exp(\alpha p_\xi)\left|x_\xi\right\rangle = \left|x_\xi + i\alpha\right\rangle. \tag{C.29}$$

In general, the state vector $\left|x_\xi + i\alpha\right\rangle$ is only defined for $\mathrm{Im}[i\alpha] = 0$, however in this case one can use this notation with complex arguments to evaluate the trace (C.27) since the equilibrium density matrix is of Gaussian shape in momentum as well as in coordinate representation. Inserting the unity operator $\frac{1}{2\pi}\int dp_\xi \left|p_\xi\right\rangle\left\langle p_\xi\right|$ next to one of the shift operators yields an integral over an exponential function with argument linear in p_ξ, i.e., the Gaussian equilibrium density matrix decays faster and the integral converges. Therefore Eq. (C.27) can then be written as

$$
\begin{aligned}
\mathrm{tr}\left\{R^\xi_{\mathrm{eq}}\tilde U^\xi_-(t)\tilde U^\xi_+(t)\right\} \;=&\; \int_{-\infty}^\infty dx_\xi \left\langle x_\xi\right| R^\xi_{\mathrm{eq}}\left|x_\xi + i\left(C^\xi_+ + C^\xi_-\right)\right\rangle \\
&\quad \exp\left[\left(x + iC^\xi_+\right)\left(B^\xi_+ + B^\xi_-\right) + A^\xi_+ + A^\xi_-\right],
\end{aligned}
\tag{C.30}
$$

i.e., replacing $x'_\xi = x_\xi + i\left(C^\xi_+ + C^\xi_-\right)$ in Eq. (C.28) and inserting this expression in Eq. (C.30) yields a Gaussian integral of type

$$\int\limits_{-\infty}^{\infty} dx \, \exp\left(-ax^2 + bx + c\right) = \sqrt{\frac{\pi}{a}} \exp\left(\frac{b^2}{4a} + c\right). \qquad (C.31)$$

After some algebra using the relations of hyperbolic functions one arrives at

$$
\begin{aligned}
\mathrm{tr}\left\{R^\xi_{\mathrm{eq}} \tilde{U}^\xi_-(t) \tilde{U}^\xi_+(t)\right\} &= \exp\left(A^\xi_+ + A^\xi_- + \tfrac{i}{2}\left(C^\xi_+ - C^\xi_-\right)\left(B^\xi_+ + B^\xi_-\right)\right) \\
&\quad \exp\left(\tfrac{1}{4m_\xi\omega_\xi} \coth\left(\tfrac{\beta\omega_\xi}{2}\right)\left(B^\xi_+ + B^\xi_-\right)^2\right) \\
&\quad \exp\left(\tfrac{1}{4}m_\xi\omega_\xi \coth\left(\tfrac{\beta\omega_\xi}{2}\right)\left(C^\xi_+ + C^\xi_-\right)^2\right).
\end{aligned} \qquad (C.32)
$$

Inserting the expressions for $A^\xi_\pm$, $B^\xi_\pm$ and $C^\xi_\pm$ and using the abbreviations

$$
\begin{aligned}
f_\xi(\tau) &= \sum_k \frac{c_{k\xi}}{2\sqrt{m_\xi\omega_\xi}}\left(\nu_{1,k}(\tau) - i\nu_{2,k}(\tau)\right), \\
h_\xi(\tau) &= \sum_k \frac{c_{k\xi}}{2\sqrt{m_\xi\omega_\xi}}\left(\nu_{3,k}(\tau) + i\nu_{4,k}(\tau)\right)
\end{aligned} \qquad (C.33)
$$

yields

$$
\begin{aligned}
\tfrac{1}{4}m_\xi\omega_\xi\left(C^\xi_+ + C^\xi_-\right)^2 &= \int\limits_0^t \sin\left(\omega_\xi\tau\right) df_\xi(\tau) \int\limits_0^t \sin\left(\omega_\xi\tau'\right) df_\xi(\tau') \\
&= \tfrac{1}{2}\int\limits_0^t \int\limits_0^t \left[\cos\left(\omega_\xi\left(\tau-\tau'\right)\right) - \cos\left(\omega_\xi\left(\tau+\tau'\right)\right)\right] df_\xi(\tau) df_\xi(\tau')
\end{aligned} \qquad (C.34)
$$

and

$$
\begin{aligned}
\tfrac{1}{4m_\xi\omega_\xi}\left(B^\xi_+ + B^\xi_-\right)^2 &= \int\limits_0^t \cos\left(\omega_\xi\tau\right) df_\xi(\tau) \int\limits_0^t \cos\left(\omega_\xi\tau'\right) df_\xi(\tau') \\
&= \tfrac{1}{2}\int\limits_0^t \int\limits_0^t \left[\cos\left(\omega_\xi\left(\tau-\tau'\right)\right) + \cos\left(\omega_\xi\left(\tau+\tau'\right)\right)\right] df_\xi(\tau) df_\xi(\tau').
\end{aligned} \qquad (C.35)
$$

In the sum of Eqs. (C.34) and (C.35) the terms containing $\cos\left(\omega_\xi\left(\tau+\tau'\right)\right)$ cancel such that

$$\tfrac{1}{4}m_\xi\omega_\xi\left(C^\xi_+ + C^\xi_-\right)^2 + \tfrac{1}{4m_\xi\omega_\xi}\left(B^\xi_+ + B^\xi_-\right)^2 = 2\int\limits_0^t \int\limits_0^\tau \cos\left(\omega_\xi\left(\tau-\tau'\right)\right) df_\xi(\tau) df_\xi(\tau'). \qquad (C.36)$$

Here the symmetry of the integrand has been used to change the integral boundaries. In the same way one gets

$$
\begin{aligned}
\tfrac{i}{2}\left(C^\xi_+ - C^\xi_-\right)\left(B^\xi_+ + B^\xi_-\right) + A^\xi_+ + A^\xi_- &= \int\limits_0^t \int\limits_0^t \sin\left(\omega_\xi\left(\tau-\tau'\right)\right) dh_\xi(\tau) df_\xi(\tau') \\
&\quad + \int\limits_0^t \int\limits_0^t \sin\left(\omega_\xi\left(\tau+\tau'\right)\right) dh_\xi(\tau) df_\xi(\tau') \\
&\quad - \int\limits_0^t \int\limits_0^\tau \sin\left(\omega_\xi\left(\tau-\tau'\right)\right)\left[dh_\xi(\tau) df_\xi(\tau') + dh_\xi(\tau') df_\xi(\tau)\right] \\
&\quad - \int\limits_0^t \int\limits_0^\tau \sin\left(\omega_\xi\left(\tau+\tau'\right)\right)\left[dh_\xi(\tau) df_\xi(\tau') + dh_\xi(\tau') df_\xi(\tau)\right].
\end{aligned} \qquad (C.37)
$$

Again considering symmetry properties of the integrands in Eq. (C.37) one notices that the second integral expression on the right hand side can be written as

$$
\begin{aligned}
\int_0^t \int_0^t \sin\left(\omega_\xi\left(\tau + \tau'\right)\right) dh_\xi(\tau) df_\xi(\tau') &= \tfrac{1}{2} \int_0^t \int_0^t \sin\left(\omega_\xi\left(\tau + \tau'\right)\right) \left[dh_\xi(\tau) df_\xi(\tau') + dh_\xi(\tau') df_\xi(\tau) \right] \\
&= \int_0^t \int_0^\tau \sin\left(\omega_\xi\left(\tau + \tau'\right)\right) \left[dh_\xi(\tau) df_\xi(\tau') + dh_\xi(\tau') df_\xi(\tau) \right]
\end{aligned}
$$

(C.38)

so that the second and the forth integral terms in Eq. (C.37) cancel. In the same way the first integral terms in Eq. (C.37) can be re-written as

$$
\begin{aligned}
\int_0^t \int_0^t \sin\left(\omega_\xi\left(\tau - \tau'\right)\right) dh_\xi(\tau) df_\xi(\tau') &= \tfrac{1}{2} \int_0^t \int_0^t \sin\left(\omega_\xi\left(\tau - \tau'\right)\right) \left[dh_\xi(\tau) df_\xi(\tau') - dh_\xi(\tau') df_\xi(\tau) \right] \\
&= \int_0^t \int_0^\tau \sin\left(\omega_\xi\left(\tau - \tau'\right)\right) \left[dh_\xi(\tau) df_\xi(\tau') - dh_\xi(\tau') df_\xi(\tau) \right],
\end{aligned}
$$

(C.39)

which cancels parts of the third integral in Eq. (C.37), i.e.,

$$
\tfrac{i}{2}\left(C_+^\xi - C_-^\xi\right)\left(B_+^\xi + B_-^\xi\right) + A_+^\xi + A_-^\xi = -2 \int_0^t \int_0^\tau \sin\left(\omega_\xi\left(\tau - \tau'\right)\right) df_\xi(\tau) dh_\xi(\tau')
$$

(C.40)

Inserting Eqs. (C.33), (C.36) and (C.40) into Eq. (C.26) the trace over the stochastic bath density matrix finally yields

$$
\begin{aligned}
\text{tr}\left\{\tilde{U}_+ R_{\text{eq}} \tilde{U}_-\right\} = \exp\Bigg(&\sum_{kj}\sum_\xi \frac{c_{k\xi} c_{j\xi}}{2 m_\xi \omega_\xi}\Bigg[\coth\left(\frac{\beta\omega_\xi}{2}\right) \\
&\int_0^t \int_0^\tau \cos\left(\omega_\xi\left(\tau - \tau'\right)\right)\left(d\nu_{1,j}(\tau') - i d\nu_{2,j}(\tau')\right)\left(d\nu_{1,k}(\tau) - i d\nu_{2,k}(\tau)\right) \\
&- \int_0^t \int_0^\tau \sin\left(\omega_\xi\left(\tau - \tau'\right)\right)\left(d\nu_{3,j}(\tau') + i d\nu_{4,j}(\tau')\right)\left(d\nu_{1,k}(\tau) - i d\nu_{2,k}(\tau)\right)\Bigg]\Bigg).
\end{aligned}
$$

(C.41)

Using the definition of the bath correlation functions (2.56) Eq. (C.41) simplifies to

$$
\begin{aligned}
\text{tr}\left\{\tilde{U}_+ R_{\text{eq}} \tilde{U}_-\right\} = \exp\Bigg(&\sum_{kj}\Bigg[\int_0^t \int_0^\tau a_{kj}(\tau - \tau')\left(d\nu_{1,j}(\tau') - i d\nu_{2,j}(\tau')\right)\left(d\nu_{1,k}(\tau) - i d\nu_{2,k}(\tau)\right) \\
&+ \int_0^t \int_0^\tau b_{k,j}\left(\tau - \tau'\right)\left(d\nu_{3,j}(\tau') + i d\nu_{4,j}(\tau')\right)\left(d\nu_{1,k}(\tau) - i d\nu_{2,k}(\tau)\right)\Bigg]\Bigg),
\end{aligned}
$$

(C.42)

where $a_{ij}(t)$ and $b_{ij}(t)$ are the real and imaginary parts of the bath correlation functions according to Eq. (2.65) but without the local bath approximation (2.58).

Bibliography

[1] H. Haken and H. C. Wolf, *Molekülphysik und Quantenchemie* (Springer, Berlin, 1998).

[2] V. May and O. Kühn, *Charge and Energy Transfer in Molecular Systems* (Wiley-VCH, Berlin, 2000).

[3] S. Scheuring *et al.*, Proc. Natl. Acad. Sci. USA **101**, 11293 (2004).

[4] J. Koepke *et al.*, Structure **4**, 581 (1996).

[5] X. Hu and K. Schulten, Physics Today **8**, 28 (1997).

[6] H. van Amerongen, L. Valkunas, and R. van Grondelle, *Photosynthetic Excitons* (World Scientific, Singapore, 2000).

[7] X. Hu, T. Ritz, A. Damjanović, and K. Schulten, J. Phys. Chem. B **101**, 3854 (1997).

[8] R. Kubo, in *Fluctuation, Relaxation and Resonance in Magnetic Systems*, edited by D. ter Haar (Oliver & Boyd, Edinburgh, 1962), p. 23.

[9] S. Mukamel, *Principles of Nonlinear Optical Spectroscopy* (Oxford University Press, New York, 1995).

[10] J. Y. Sung and M. H. Cho, J. Chem. Phys. **113**, 7072 (2000).

[11] J. Y. Sung and R. J. Silbey, J. Chem. Phys. **115**, 9266 (2001).

[12] A. Matro and J. Cina, J. Phys. Chem. **99**, 2568 (1995).

[13] T. Renger and V. May, Phys. Rev. Lett. **78**, 3406 (1997).

[14] T. Renger and V. May, Phys. Rev. Lett. **84**, 5228 (2000).

[15] K. Ohta, M. Yang, and G. R. Fleming, J. Chem. Phys. **115**, 7609 (2001).

[16] T. Renger and R. A. Marcus, J. Chem. Phys. **116**, 9997 (2002).

[17] W. M. Zhang, T. Meier, V. Chernyak, and S. Mukamel, J. Chem. Phys. **108**, 7763 (1998).

[18] A. Damjanović, I. Kosztin, U. Kleinekathöfer, and K. Schulten, Phys. Rev. E **65**, 031919 (2002).

[19] M. Schröder, U. Kleinekathöfer, and M. Schreiber, J. Chem. Phys. **124**, 084903 (2006).

[20] U. Kleinekathöfer, M. Schröder, and M. Schreiber, J. Lumin. **112**, 461 (2005).

[21] M. Schröder, U. Kleinekathöfer, and M. Schreiber, J. Lumin. (2006), accepted.

[22] S. Welack, M. Schreiber, and U. Kleinekathöfer, J. Chem. Phys. **124**, 044712 (2006).

[23] M. Bixon and J. Jortner, Chem. Phys. **281**, 393 (2002).

[24] T. Renger and R. A. Marcus, J. Phys. Chem. A **107**, 8404 (2003).

[25] T. Cramer, S. Krapf, and T. Koslowski, J. Phys. Chem. B **106**, 11812 (2004).

[26] U. Kleinekathöfer, G. Li, and M. Schreiber, J. Lumin. **119-120**, 91 (2006).

[27] T. Fiebig *et al.*, Proc. Natl. Acad. Sci. USA **96**, 1187 (1999).

[28] C. Wan *et al.*, Proc. Natl. Acad. Sci. USA **97**, 14052 (2000).

[29] Y. Tanimura and R. Kubo, J. Phys. Soc. Jpn. **58**, 101 (1998).

[30] Y. Tanimura, Phys. Rev. A **41**, 6676 (1990).

[31] Y. Tanimura and P. G. Wolynes, Phys. Rev. A **43**, 4131 (1991).

[32] Y. Tanimura and S. Mukamel, J. Phys. Soc. Jpn. **63**, 66 (1994).

[33] J. Shao, J. Chem. Phys. **120**, 5053 (2004).

[34] Y. Yan, F. Yang, and J. Shao, Chem. Phys. Lett. **395**, 216 (2004).

[35] A. Ishizaki and Y. Tanimura, J. Phys. Soc. Jpn. **74**, 3131 (2005).

[36] R.-X. Xu *et al.*, J. Chem. Phys. **122**, 041103 (2005).

[37] Y. Tanimura, J. Phys. Soc. Jpn. **75**, 082001 (2006).

[38] H. P. Breuer, D. Burgarth, and F. Petruccione, Phys. Rev. B **70**, 045323 (2004).

[39] V. May and M. Schreiber, Phys. Rev. A **45**, 2868 (1992).

[40] V. May, O. Kühn, and M. Schreiber, J. Phys. Chem. **97**, 12591 (1993).

[41] J. Manz, in *Femtochemistry and Femtobiology*, edited by V. Sundström (Imperial College Press, London, 1997).

[42] F. C. DeSchryver, S. DeFeyter, and G. Schweitzer, *Femtochemistry* (Wiley-VCH, Berlin, 2001).

[43] A. Douhal and J. Santamaria, *Femtochemistry and Femtobiology: Ultrafast Dynamics in Molecular Science* (World Scientific, Singapore, 2002).

[44] V. Buch, J. Chem. Phys. **117**, 4738 (2002).

[45] C. Leforestier *et al.*, J. Comp. Phys. **94**, 59 (1991).

[46] R. Kosloff, Annu. Rev. Phys. Chem. **45**, 145 (1994).

[47] R. Kosloff, in *Dynamics of Molecules and Chemical Reactions*, edited by R. E. Wyatt and J. Z. H. Zhang (Marcel Dekker, New York, 1996).

[48] N. Balakrishnan, C. Kalyanaraman, and N. Sathyamurthy, Phys. Rep. **280**, 79 (1997).

[49] P. A. M. Dirac, Proc. Cambridge Philos. Soc. **26**, 376 (1930).

[50] A. D. McLachlan, Mol. Phys. **8**, 39 (1964).

[51] H.-D. Meyer, U. Manthe, and L. Cederbaum, Chem. Phys. Lett. **165**, 73 (1990).

[52] M. H. Beck, A. Jäckle, G. A. Worth, and H.-D. Meyer, Phys. Rep. **324**, 1 (2000).

[53] H.-D. Meyer and G. A. Worth, Theor. Chim. Acta **109**, 251 (2003).

[54] H. Wang, M. Thoss, and W. H. Miller, J. Chem. Phys. **115**, 2979 (2001).

[55] M. Thoss, H. Wang, and W. H. Miller, J. Chem. Phys. **115**, 2991 (2001).

[56] B. Wolfseder and W. Domcke, Chem. Phys. Lett. **235**, 370 (1995).

[57] B. Wolfseder and W. Domcke, Chem. Phys. Lett. **259**, 113 (1996).

[58] O. Linden and V. May, Eur. Phys. J. D **12**, 473 (2000).

[59] J. Steinbach, B. N. Garraway, and P. L. Knight, Phys. Rev. A **51**, 3302 (1995).

[60] W. T. Strunz, L. Diosi, N. Gisin, and T. Yu, Phys. Rev. Lett. **83**, 4909 (1999).

[61] T. Yu, L. Diósi, N. Gisin, and W. T. Strunz, Phys. Rev. A **60**, 91 (1999).

[62] U. Kleinekathöfer, I. Kondov, and M. Schreiber, Phys. Rev. E **66**, 037701 (2002).

[63] I. Kondov, U. Kleinekathöfer, and M. Schreiber, J. Chem. Phys. **119**, 6635 (2003).

[64] H. P. Breuer, B. Kappler, and F. Petruccione, Phys. Rev. A **56**, 2334 (1997).

[65] T. Felbinger and M. Wilkens, J. Mod. Opt. **46**, 1401 (1999).

[66] M. Schröder and U. Kleinekatöfer, phys. stat. sol. (b) **241**, 2157 (2004).

[67] S. Nakajima, Prog. Theor. Phys. **20**, 948 (1958).

[68] R. Zwanzig, in *Lectures in Theoretical Physics*, edited by W. E. Brittin, B. W. Downs, and J. Downs (Interscience, New York, 1961), Vol. 3, p. 106.

[69] R. Zwanzig, Physica **30**, 1109 (1964).

[70] N. Hashitsume, F. Shibata, and M. Shingu, J. Stat. Phys. **17**, 155 (1977).

[71] F. Shibata, Y. Takahashi, and N. Hashitsume, J. Stat. Phys. **17**, 171 (1977).

[72] Q. Shi and E. Geva, J. Chem. Phys. **119**, 12063 (2003).

[73] S. Jang, J. Cao, and R. J. Silbey, J. Chem. Phys. **116**, 2705 (2002).

[74] H.-P. Breuer and F. Petruccione, *The theory of open quantum systems* (Oxford University Press, New York, 2002).

[75] H. Grabert, P. Schramm, and G.-L. Ingold, Phys. Rep. **168**, 115 (1988).

[76] U. Kleinekathöfer, J. Chem. Phys. **121**, 2505 (2004).

[77] J. E. Hirsch, Phys. Rev. B **28**, 4059 (1983).

[78] D. Lacroix, Phys. Rev. A **72**, 013805 (2005).

[79] Y. Mo, R.-X. Xu, P. Cui, and Y. Yan, J. Chem. Phys. **120**, 084115 (2005).

[80] Y. Zhou, Y. Yan, and J. Shao, Europhys. Lett. **72**, 334 (2005).

[81] J. Shao, Chem. Phys. **322**, 187 (2006).

[82] E. Geva, E. Rosenman, and D. J. Tannor, J. Chem. Phys. **113**, 1380 (2000).

[83] W. H. Louisell, *Quantum Statistical Properties of Radiation* (Wiley, New York, 1990).

[84] D. Kohen, C. C. Marston, and D. J. Tannor, J. Chem. Phys. **107**, 5236 (1997).

[85] C. Meier and D. J. Tannor, J. Chem. Phys. **111**, 3365 (1999).

[86] B. Øksendal, *Stochastic Differential Equations* (Springer, Berlin, 1995).

[87] C. W. Gardiner, *Handbook of Stochastic Methods*, 2nd ed. (Springer, Berlin, 1985).

[88] H. Kleinert, *Path Integrals in Quantum Mechanics, Statistics and Polymer Physics*, 2nd ed. (World Scientific, Singapore, 1995).

[89] M. Yang and G. R. Fleming, Chem. Phys. **275**, 355 (2002).

[90] F. Neugebauer, D. Malzahn, and V. May, Chem. Phys. **201**, 151 (1995).

[91] D. Egorova, M. Thoss, W. Domcke, and H. Wang, J. Chem. Phys. **119**, 2761 (2003).

[92] T. Renger, V. May, and O. Kühn, Phys. Rep. **343**, 137 (2001).

[93] H. P. Breuer, B. Kappler, and F. Petruccione, Phys. Rev. A **59**, 1633 (1999).

[94] V. Novoderezhkin, M. A. Palacios, H. van Amerongen, and R. van Grondelle, J. Phys. Chem. B **108**, 10363 (2004).

[95] J. M. Jean, J. Chem. Phys. **101**, 10464 (1994).

[96] S. Georgakopoulou *et al.*, Biophys. J. **82**, 2184 (2002).

[97] C. Warns, P. Reineker, and I. Barvík, Chem. Phys. **290**, 1 (2003).

[98] J. Linnanto, J. E. I. Korppi-Tommola, and V. Helenius, J. Phys. Chem. B **103**, 8739 (1999).

[99] J. A. Ihalainen *et al.*, J. Phys. Chem. B **105**, 9849 (2001).

[100] V. Nagarajan, R. G. Alden, J. C. Williams, and W. W. Parson, Proc. Natl. Acad. Sci. USA **93**, 13774 (1996).

[101] M. Nest and H.-D. Meyer, J. Chem. Phys. **119**, 24 (2003).

[102] F. E. van Dorsselaer and G. Nienhuis, J. Opt. B **2**, L5 (2000).

[103] M. B. Plenio and P. L. Knight, Rev. Mod. Phys. **70**, 101 (1998).

[104] S. Jang and R. J. Silbey, J. Chem. Phys. **118**, 9312 (2003).

[105] S. Jang and R. J. Silbey, J. Chem. Phys. **118**, 9324 (2003).

[106] C. Hofmann, T. J. Aartsma, and J. Köhler, Chem. Phys. Lett. **395**, 373 (2004).

[107] C. Hofmann, H. Michel, M. van Heel, and J. Köhler, Phys. Rev. Lett. **94**, 195501 (2005).

List of Figures

List of Tables

Danksagung

Ich möchte mich an dieser Stelle bei all jenen bedanken, die mich bei dieser Arbeit unterstützt haben und ohne deren Zutun ihre Entstehung schwerlich möglich gewesen wäre.

Besonders bedanken möchte ich mich bei Professor Dr. Michael Schreiber, der es mir ermöglichte in seiner Arbeitsgruppe tätig zu sein. Er unterstützte und betreute mich stets während meiner Aufenthalte sowohl in Bremen als auch in Chemnitz.

Dieses gilt in gleichem Maße für Professor Dr. Ulrich Kleinekathöfer, der diese Arbeit direkt betreute. Er hat mich in ein interessantes und faszinierendes Themengebiet eingeführt und war immer ein engagierter Ansprechpartner, der stets Zeit und ein offenes Ohr für Diskussionen hatte.

Ebenfalls bedanken möchte ich mich bei Dr. Thomas Renger, mit dem ich am Rande seines Besuches in Chemnitz Gelegenheit zur Diskussion hatte.

Hervorheben möchte ich außerdem das sehr gute Verhältnis zu den Mitgliedern der Arbeitsgruppe. Ich habe die freundschaftliche Atmosphäre in dieser Gruppe sehr genossen.

Nicht zuletzt stehen hinter all dem Freunde und Familie, meine Eltern Kurt und Astrid Schröder und meine Schwester Anke. Besonderer Dank gilt auch meinen Freunden Thomas Blecha, Steffen Gräfe, Jörg Liebers, Carsten Olbrich, Stephanie Röper, Susanne Schübel und Mario Zerson.

Vielen Dank!

Selbständigkeitserklärung nach § 6 Promotionsordnung

Hiermit erkläre ich, dass ich die vorliegende Arbeit selbständig und nur unter Verwendung der angegebenen Literatur und Hilfsmittel angefertigt habe. Die Stellen in der Arbeit, die in Sinn und Wortlaut anderen Werken entnommen wurden, habe ich entsprechend gekennzeichnet. Ich erkläre, nicht bereits früher oder gleichzeitig bei anderen Hochschulen oder an der Technischen Universität Chemnitz ein Promotionsverfahren beantragt zu haben. Die derzeit gültige Promotionsordnung der Fakultät für Naturwissenschaften der Technischen Universität Chemnitz vom 10. Oktober 2001 ist mir bekannt.

Chemnitz, den 18.10.2006

Markus Schröder

Lebenslauf

Persönliche Angaben

Name	Markus Schröder
Geburtsdatum	15. Mai 1977
Geburtsort	Verden (Aller)
Staatsangehörigkeit	deutsch
Familienstand	ledig

Schulbildung

1983 - 1987	Grundschule am Sachsenhain in Verden (Aller)
1987 - 1989	Orientierungsstufe in Verden (Aller)
1989 - 1993	Realschule Verden (Aller)
1993 - 1996	Domgymnasium Verden (Aller)
Mai 1996	Abitur

Studium und Beruf

01. 09. 1996 - 30. 06. 1997	Grundwehrdienst
01. 10. 1997 - 30. 09. 1999	Studium der Physik, Universität Bremen, Abschluss: Vordiplom in Physik, Note: 1.8
01. 10. 1999 - 28. 02. 2003	Studium der Physik, Technische Universität Chemnitz, Abschluss: Diplom in Physik, Note: 1.2
01. 03. 2003 - 29. 02. 2004	Graduate Student, School of Engineering and Science, International University Bremen
01. 03. 2004 - 30. 09. 2006	Wissenschaftlicher Mitarbeiter an der Professur "Theorie ungeordneter Systeme", Institut für Physik, Technische Universität Chemnitz

Publikationen

1. M. Schröder and U. Kleinekathöfer, "A Monte Carlo method for propagating multi-dimensional wave packets", Phys. Stat. Sol. (b) **241**, 2157-2167 (2004)

2. U. Kleinekathöfer, M. Schröder and M. Schreiber, "Absorption spectra for a model light-harvesting system using non-Markovian theories", J. Lumin. **112**, 461-464 (2005)

3. M. Schröder, U. Kleinekathöfer and M. Schreiber, "Absorption spectra for light harvesting systems based on different quantum master equations", J. Chem. Phys. **124**, 084903/1-14 (2006)

4. M. Schröder, M. Schreiber and U. Kleinekathöfer, "A time-dependent modified Redfield theory for absorption spectra applied to light-harvesting systems", J. Lumin. (akzeptiert)

5. M. Schröder, M. Schreiber and U. Kleinekathöfer, "Reduced dynamics of coupled harmonic and anharmonic oscillators using higher-order perturbation theory", J. Chem. Phys. (akzeptiert)

Konferenzbeiträge

1. M. Schröder, U. Kleinekathöfer and M. Schreiber, "Monte Carlo methods for propagating multi-dimensional wave packets and density matrices", DPG Frühjahrstagung, Regensburg (2004)

2. M. Schröder, U. Kleinekathöfer and M. Schreiber, "Absorption spectra for a model light-harvesting system using non-Markovian theories" DPG Frühjahrstagung, Berlin (2005)

3. M. Schröder, U. Kleinekathöfer and M. Schreiber, "Absorption spectra of light-harvesting complexes using non-Markovian theories", Classical and Quantum Dynamical Simulations in Chemical and Biological Physics workshop, Dresden (2005)

4. M. Schröder, M. Schreiber and U. Kleinekathöfer, "Absorption spectra for light-harvesting systems using non-Markovian as well as modified Redfield master equations", DPG Frühjahrstagung, Dresden (2006)

5. G. Q. Li, M. Schröder, M. Schreiber and U. Kleinekathöfer, "Hierarchical and approximate quantum master equations based on a decomposition of the spectral density applied to electron injection into a DNA base pair", DPG Frühjahrstagung, Dresden (2006)